

This dissertation has been
microfilmed exactly as received

69-11,055

MUNTER, William Andrew, 1940-
MEASUREMENTS OF THERMAL RADIATION
THROUGH DUST CLOUDS.

The University of Oklahoma, Ph.D., 1969
Engineering, mechanical

University Microfilms, Inc., Ann Arbor, Michigan

THE UNIVERSITY OF OKLAHOMA
GRADUATE COLLEGE

MEASUREMENTS OF THERMAL RADIATION
THROUGH DUST CLOUDS

A DISSERTATION
SUBMITTED TO THE GRADUATE FACULTY
in partial fulfillment of the requirements for the
degree of
DOCTOR OF PHILOSOPHY

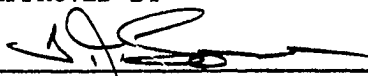
BY
WILLIAM A. MUNTER

Norman, Oklahoma

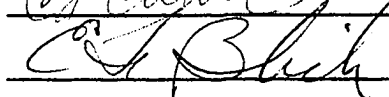
1969

MEASUREMENTS OF THERMAL RADIATION
THROUGH DUST CLOUDS

APPROVED BY



Darrel H. Harden



DISSERTATION COMMITTEE

ACKNOWLEDGEMENTS

The author wishes to acknowledge his indebtedness to Dr. Tom J. Love, Jr., whose guidance, patience and understanding made possible the success of the experimental investigation, and also to all members of the author's graduate committee, Dr. D.G. Hardin, Dr. E.F. Blick, Dr. C.P. Colver, and Dr. J.E. Francis.

A tribute must also be paid to those colleagues and employees at the University of Oklahoma, North Campus, for the many ideas, suggestions and aid which they brought to this problem. Specifically: Mr. E.F. Finch and Mr. M.J. Holland.

The author wants to express his appreciation to Mary Ann Parton for being patient and kind enough to translate his handwritten hieroglyphics into a legible typewritten dissertation.

Finally, the author wishes to thank his family, his wife Peggy, and daughter Paula, for their patience and support throughout this investigation.

ABSTRACT

Predicting and understanding the transfer of thermal radiation through a scattering, absorbing and emitting medium is important in many engineering calculations. A method of analysis for prediction of radiative heat transfer through isothermal media and media in radiative equilibrium with plane parallel geometry exists. Therefore it was necessary to develop an experimental method for evaluation of the computational analysis.

An apparatus was developed and an experimental investigation was undertaken for the determination of radiative flux through a scattering, absorbing and emitting medium bounded by two parallel and directly opposite walls.

To evaluate the experimental results obtained in a particle tunnel, a computational method for determination of the radiative flux through an isothermal media bounded by infinite plane parallel geometry was used. The application of this computational method was found to be acceptable for a wall spacing of 3.00 inches and a media composed of air and glass beads. The case of radiative equilibrium is also considered experimentally.

The data are presented in terms of a plot of the dimensionless radiative heat flux versus a dimensionless parameter defined as optical thickness.

Experimental results for the effect of convective heat transfer is considered and results are presented in graphic form for comparison.

TABLE OF CONTENTS

	Page
LIST OF TABLES	vii
LIST OF FIGURES	viii
LIST OF SYMBOLS	xi
 Chapter	
I. INTRODUCTION	1
II. EXPERIMENTAL APPARATUS	5
III. PARTICLE TUNNEL	26
IV. EXPERIMENTAL PROCEDURE	37
V. EXPERIMENTAL OBSERVATIONS AND RESULTS	41
VI. CONCLUSIONS	55
LIST OF REFERENCES	57
 APPENDICES	
I. A CLOUD OF DUST IN RADIATIVE EQUILIBRIUM	61
II. RADIATIVE HEAT TRANSFER BETWEEN PARALLEL WALLS	70
III. CALIBRATION OF HEAT FLOW METER	74
IV. CONVECTIVE HEAT TRANSFER COEFFICIENTS	78
V. GLASS BEADS	83
VI. DIMENSIONLESS RADIATIVE HEAT TRANSFER PARAMETERS	88
VII. SAMPLE DATA RECORDING	91
VIII. EXAMPLE CALCULATIONS	94
IX. EQUIPMENT	101

LIST OF TABLES

Table	Page
I. Comparison of Radiative Equilibrium Results	65
II. Dimensionless Parameters for Isotropic Scattering, Where Scattering to Extinction Ratio Equals 0.6	88
III. Dimensionless Parameters for Isotropic Scattering, Where Scattering to Extinction Ratio Equals 0.475	89
IV. Dimensionless Parameter for Radiative Equilibrium Case. .	90

LIST OF FIGURES

Figure		Page
1	Sketch of Hot Wall	6
2	Control Circuit for Center Heater	7
3	Control Circuit for Back Heater	8
4	Control Circuit for Border Heater	8
5	Exploded View of Cold Wall	11
6	Cutaway of Cold Wall	12
7	Labyrinth Water Channel	14
8	General Information for Test Section	16
9	Temperature Measuring Circuit Using Electromagnetic Galvanometer	17
10	Recording Circuit With Heat Flow Meter	18
11	Amplifier and Recording Circuit With Thermocouple	19
12	Amplifier and Recording Circuit for Photocell	20
13	Voltage Dividing Circuit With Photocell	21
14	Stream Thermocouple Probe	23
15	View of Instrumentation	25
16	Sketch of Dust Collector	28
17	Sketch of Dust Cloud Generator	31
18	View of Inlet Section	32
19	View of Dust Collector and Main Fan	33

Figure	Page
20	View of Dust Cloud Generator 34
21	View of Experimental Apparatus 35
22	View of Test Section 36
23	Dimensionless Temperature Profile 42
24	View of Test Section With Dust Cloud 43
25	Dimensionless Heat Flux Ratio Versus Optical Thickness 47
26	Dimensionless Heat Flux Ratio Versus Thring's Radiation Group 48
27	Mass Flow Versus Optical Thickness 51
28	Apparent Density Per Unit Depth Versus Optical Depth . . 52
29	Dimensionless Velocity Profile 54
30	Sketch of Overall System 62
31	Sketch of Original Data From Vacuum 67
32	Original Data Continued 68
33	View of Parallel Walls 69
34	Vacuum Data for Finite Parallel Walls 73
35	Calibration of Heat Flow Meter 76
36	Heat Flux Input Versus Hot Wall Surface Temperature . . 77
37	Force Convection Heat Transfer Data 81
38	Free Convection Heat Transfer Data 82
39	Variation of σ/β With Wave Length 84
40	Variation of Mass Extinction With Wave Length 85
41	Photomicrographs of Corning Beads 86
42	Photomicrographs of Kenco Beads 87

Figure		Page
43	Sample Data Recording From Tunnel	92
44	Sample Data Recording From Tunnel	93

LIST OF SYMBOLS

A	= area (ft ²)
C _p	= specific heat (BTU lb ⁻¹ °F ⁻¹)
Gr	= Grashof number
M	= dimensionless parameter
\dot{m}	= mass flow (lb sec ⁻¹)
N	= dimensionless parameter
N _{th}	= Thring's radiation number
Nu	= Nusselt number
Pr	= Prandtl number
Q	= dimensionless parameter
q	= heat flux (BTU hr ⁻¹ ft ⁻²)
q(1), etc.	= heat flux input (BTU hr ⁻¹ ft ⁻²)
S	= wall spacing (ft)
T	= temperature (°R)
u, v	= velocity (ft sec ⁻¹)
x, y	= distance (ft)
β	= mass extinction coefficient (ft ² lb ⁻¹)
ε	= total hemispherical emittance
ρ	= mass density (lb ft ⁻³)
π	= 3.1416
σ	= mass scattering coefficient (lb ft ⁻³)

σ = Stefan-Boltzman constant (BTU ft⁻² °R⁻¹)

τ = optical depth

subscript

cw = cold wall

hw = hot wall

m = mean value

max = maximum value

1 = refer to surface 1

2 = refer to surface 2

∞ = free stream

MEASUREMENTS OF THERMAL RADIATION
THROUGH DUST CLOUDS

CHAPTER I

INTRODUCTION

Engineering interest in high speed atmospheric flight, high energy sources, and space flight have stimulated the study of radiative heat transfer through clouds of particles which emit, scatter and absorb radiant energy. Specific examples of the transmission of radiant energy through a scattering media are the cases of an ablative material in the boundary layer of a nose cone during re-entry and of particles in the exhaust gas of a rocket engine.

This experimental study is primarily concerned with the transfer of thermal radiation through a plane parallel emitting, scattering and absorbing dust cloud, where the dust clouds are composed of mixtures of air and solid particles, bounded by diffusely emitting and reflecting surfaces at different temperatures.

Love (1)*, (2) proposed an analysis for considering the radiant energy exchange in various media. The equation for the transfer of radiant energy is presented for analyzing the problem of an isothermal plane parallel cloud of particles which emit, scatter and

*Number in parentheses refers to corresponding number in references.

absorb radiant energy. This cloud of particles is assumed to be bounded by diffusely reflecting and emitting infinite surfaces at different temperatures.

Hsia and Love (3) considered the problem of radiant energy exchange in a nonisothermal medium. The medium is assumed to be a cloud of particles which scatters radiant energy in an anisotropic fashion for plane parallel boundaries.

Love and Wheasler (4) and Love and Beattie (5) measured scattering functions experimentally for several different materials. Lee (6) utilized the experimental data presented by Love and Beattie (5) for determination of the dimensionless parameters developed by Love (2) for radiant heat transfer computations. Lee (6) transformed the data by numerical integration to obtain the dimensionless parameters. From this data Lee (6) concluded that the approximation of isotropic scattering was reasonable for radiant heat transfer calculations in most engineering situations.

Thermal radiation between finite parallel walls was considered by Love and Gilbert (7). The purpose of this experimental investigation was to determine how closely infinite plane parallel walls could be approximated by finite plane parallel walls. Schornhorst and Viskanta (8) experimentally investigated the validity and accuracy of simplified methods for computing radiant heat transfer.

Usiskin and Sparrow (9) present a numerical solution to the problem of thermal radiation between parallel plates separated by an absorbing-emitting nonisothermal gas. The Monte Carlo method has been applied to a similar problem by Howell and Perlmutter (10).

Transfer of thermal radiation often occurs simultaneously with other modes of heat transfer. Numerous literature has been recently published on simultaneous heat transfer problems specifically: Sparrow and Cess (11), Cess (12), and Pai (13) present a survey of this field of heat transfer.

The effects of gas-solid suspensions, or multiphase systems, on heat transfer from surfaces and flow properties is discussed by Soo (14). Brillier and Peskin (15) performed an experiment to determine the convective heat transfer coefficient to heated and cooled gas-solid suspensions.

The preceding discussion presents some of the more pertinent literature on radiative heat transfer, combined heat transfer, and heat transfer to multiphase systems. In the field of experimental work, most investigations considered only the steady state transfer of thermal radiation between simple configurations without an intervening media.

This experimental study has been subdivided into three basic parts:

I. An experimental determination of the change in net thermal radiation due to an absorbing, emitting, and scattering media.

II. An experimental measurement of thermal radiation through a dust cloud in radiative equilibrium.

III. Determination of forced convection heat transfer coefficients.

The consideration of Part I is paramount in this investigation and is presented in the main part of the test. Whereas, the other

parts are presented in the appendices.

The experimental measurements were performed for a system of plane parallel walls separated by a cloud of particles. For the isothermal case this was performed in air in order that the dust cloud could be forced between the parallel walls at a controlled speed. In the case of radiative equilibrium the experiment was performed in a vacuum chamber and the dust cloud passed through the system with a speed determined by the acceleration of gravity.

The solid particles used for the dust cloud were glass beads, which had a diameter on the order of 100 microns. In previous experimentation with solid aerosols it had been found that the characteristics of glass beads were ideally suited for this type of situation. Glass beads proved to be readily available as they have a considerable number of industrial applications and could be purchased in a variety of different sizes locally. Another important factor in selecting glass beads was the experimental data of Love and Beattie (5) because Lee (6) concluded from this data that isotropic scattering data may be used to represent anisotropic scattering with good accuracy for the plane parallel cloud case.

The properties of glass beads in a vacuum chamber, for the radiative equilibrium case, showed superior characteristics as compared to other materials tested.

CHAPTER II

EXPERIMENTAL APPARATUS

In order to obtain measurements of radiative energy transfer between parallel walls separated by an isothermal cloud of dust an experimental apparatus had to be constructed. This apparatus consisted of a particle tunnel with an integral heat transfer section and a secondary system for generating clouds of dust. Located inside the test section of the particle tunnel was the heat transfer apparatus where one wall serves as a heater and has a guarded heater section at the center. The opposite wall is cooled by circulating water through an internally located water channel. A detailed description of the heat transfer section and instrumentation used in this study follows. The particle tunnel description is given in the next chapter.

The heater consisted of three zones: border, back, and center, which were controlled by means of a variable auto transformer, see figure 1. In figures 2, 3, and 4 the heater circuits are displayed along with their measuring circuits.

A primary requirement of the heater and its controls was the consideration of thermal inertia. This criteria was important in determining the time required to attain a desired temperature and the thermal stability to maintain this temperature. Because of this property of the heater, stainless steel was utilized in construction of the

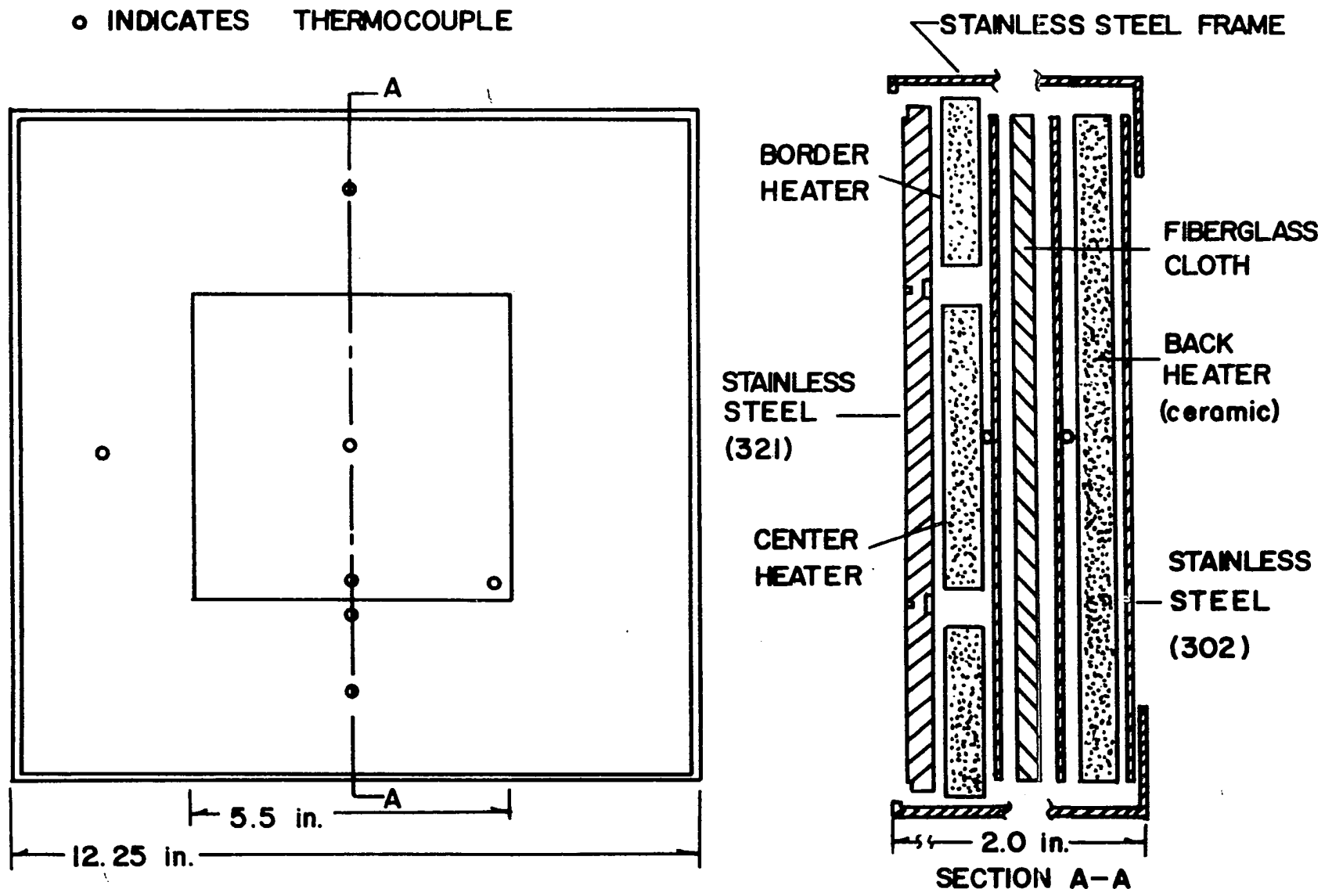


FIGURE I. SKETCH OF HOT WALL

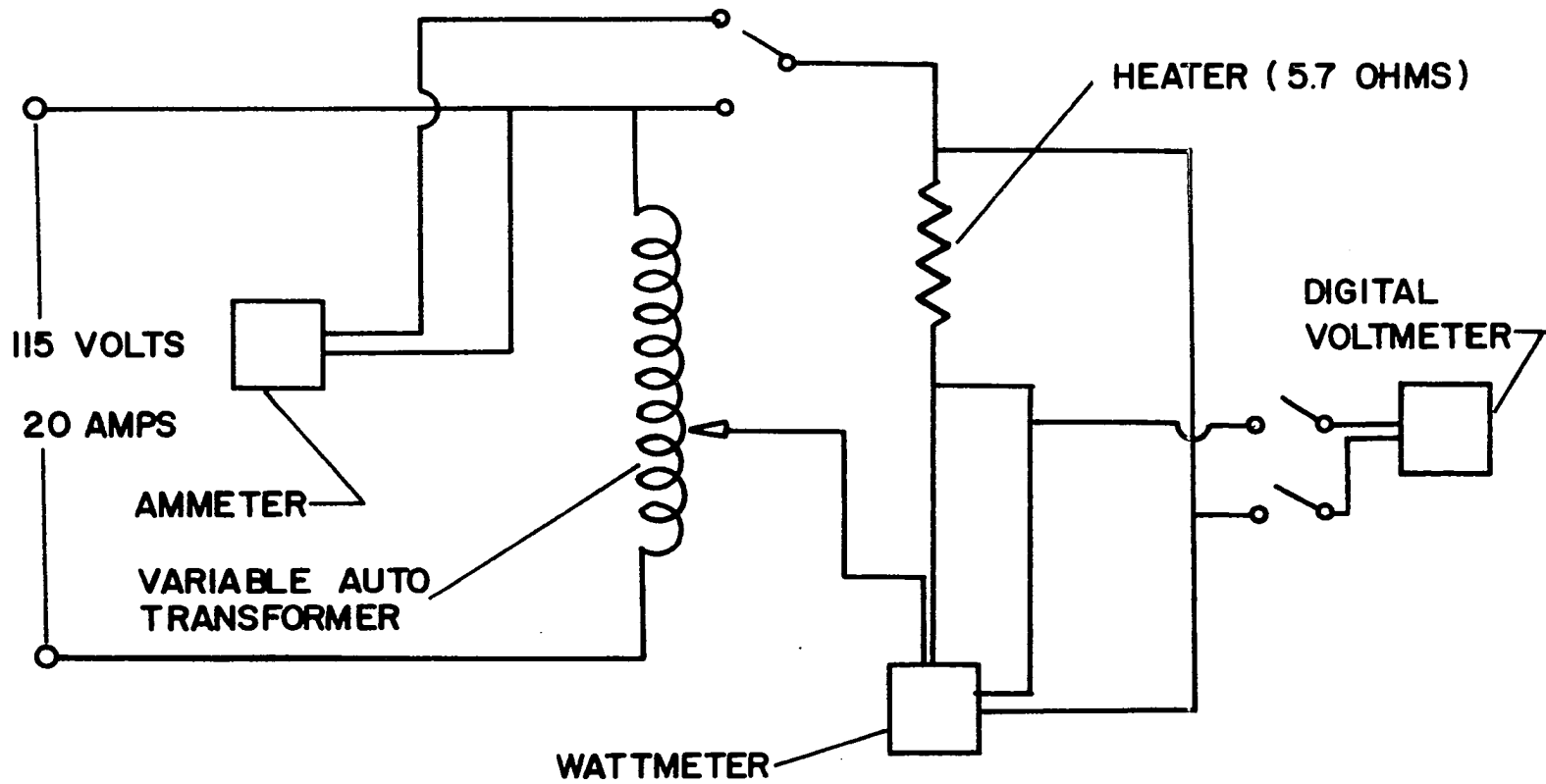


FIGURE 2. CONTROL CIRCUIT FOR CENTER HEATER

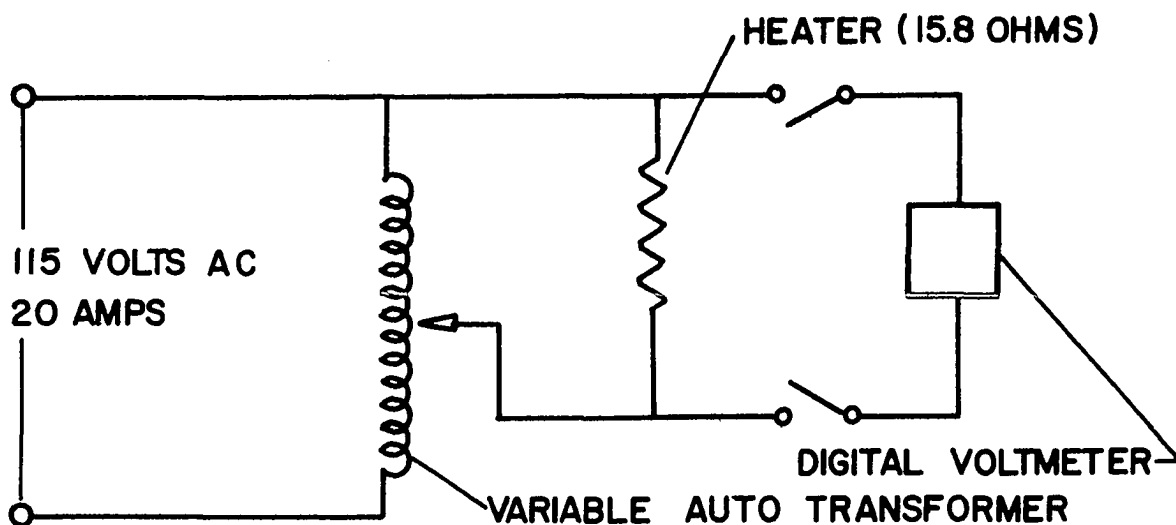


FIGURE 3. CONTROL CIRCUIT FOR BACK HEATER

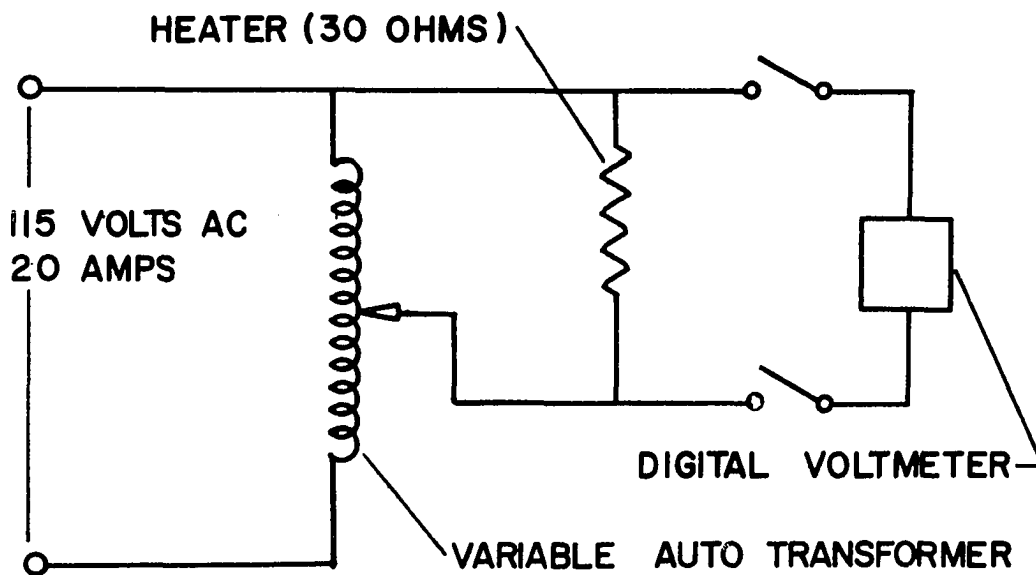


FIGURE 4. CONTROL CIRCUIT FOR BORDER HEATER

heater components since its poor thermal conductivity does not permit the dissipation of energy readily.

The purpose of the three heater zones was to create a thermal environment such that the energy being dissipated in the center heater could be assumed to be transmitted perpendicularly to the heater face with a minimum of edge or back losses. The reduction of energy losses through the back of the heater was minimized with the back heater. Whereas the border heater restricted the energy losses from the sides of the center heater. An attempt to isolate the center section was made by machining a border around the center section. Gilbo (16) employed a heater of similar design as did Gilbert (7).

Hot wall temperature measurements were taken with chromel-alumel thermocouples, 24 gauge, fastened to the inside of the stainless steel face by means of an electric discharge welder using 40-watt-seconds and on either side of the insulation separating the back heater from the border and the center heater. Also, a pair of thermocouples were used to regulate the electrical power to the border and center heaters to minimize edge losses from the center heater.

The hot wall face thermocouples were covered with 0.002 inch stainless steel, type 302, after being fastened to the inside of the face. This very thin stainless steel was placed over the thermocouple and then welded to the hot wall with an electric discharge welder. The possibility of the thermocouple shorting to the heater coil was minimized by this type of installation. This technique is widely employed in the instrumentation of engines to protect wires.

The resistance of the three heaters, shown in figures 2, 3,

and 4, was a function of the diameter and length of the heater wire. Therefore, it was necessary to increase the line voltage in order to increase the current load, which generated the thermal energy, for a fixed resistance. The border heater required 120 volts at its peak setting. Therefore, the overall performance was limited by the line voltage capacity.

The opposite wall, referred to as the cold wall, provided the heat transfer section with a heat sink. Figure 5 presents an exploded section of the cold wall.

The cold wall was constructed with the purpose in mind that it would be used for measuring unsteady state radiant heat transfer. The changes in thermal energy due to the intervening media were measured with a multi-junction thermopile located in the cold wall. Figure 5 shows the position of the thermopile in the cold wall.

The thermocouples for the thermopile were constructed by electroplating copper on 30 gauge constantan wires. This was accomplished by wrapping the 30 gauge constantan wire over a cylinder whose circumference was equal to the thermopile circumference and placing in an electrolyte. The level of the electrolyte on the cylinder determines the line of the junctions. This type of thermopile is possible only because the electrical resistance of the constantan wires is so much greater than the copper plating on one-half of the coil of wire, that the constantan wire is essentially shunted over that length. See (17), (18), (19), (20), and (21) for a more complete discussion of thermopiles. After plating the series thermocouples were removed from the cylinder and prepared for installation on an aluminum core. But,

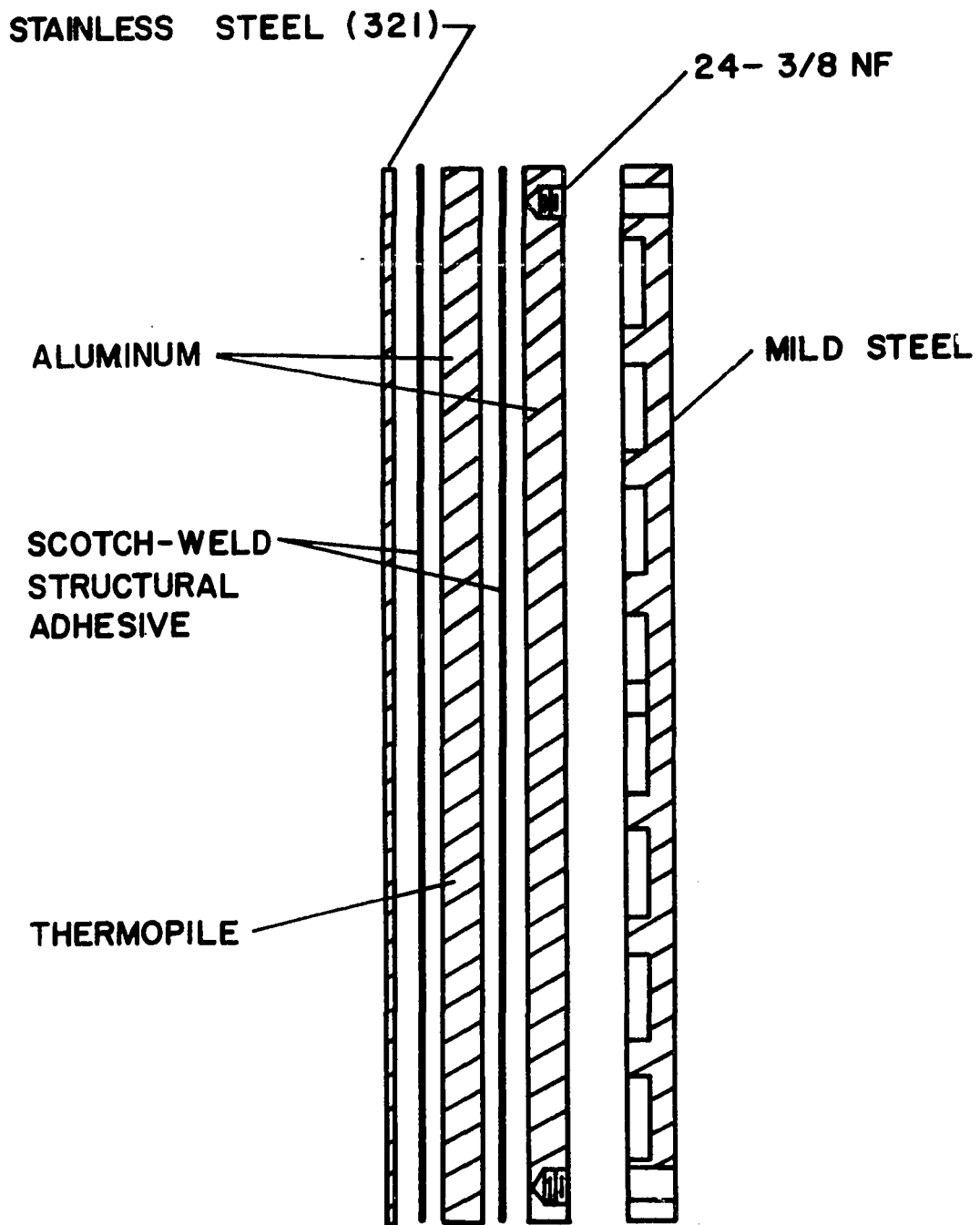


FIGURE 5. EXPLODED VIEW OF COLD WALL

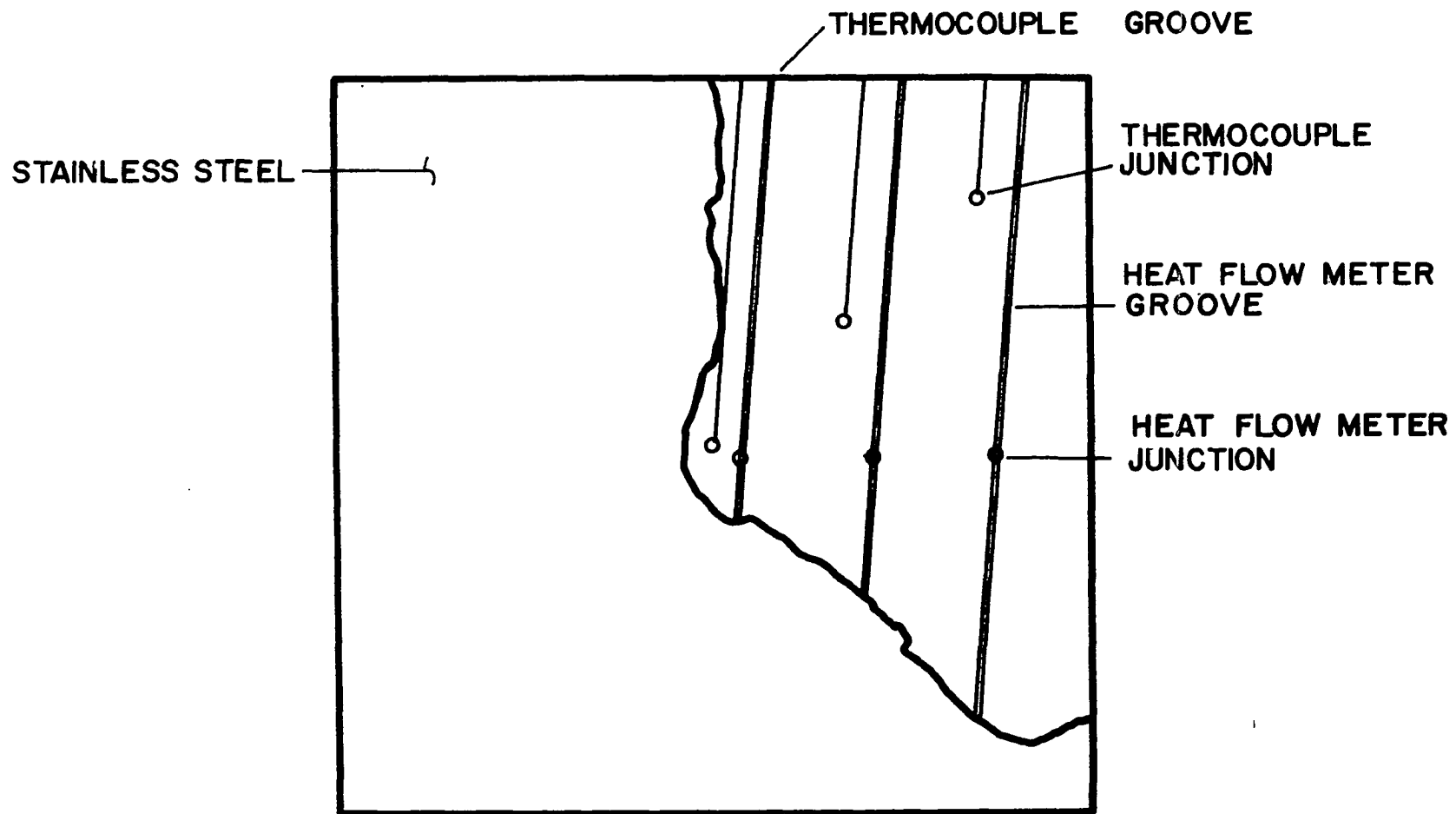


FIGURE 6. CUTAWAY OF COLD WALL

first they had to be insulated electrically from each other to prevent shorting of the thermopile. This was accomplished by covering the thermocouples with teflon tubing, the wire was threaded through a continuous section of teflon tubing.

The installation involved winding the series thermocouples over the aluminum frame and making sure the copper-constantan interface was in the center. A cutaway of the cold wall showing location of the thermopile junction is shown in figure 5.

Stainless steel, type 321, 0.020 inches thick was bonded to one face of the thermopile with Scotch-Weld structural adhesive, type AF-110. Scotch-Weld, AF-110, is a non-volatile thermosetting film adhesive for use in the bonding of metals. This adhesive was used in bonding the stainless steel face to the thermopile because of its high bond strength. Also, its thermal resistance was low as a result of its compression to only a few thousandths of an inch. Surface preparation of the two faces to be bonded consisted of sandblasting them with a 60 mesh fused aluminum oxide grit. This was followed by submerging the surfaces in an acetone bath repeatedly until clean. Next, the surface with the adhesive was placed in a press where a contact pressure of 10 pounds per square inch was applied while the platlets of the press were heated to 350°F.

By employing the same techniques discussed above for bonding, the thermopile was then bonded to a 0.500 inch aluminum plate. This aluminum plate would also serve as the cover plate for the water channel. The water channel was joined to the aluminum spacer plate by 24-3/8NF Bolts. A silicone rubber gasket was used to seal between

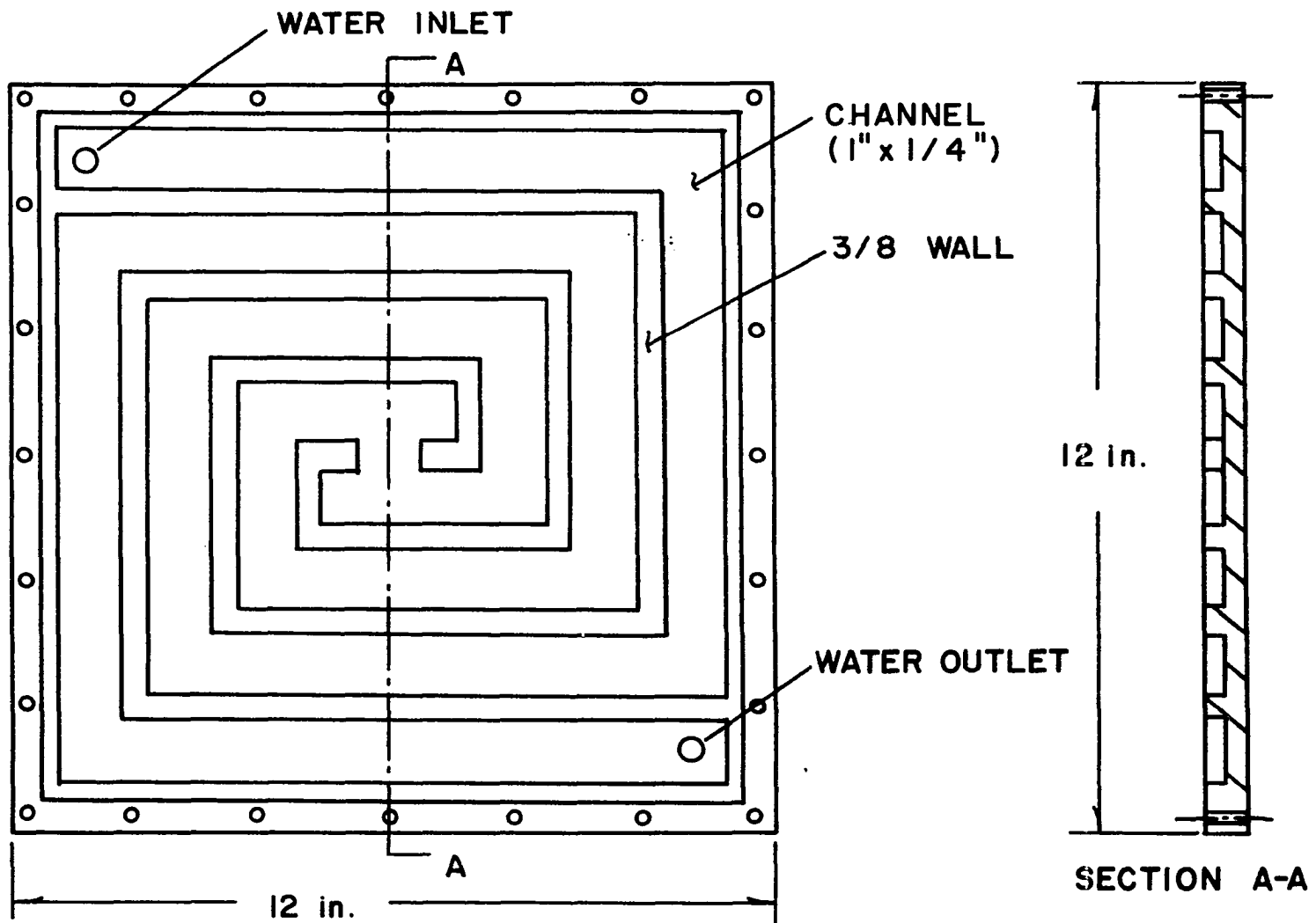


FIGURE 7. LABYRINTH WATER CHANNEL

the aluminum cover plate and the water channel. Figure 5 presents an exploded view of the cold wall and figure 7 shows the details of the labyrinth water channel.

Thermocouples were silver soldered to the stainless steel cold wall face, on the back side facing the thermopile, prior to bonding to the thermopile. This type of construction was necessary to have a smooth surface free of wires. Copper-constantan were used on the cold wall because of the lower temperatures and their ability to solder.

Preparation of the exposed surfaces, hot and cold wall faces, was identical to that discussed by Gilbert (7). The surfaces were sandblasted to obtain a diffuse surface and the determination of the emittance of the surface could be obtained from the literature.

All temperature measurements were taken by means of a Leeds and Northrup Model 8686 millivolt potentiometer, which was connected to a Leeds and Northrup Model 8248-16 rotary selector switch. The rotary selector switch used solid silver contacts with durable silver alloy brushes to reduce errors in the EMF readings due to contact resistance. Copper leads were used to connect the rotatory switch to the thermocouple wires. These connections were carried out in heavy metal boxes to insure the connections were both thermally and electrically insulated from the surroundings.

Temperatures of the hot wall and cold wall were monitored on a Honeywell 906C Visicorder Oscillograph during operation of the secondary air stream with particles. Two basic circuits were used to display the thermocouple signals on the oscillograph. First, the most sensitive circuit used a Hewlett-Packard differential amplifier, model 8875A,

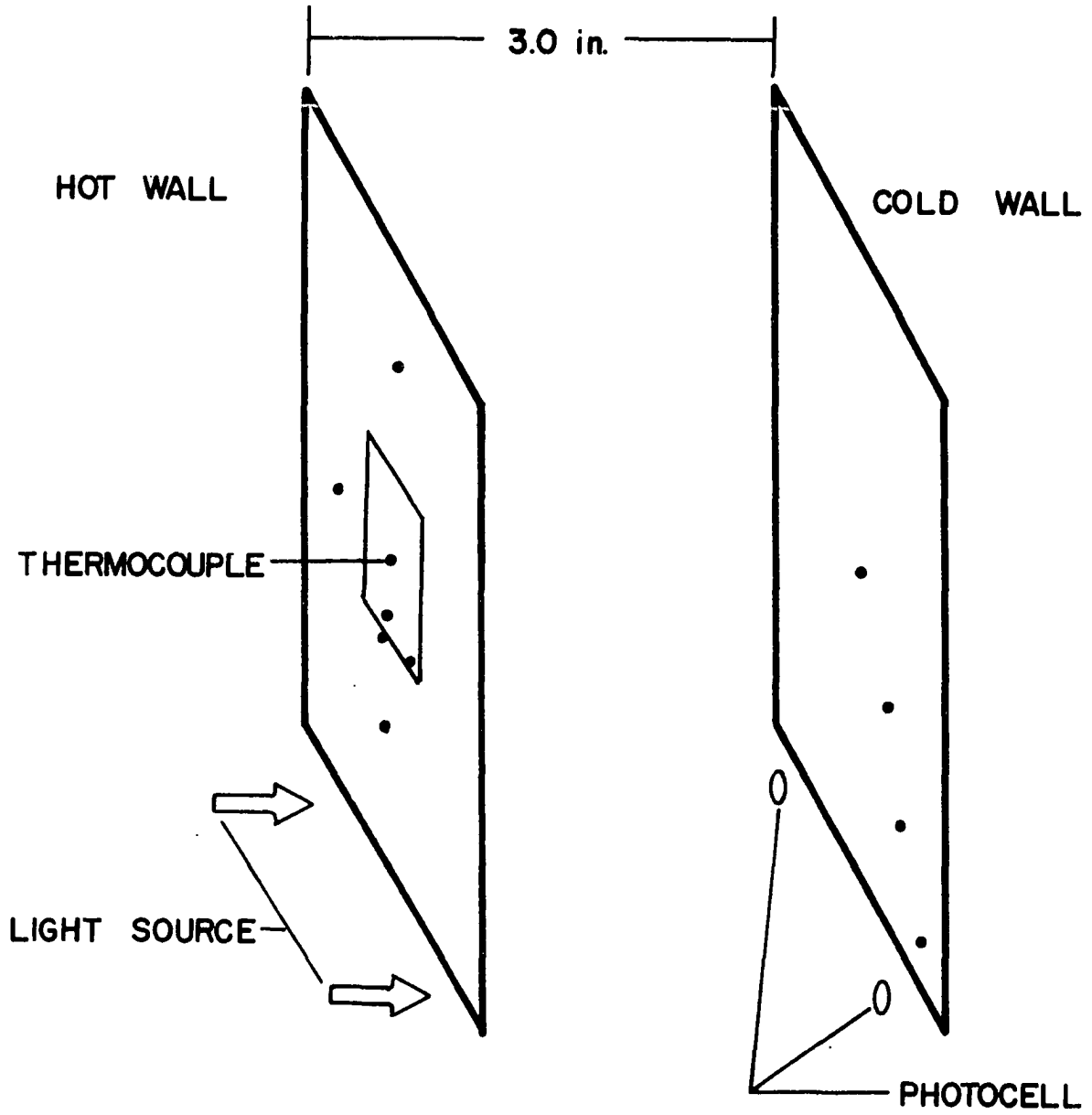


FIGURE 8. GENERAL INFORMATION FOR TEST SECTION

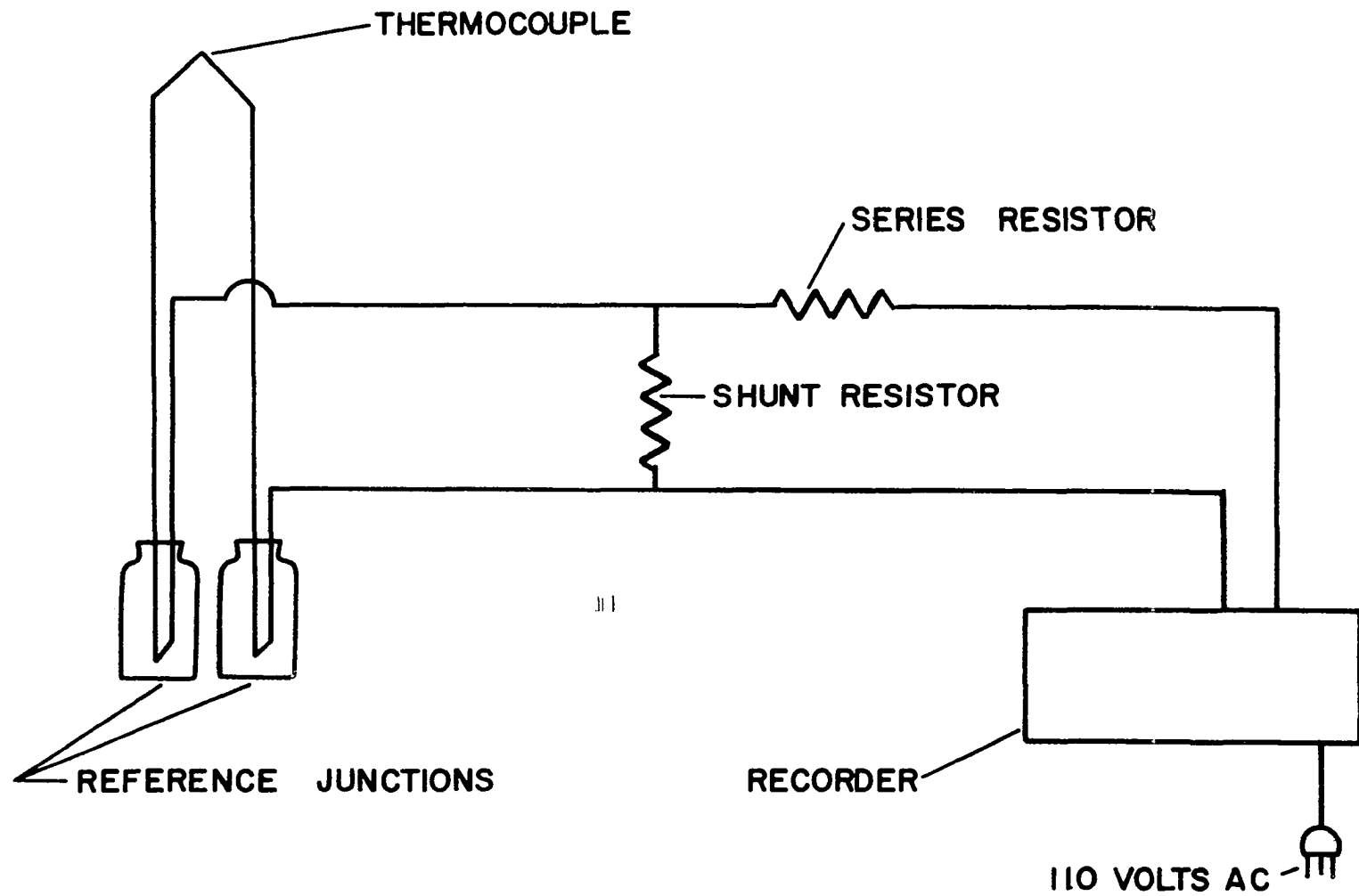


FIGURE 9. TEMPERATURE MEASURING CIRCUIT USING ELECTROMAGNETIC GALVANOMETER

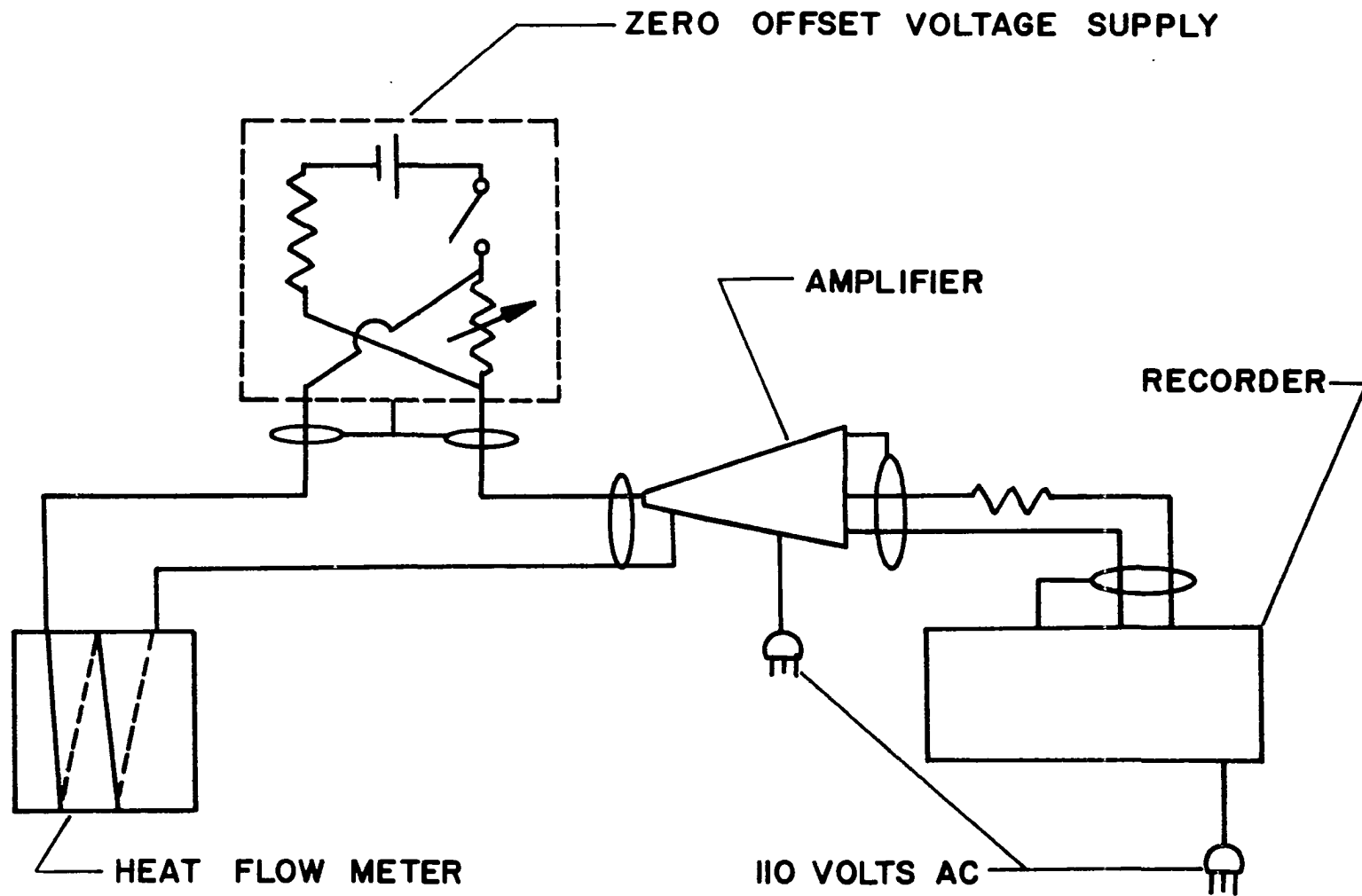


FIGURE 10. RECORDING CIRCUIT WITH HEAT FLOW METER

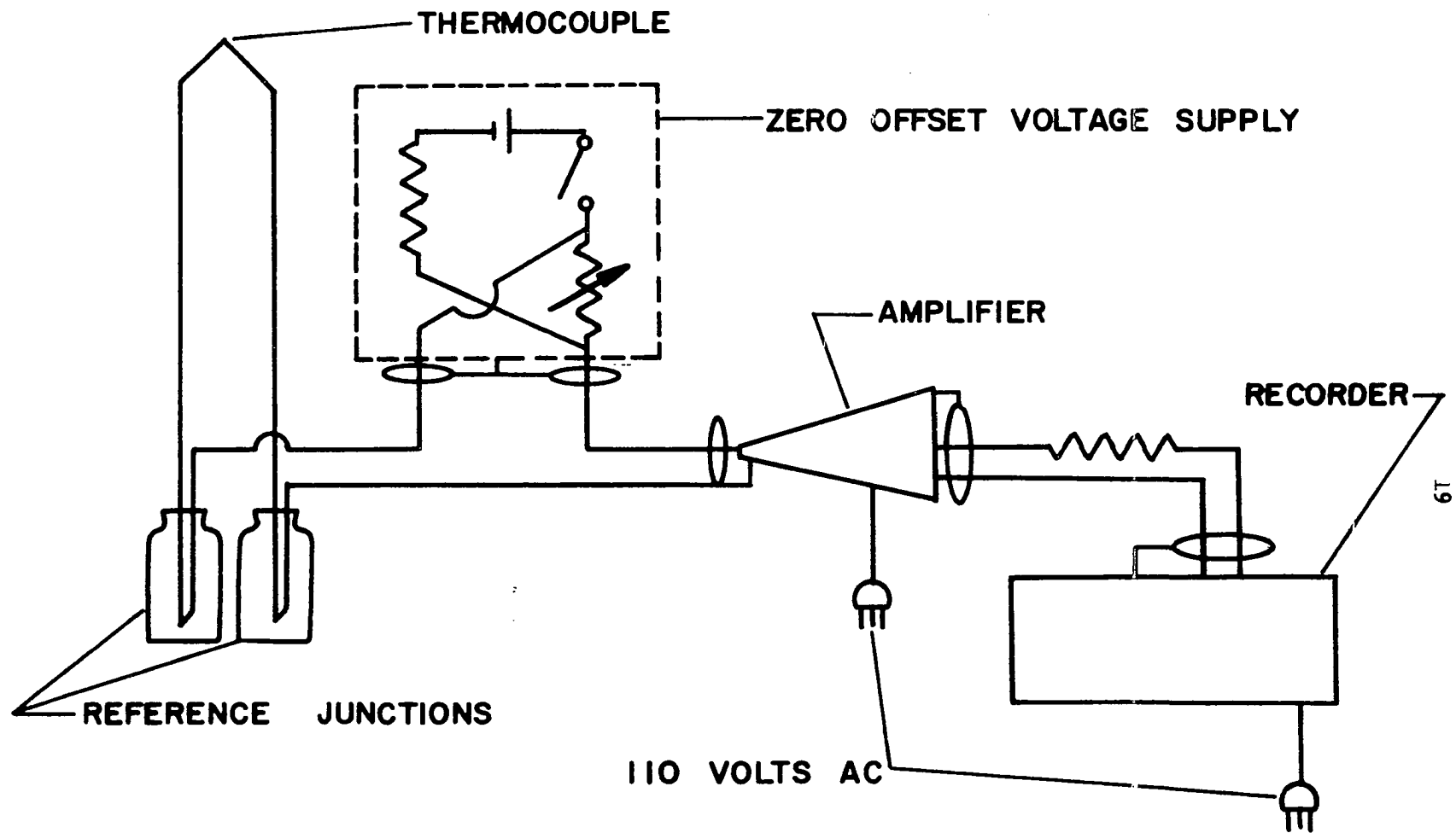


FIGURE 11. AMPLIFIER AND RECORDING CIRCUIT WITH THERMOCOUPE

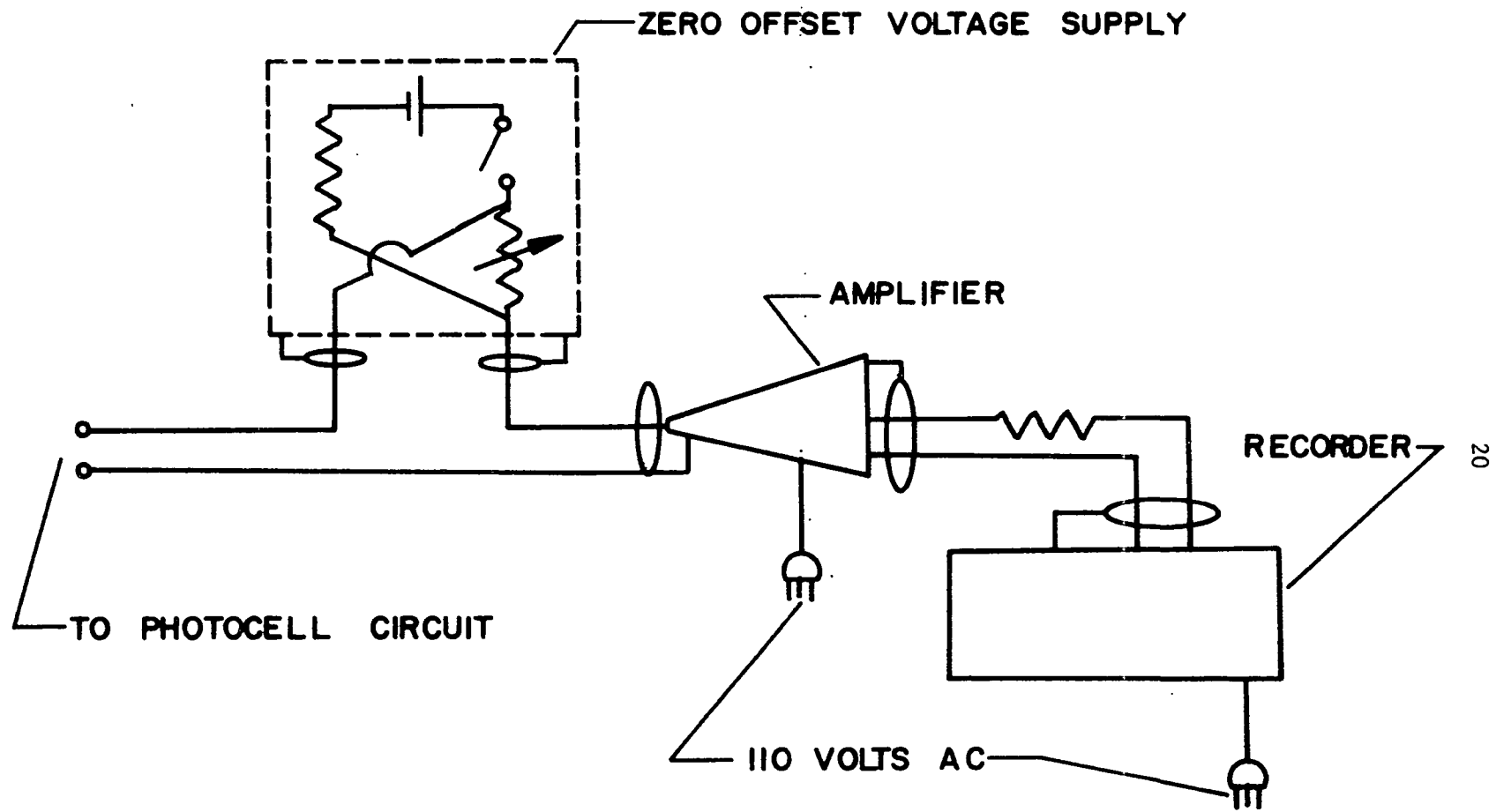


FIGURE 12. AMPLIFIER AND RECORDING CIRCUIT FOR PHOTOCELL

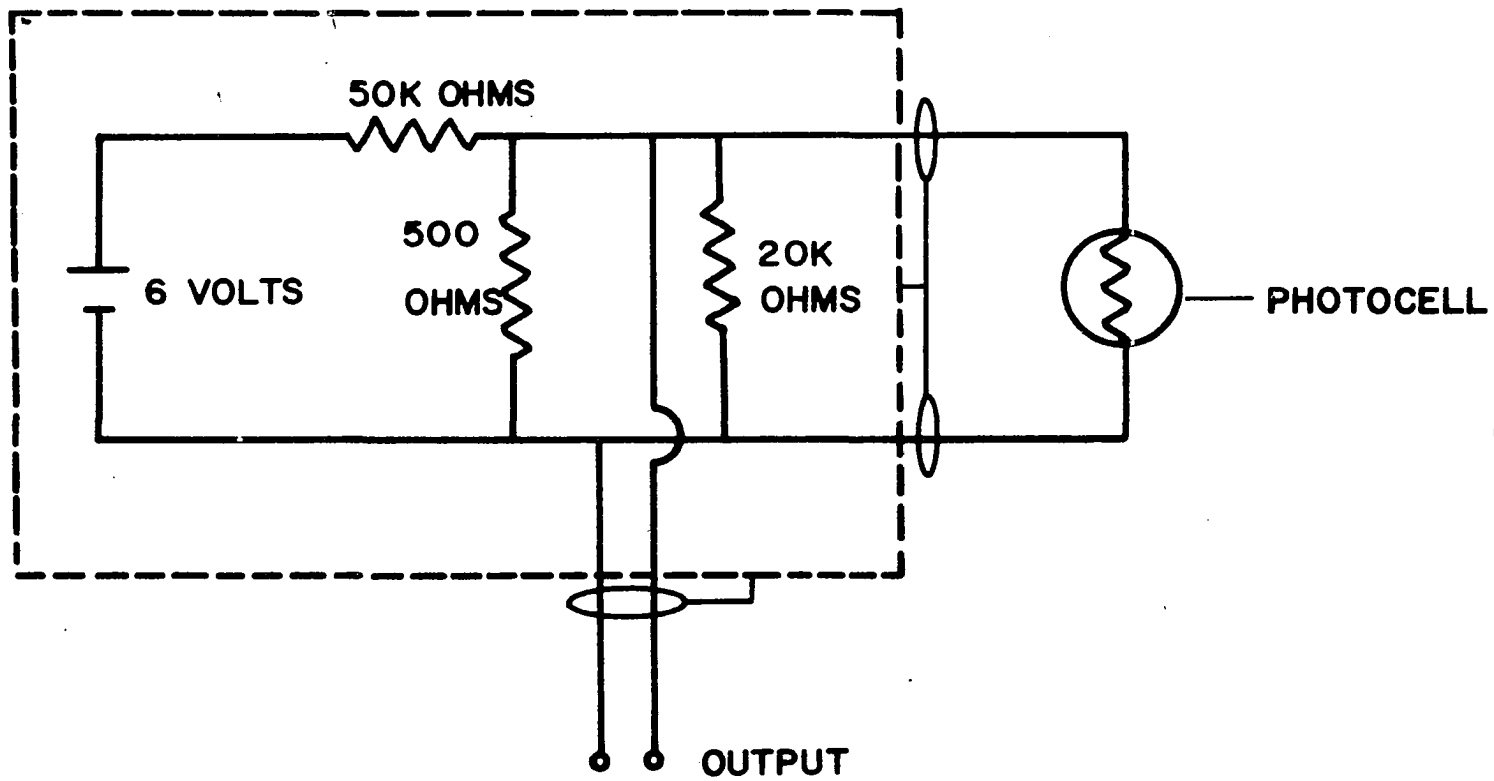


FIGURE 13. VOLTAGE DIVIDING CIRCUIT WITH PHOTOCELL

to amplify the signal in combination with a M1650 fluid damped galvanometer, figure 11. Also, a 50 millivolt voltage source was connected in the thermocouple circuit to provide a zero offset. This permitted use of the maximum gain of the amplifiers without damage to the galvanometers. Figure 11 gives a wiring diagram for the above described circuit. In the second circuit the thermocouple was wired directly to a M40-350A Honeywell electro-magnetic damped galvanometer, see figure 9.

Air stream temperature measurements were taken with a copper-constantan stream thermocouple. An open end "T" shaped metal shield over the measuring junction reduced the effect of radiant heat transfer between test section walls and the thermocouple. A sketch of this thermocouple is presented in figure 14. The output from this thermocouple was recorded with a circuit similar to the first type discussed previously.

Optical depth of the cloud was monitored by using a Clairex CL-5M CdSe fast switching photocell in a voltage dividing circuit, which is shown in figure 13. The photocell was activated by means of general electric 40 watt lamp, appliance type, located outside the test section on the hot wall side and the voltage supply was varied by means of a variac for calibration purpose. This particular type of appliance bulb is designed for high temperature operation, such as ovens. The voltage drop across the photocell, which is dependent upon resistance, was amplified by means of a Hewlett-Packard differential amplifier, model 8875A; the signal was then displayed on a Honeywell 906C Visicorder Oscillograph, which was equipped with a fluid damped galvanometer, type M1650, for this particular channel. Figures 12 and 13 show the wiring

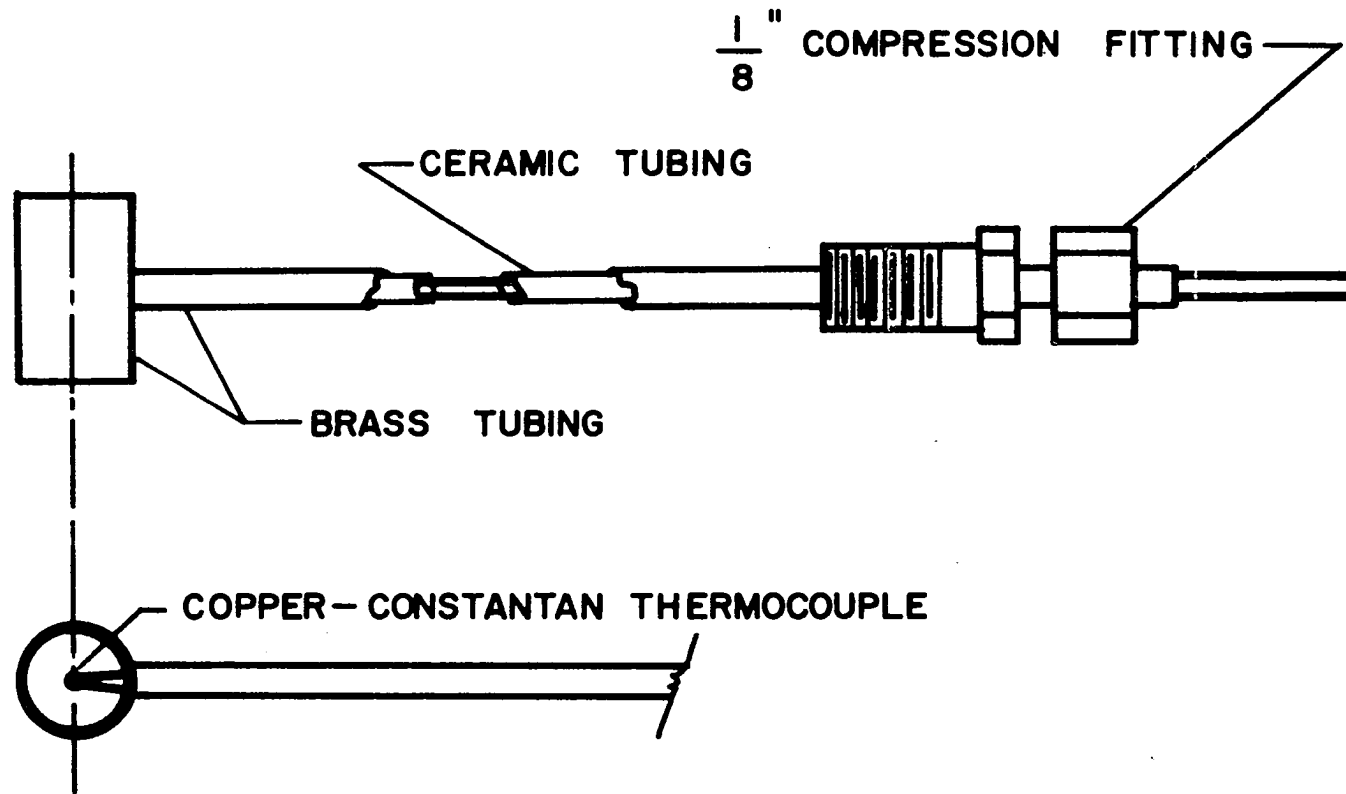


FIGURE 14. STREAM THERMOCOUPLE PROBE

diagram required for the above sensing and recording instruments. Location of the photocells is shown in figure 8, two are shown in this illustration but during some data runs only one was used do to the limited number of recording channels.

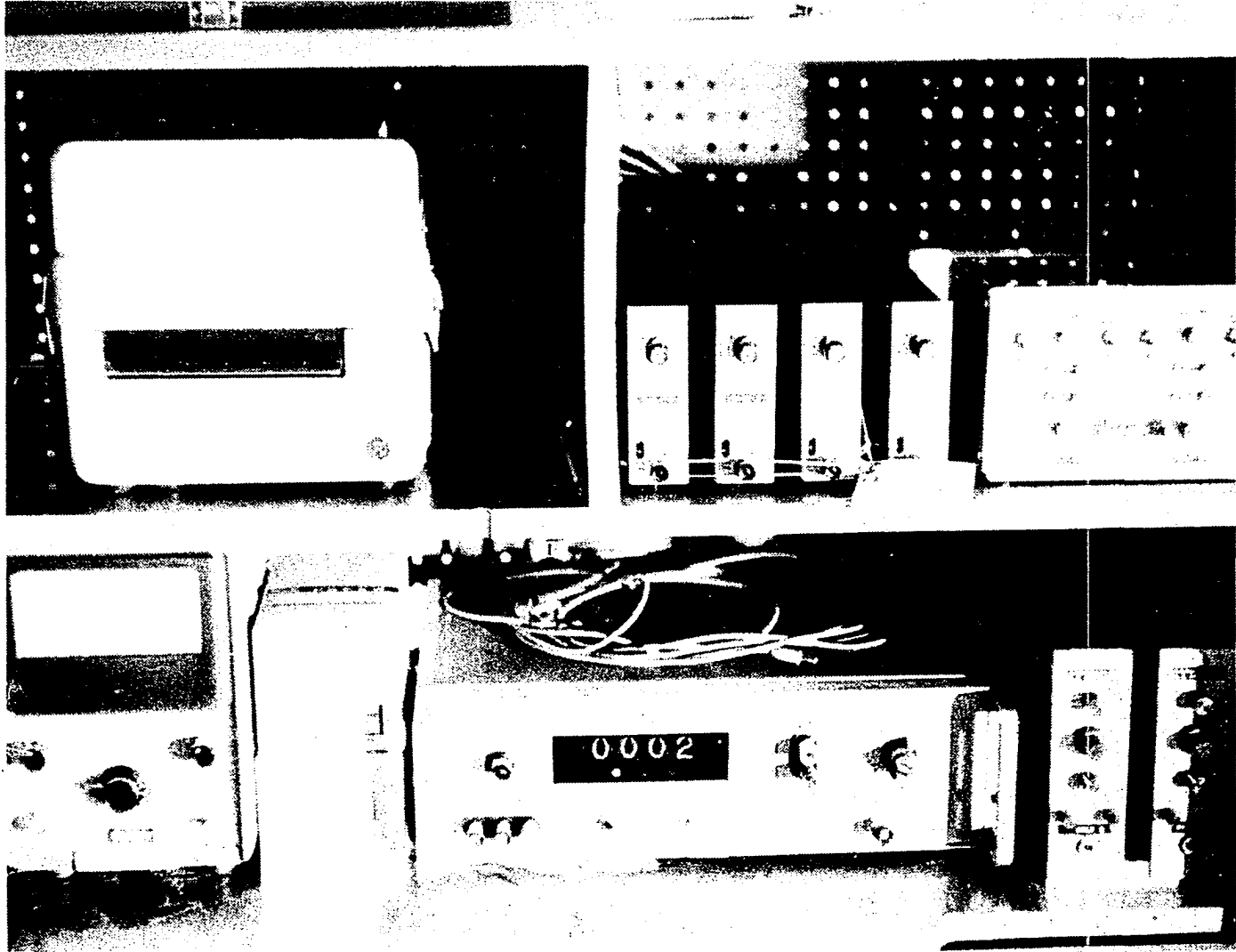


FIGURE 15. VIEW OF INSTRUMENTATION

CHAPTER III

PARTICLE TUNNEL

Upon formulation of the experimental testing to be performed an investigation was initiated for a suitable tunnel design. From previous experimentation and available literature it was determined that the test section dimensions would have to be 3.0 inches x 13.0 inches. Also, it was desirable to utilize existing apparatus wherever possible to minimize construction and development time.

Since, the test section dimensions were established the remaining portions of the tunnel could be designed. Streeter (22) states that the contraction ratio, ratio of the inlet cross sectional area to the cross sectional area of test section, should never be less than 10.0. Hence a conservative number of 11.0 was used for the contraction ratio. Also, Lawrence (23) suggests an entrance cone angle of 15.0 degrees is considered adequate for most designs. Again a conservative number was utilized based on available space, 12.5 degrees. Preceding the entrance cone a parallel-flow section, settling length, was designed according to Streeter (22). He suggests a settling length of 500 mesh lengths is usually sufficient, where mesh lengths refers to damping screens used to cover the inlet area for reducing the intensity of incident turbulence. For most suitable screens this would yield a settling length of approximately 36.0 inches. The use of damping screens is discussed by

Dryden and Schubauer (24). This concluded the design of the inlet section, up to the test section.

Pope and Harper (25) and Pankhurst and Holder (26) suggest the exit cone should expand at an angle of from 6.0 to 10.0 degrees, depending on available space. Again a conservative number was chosen, as the consideration of space was not paramount. But, in order to complete the design of the exit cone a fan had to be selected since the exit cone couples the test section to the fan.

A decision was made that the diameter of the fan be equal to or greater than the diagonal of the test section based on the cross-sectional area. A Clarage, type NH, fan was purchased from the Oklahoma State Surplus and rebuilt for use as the fan on the main air stream. The fan wheel diameter was 18.25 inches and the fan capacities were well above our expectations.

Completion of the exit cone was routine since the dimensions of the ends and the expansion angle had been specified.

The remaining sections of the particle tunnel were built considering those effects of the system on the fan's operation, which, in turn, have an important bearing on the operation of the system.

Proceeding the fan a vibration isolating section was added to prevent fan or motor vibrations from being transmitted along the tunnel walls to the test section. This section was constructed with a plastic coated canvas attached to two frames, these frames were then fastened to the tunnel and the fan housing. This flexible section functioned very successfully as a vibration isolator.

The fan used for the main air stream was as mentioned previously

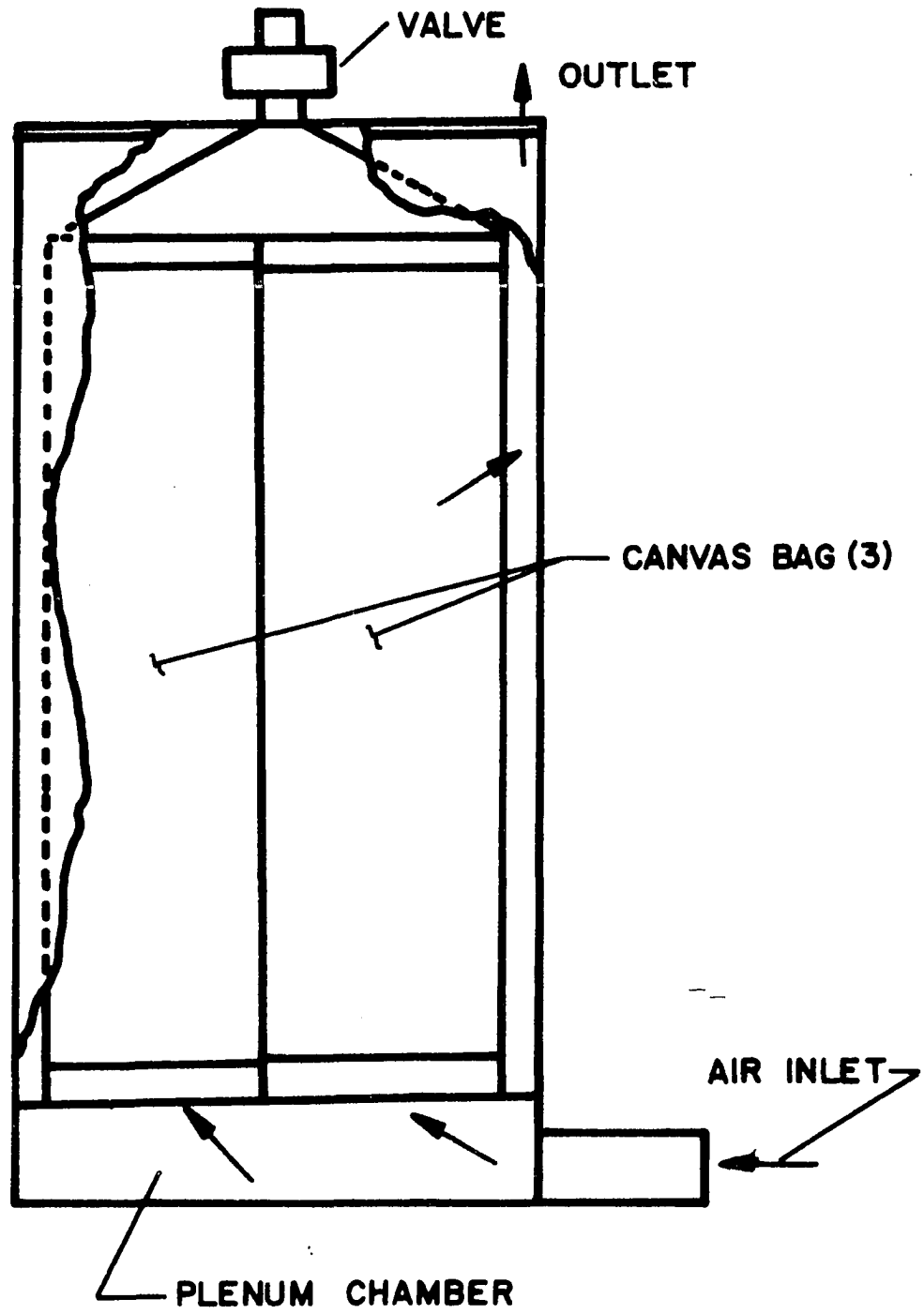


FIGURE 16. SKETCH OF DUST COLLECTOR

a Clarage fan, type NH, size 36 1/2. Power to drive the fan was supplied by means of a US Motor, 5 horsepower, coupled to a variable speed drive unit which was connected to the fan by three belts. Both the fan and power supply were mounted on an aluminum channel frame that was isolated from the floor with rubber pads to prevent walking and vibration. In addition an aircraft type tachometer was attached to the fan shaft to provide information on fan revolutions per minute.

On the outlet side of the fan, as the air was pulled through the tunnel, two large dust collectors were located. These dust collectors were of the bag type as illustrated in figure (16) and were donated by the Halliburton Company.

The secondary air stream which was used to supply the particles to the main air stream was driven by a New York fan, size 75 Junior fan, with a 1/3 horsepower motor. This particular type of fan had a cast aluminum forward curved wheel of spark resistant construction which proved to be the best suited for generating an aerosol (dust cloud). Silverman and Billings (27) suggested using this particular type of fan with one alteration. This alteration consisted of a rotating plate located in the fan and the action of centrifugal force plus the inward moving air causes the material, dust, to be carried out to the fan blades where it is dispersed.

Located above the center of the rotating plate was a hopper consisting of a tank and a mechanism to control the material feed rate. The hopper was constructed from a five gallon plastic bottle which was inverted and had the bottom removed. This bottle was then placed in an adjustable holder which permitted alignment and control of the height

above the rotating plate. The mechanism for control of the material flow consisted of a perforated tube with a moving cylinder inside to control the area of the opening. This mechanism was then pressed into the mouth of the plastic bottle as shown in figure 15. Richmond (28) and Dumbaugh (29) present a discussion of hopper designs.

The aerosol was ducted from the fan to the test section, which is shown in figure 17, where it was discharged at the top of the walls, equidistant from the hot and cold walls, into the main air stream.

The final section to be discussed is the test section. This particular section was constructed of welded 5/16 inch aluminum, whereas the other sections were constructed of galvanized sheet metal, to insure the rigidity of the test section. Also, the test section contained the hot and cold walls which were fastened to supports that were welded to the aluminum test section allowing removal without disassembling the test section. This particular type of arrangement permitted adjustment of the walls allowing them to be placed flush with the sides of the test section. Once the walls were in place they were sealed to the test section with silicone rubber, manufactured by Dow Corning. The test section also contain several ports which could be used for either pressure, static or dynamic, or temperature measurements. These ports were constructed with brass compression fittings. Also, four photocells were located in the walls to permit optical thickness measurements to be made. Finally, one of the narrow sides of the test section was fitted with a plexiglass window, which was removeable.

The final assembly of the above mentioned section is shown in figures 18, 19 and 20.

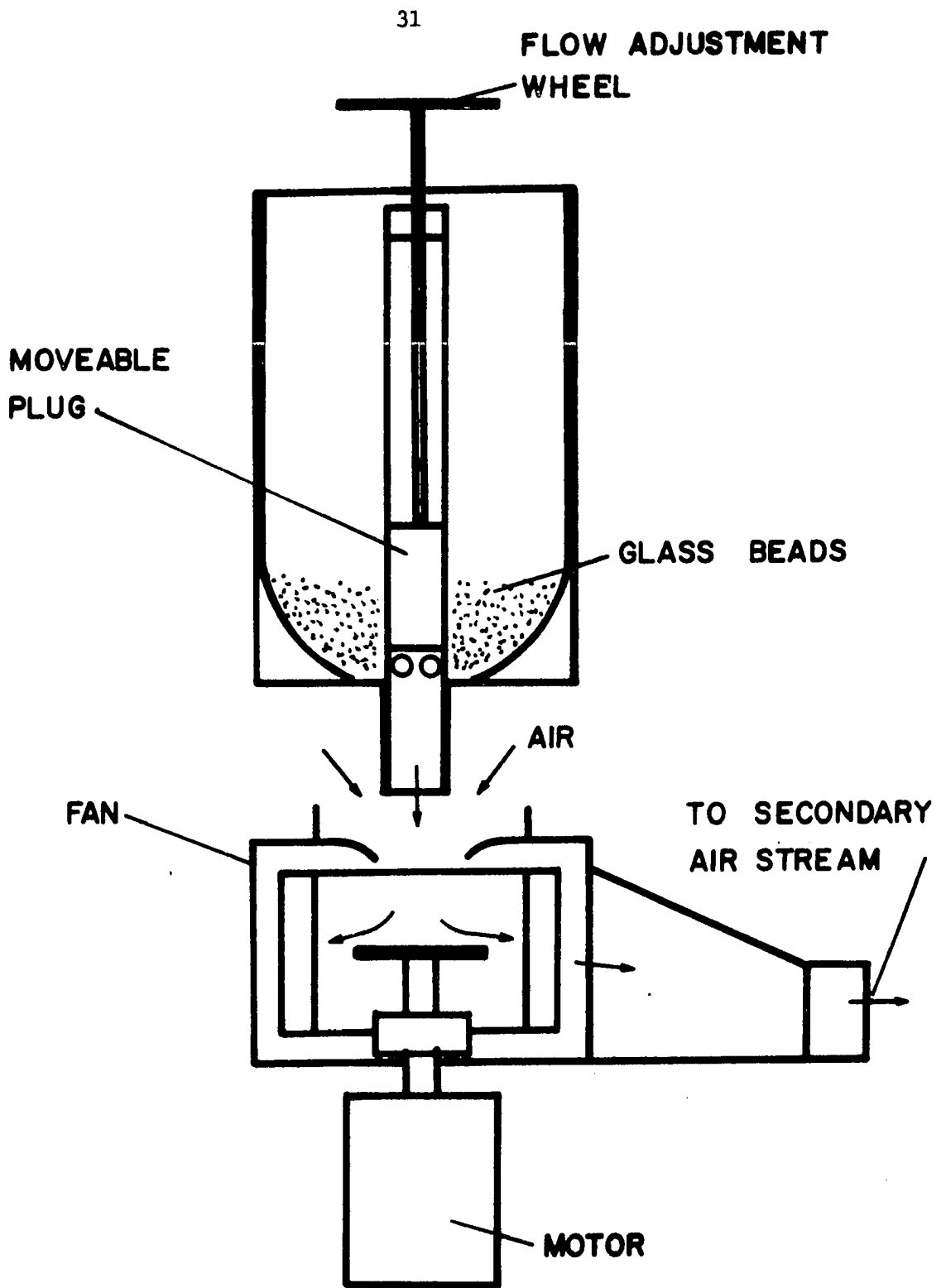


FIGURE 17. SKETCH OF DUST CLOUD GENERATOR

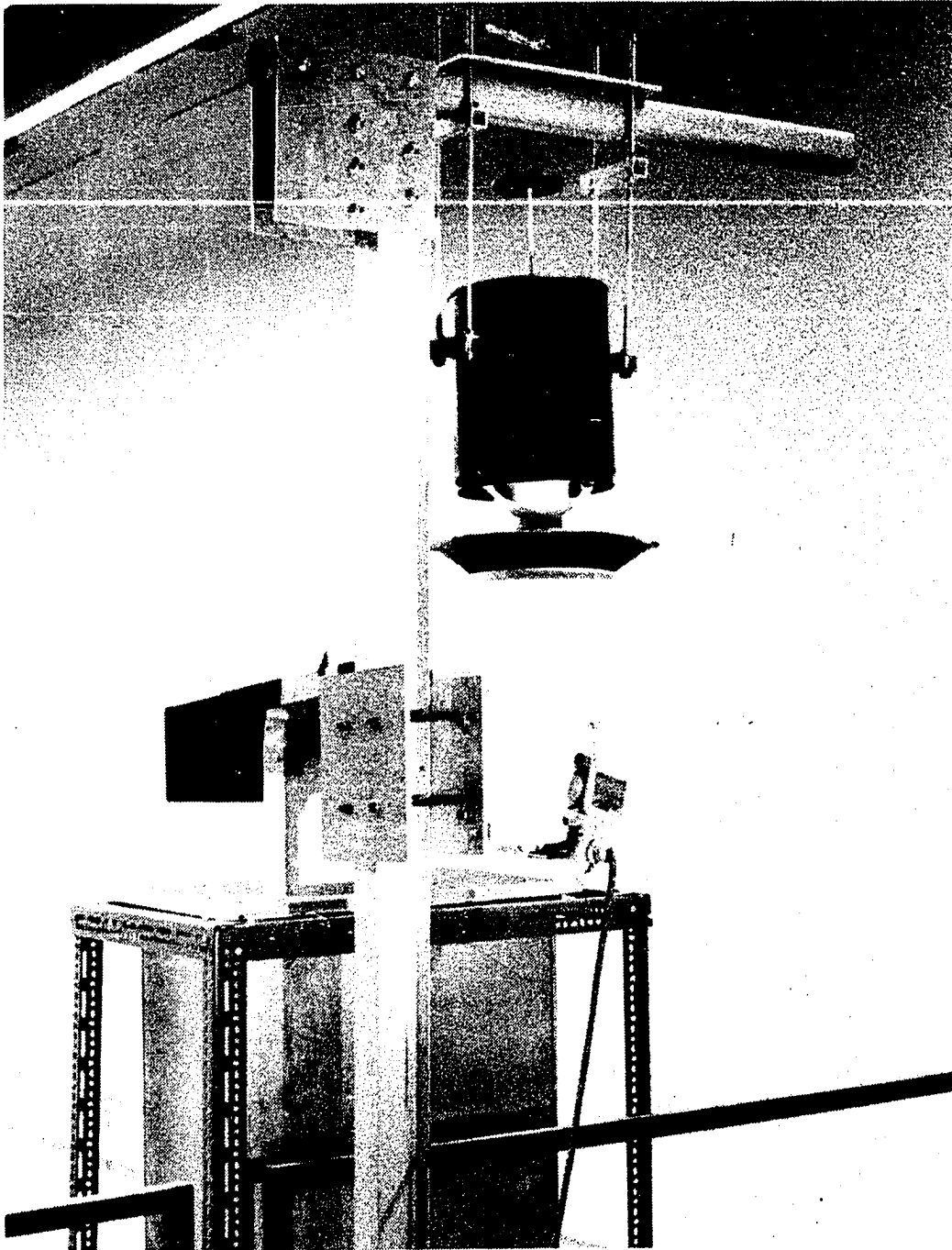


FIGURE 18. VIEW OF INLET SECTION

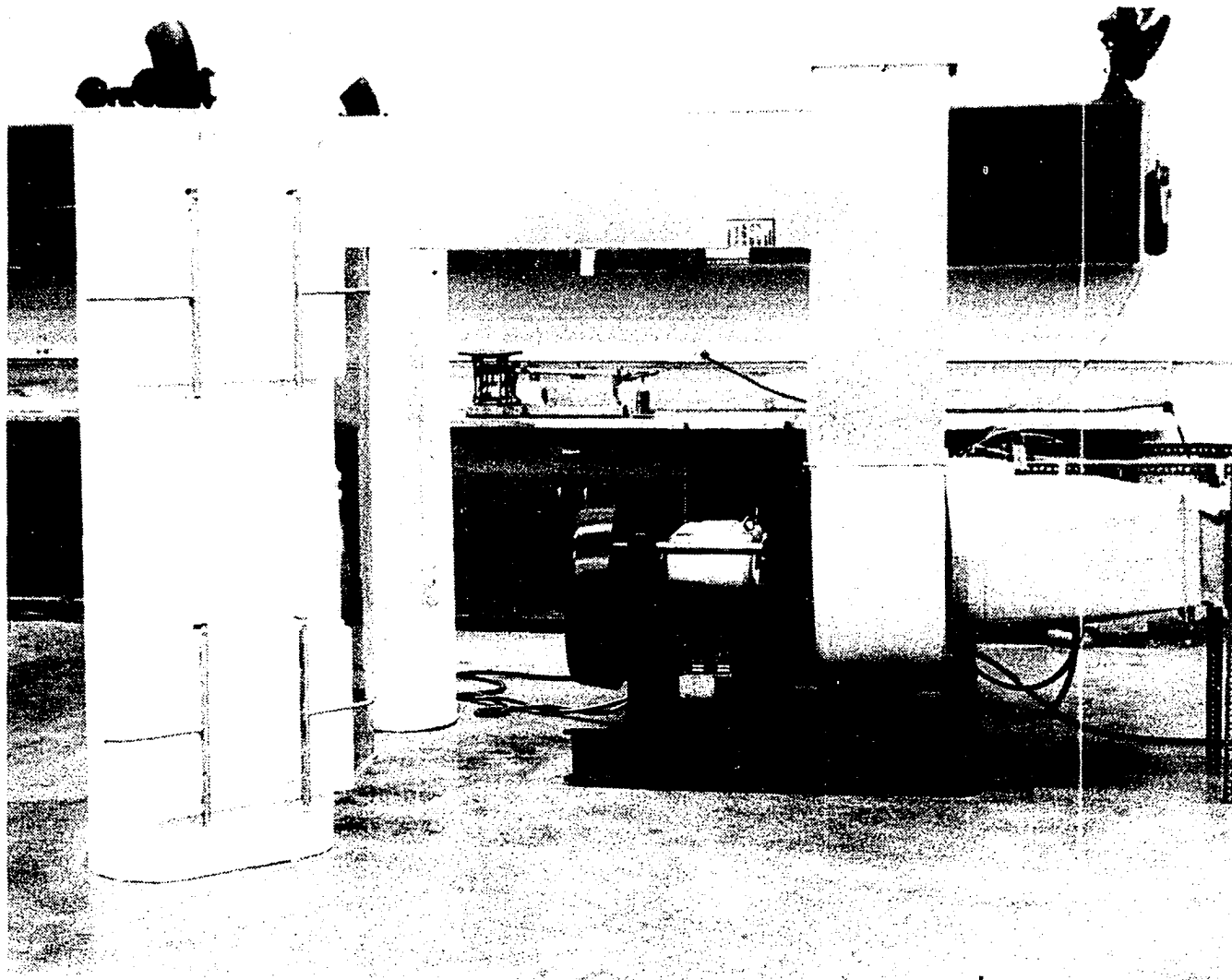


FIGURE 19. VIEW OF DUST COLLECTOR AND MAIN FAN



FIGURE 20. VIEW OF DUST CLOUD GENERATOR

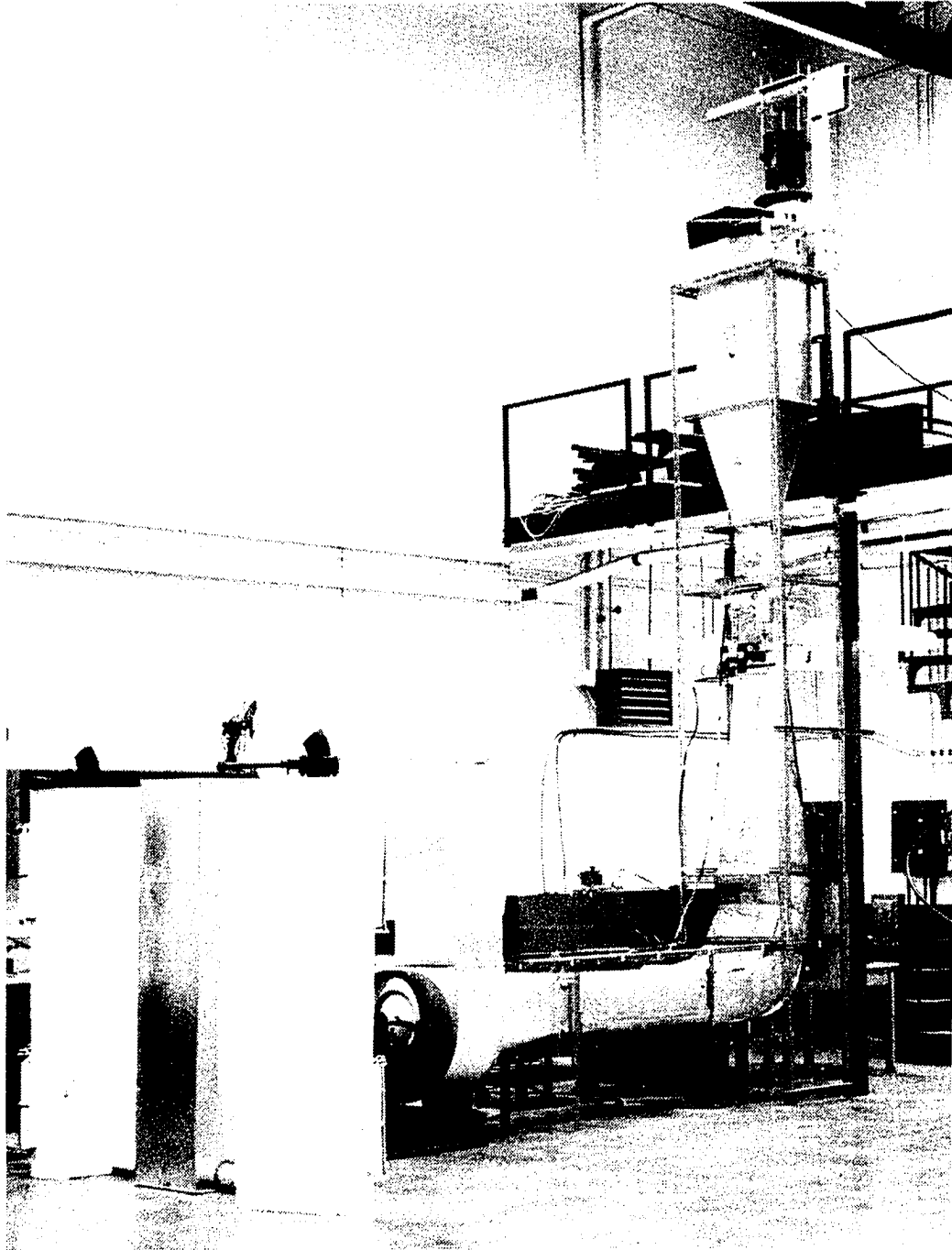


FIGURE 21. VIEW OF EXPERIMENTAL APPARATUS

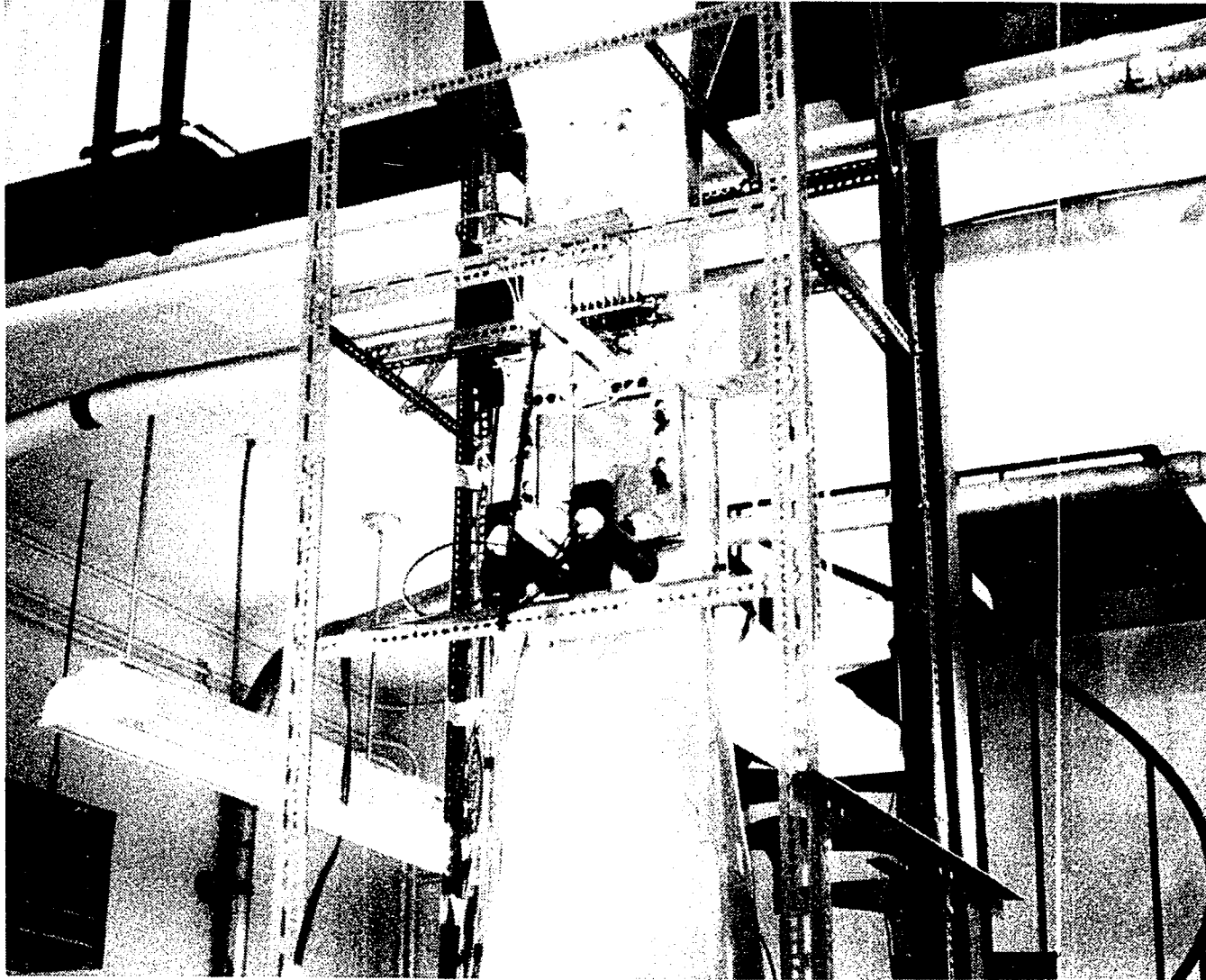


FIGURE 22. VIEW OF TEST SECTION

CHAPTER IV

EXPERIMENTAL PROCEDURE

Prior to the operation of the equipment for data, several tests were conducted for the purpose of determination of voltage inputs to the heaters, for a uniform hot wall surface temperature, and to obtain the approximate number of hours of continuous operation required for equilibrium conditions. To obtain steady state conditions as much as four hours were required. Once the experimental procedure was established the data taking procedures were conducted.

Before each data run a check-out procedure of all electrical components was administered. This consisted of standardizing the potentiometer, checking all thermocouples to determine if they read ambient temperature, running of the main blower, testing of particle stream equipment, and finally a check was made on the heaters and their monitoring equipment.

The initial step in the experimental procedure was to provide the proper voltage input to the heaters using the predetermined settings. The voltage settings and the power input to the center heater were observed at regular intervals and minor adjustments were made when required to maintain the original voltage settings. The voltage settings were checked with a Hewlett-Packard digital voltmeter, Model 344A/3445A, and the power input to the center heater was monitored by a General

Electric Company wattmeter.

When the hot wall surface temperatures exceeded the predetermined surface temperature both the main air stream and the particle air stream were started and adjusted to their predetermined speeds, subsequently cooling the hot wall to its operating temperature.

After allowing a warm-up time of approximately four hours, all temperatures were read and then re-read after thirty-minutes to test the stability of the hot wall. The hot wall is assumed stable by two conditions:

1. Internal temperature difference should be less than 10°F ,
2. Hot wall face temperature change should be less than 50°F .

Once these stability conditions have been satisfied, the cold wall temperature is adjusted to the free stream temperature of the air, the stability criteria being 1°F . This criteria is tested over a period of one hour.

The cold wall temperature is regulated by adjusting the cooling water flow rate through the labyrinth water channel located in the cold wall. This is accomplished by using two valves and a pressure gage on the water line, enabling a constant pressure to be maintained on the water channel.

At one hour, and at one-half an hour before the final reading for a data point, preliminary readings were made and recorded to indicate how closely steady state was being approached. These readings were recorded and the differences between temperature readings were noted.

Meanwhile, all recording instrumentation was checked, calibrated,

and observed under operating conditions. The multi-channel recorder permitted continuous observation of five temperatures, the heat flow meter, and the optical thickness of the particle stream.

Calibration of the photocell proceeded in the following manner; the maximum available voltage was applied to the light source and then positioned to give the greatest possible deflection on the recorder, then the voltage was decreased in small increments and the deflection noted. In Appendix VIII is an example calculation of the optical thickness.

The heat flow meter and the thermocouples deflection were calibrated by means of a Leeds and Northrup potentiometer. This was accomplished by applying a known input voltage to the recorder and noting the deflection, thus the deflections were calibrated. The deflection was later converted to millivolts for the thermocouples and translated to temperature change by means of a Leeds and Northrup calibration chart.

Calibration of the heat flow meter response is presented in Appendix III.

During the warm-up period the particles to be used were measured, the hopper opening was adjusted to give a suitable flow rate, and finally the particles were placed in the hopper.

Once the stability conditions have been satisfied, the velocity profile was taken by means of a 0.125 inch diameter pitot tube, manufactured by the F.W. Dwyer Mfg. Co., connected to a micromanometer, Model MM-3, manufactured by Flow Corporation. The temperature profile was obtained with a stream thermocouple probe, described in Chapter II,

and a Leeds and Northrup millivolt potentiometer.

Upon successful completion of all previous operations, the recording instruments were turned on, photocell activated, and the hopper gate opened allowing the particles to pass into the particle stream mechanism. This terminated the procedure for a data-run.

If another set of data was desired at these preset conditions a hold of approximately fifteen minutes was employed then the stability conditions were re-checked and the particle hopper was re-loaded. Now the check out preceeded as before but the temperature and velocity profiles were not run in their entirety. This procedure could be continued as many times as desired.

CHAPTER V

EXPERIMENTAL OBSERVATIONS AND RESULTS

As stated in the introduction the subdivision of this experimental investigation into three distinct groups is possible. In this chapter consideration is given only to the transport of thermal radiation through an emitting, scattering, and absorbing dust cloud. Consideration of the remaining groups can be found in the appendices.

Previously an analysis by Love (2) was discussed. In his analysis Love has considered the particles, which are bounded by diffusely reflecting and emitting surfaces at different temperatures, to be isothermal. To obtain this particular condition experimentally the particles would have to be contained outside the thermal boundary layer. Figure 23 presented the temperature profile obtained with the aid of a thermocouple probe shown in Chapter V. This temperature profile was taken without particles and shows definitely that there is a region which can be considered isothermal in the flow.

The release of the particles into the main air stream occurs at the top of the test section, midway between the hot and cold walls. At this point the secondary air stream duct, particle stream, is 0.5 inches in width and from figure 24 it is apparent that this stream remains relatively constant in width.

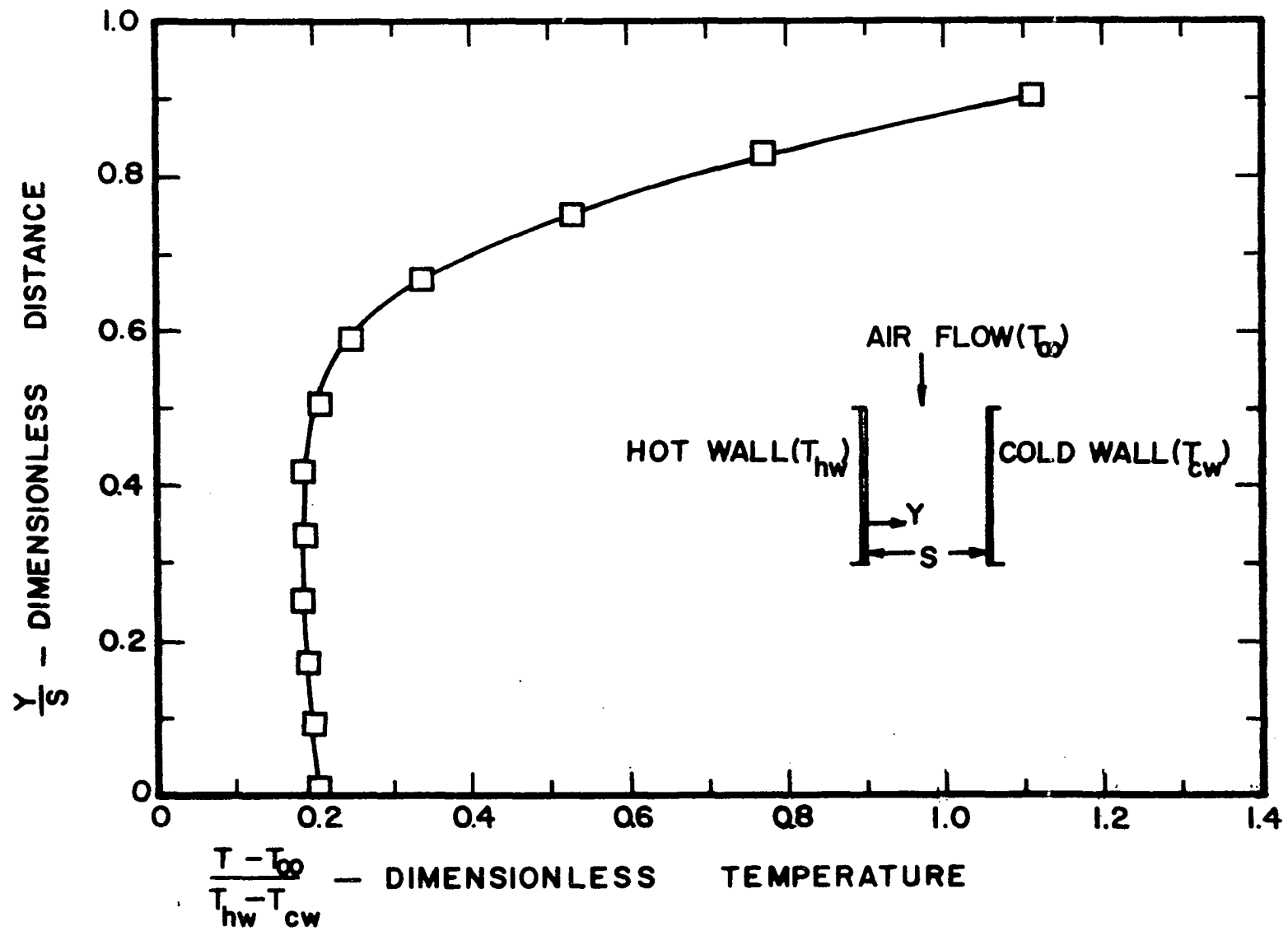


FIGURE 23. DIMENSIONLESS TEMPERATURE PROFILE



FIGURE 24. VIEW OF TEST SECTION WITH DUST CLOUD

This observation implies that the cloud of particles has been dropped into a region where only effects of thermal radiation should be considered. To determine the temperature rise of the cloud due to the radiant energy being intercepted by the cloud a rather simple but effective calculation can be performed. First consider the density of the cloud for a typical data run:

$$\text{Weight of particles} = 5298 \text{ grams}$$

$$\text{Volume of cloud} = 34.3 \text{ ft}^3$$

therefore

$$\rho = 0.3387 \text{ lb. per ft.}^3$$

The mass flow rate is merely a produce of density, cross-sectional area, and velocity:

$$\dot{m} = c_p AV$$

$$\dot{m} = 0.3387(0.0452)(49)$$

$$\dot{m} = 0.752 \text{ lb. per sec.}$$

Now to calculate the temperature rise of the cloud the assumption that the entire radiant energy leaving the hot wall is used to raise the temperature of the cloud. This should produce a limiting situation that will be higher than the actual physical problem.

$$q'' = \dot{m} c_p \Delta T$$

where

$$q'' = 300 \text{ BTU/hr ft}^2$$

$$\Delta T = \text{temperature rise}$$

$$c_p = \text{specific heat of glass beads}$$

$$\Delta T = \frac{q''}{mc_p}$$

$$\Delta T = \frac{300}{(0.752)(3600)(0.199)}$$

$$\Delta T = 0.558 \text{ } ^\circ\text{F}$$

This calculation along with the experimental measurements made of the air stream temperature support the conclusion of an isothermal cloud.

Measurements of thermal radiation through a dust cloud were made for several different sizes of glass beads. In previous work glass beads were found to be the most suitable in terms of handling and moving, reference (31). These measurements were made with the aid of a photocell, for optical thickness, and a heat flow meter, for measuring thermal changes at the cold wall. The heat flow meter was calibrated, as discussed in Appendix III, so a deflection on the recorder could be converted directly to a thermal change. This thermal change at the cold wall was correlated with its corresponding optical thickness measurement.

The steady state radiant heat transfer was obtained from figure 34 in Appendix II. This data was taken in a vacuum chamber at a sufficiently high vacuum to eliminate convective heating effects, permitting the measurement of thermal radiation only. For a given hot wall temperature a corresponding radiative heat flux is obtained.

Calculated values for the thermal change at the cold wall were obtained with the aid of the following equation:

$$q = \frac{\sigma}{\pi} [MT_1^4 - NT_2^4 - QT_2^4]$$

where

q = net radiant flux at wall 1

T = absolute temperature

N, N, Q = dimensionless parameters from table

σ = Stefan-Boltzmann constant

Subscript

1 = surface 1

2 = surface 2

a = particles

This equation was obtained by Love (2) and the dimensionless parameters are functions of optical depth, emittance, and the ratio of scattering to extinction for isotropic scattering.

To analyze the system without particles the following equation for gray parallel infinite walls was used:

$$q = \frac{\sigma(T_1^4 - T_2^4)}{\frac{1}{\epsilon_1} + \frac{1}{\epsilon_2} - 1}$$

where ϵ = total hemispherical emittance.

Figure 25 presents a comparison of the above experimental and theoretical results.

Comparison of the experimental results for gray infinite parallel walls is presented in Appendix II.

Figure 26 presents a dimensionless radiative flux ratio, which is a ratio of the radiative flux through a dust cloud to the radiative flux for gray infinite parallel walls, versus Thring's

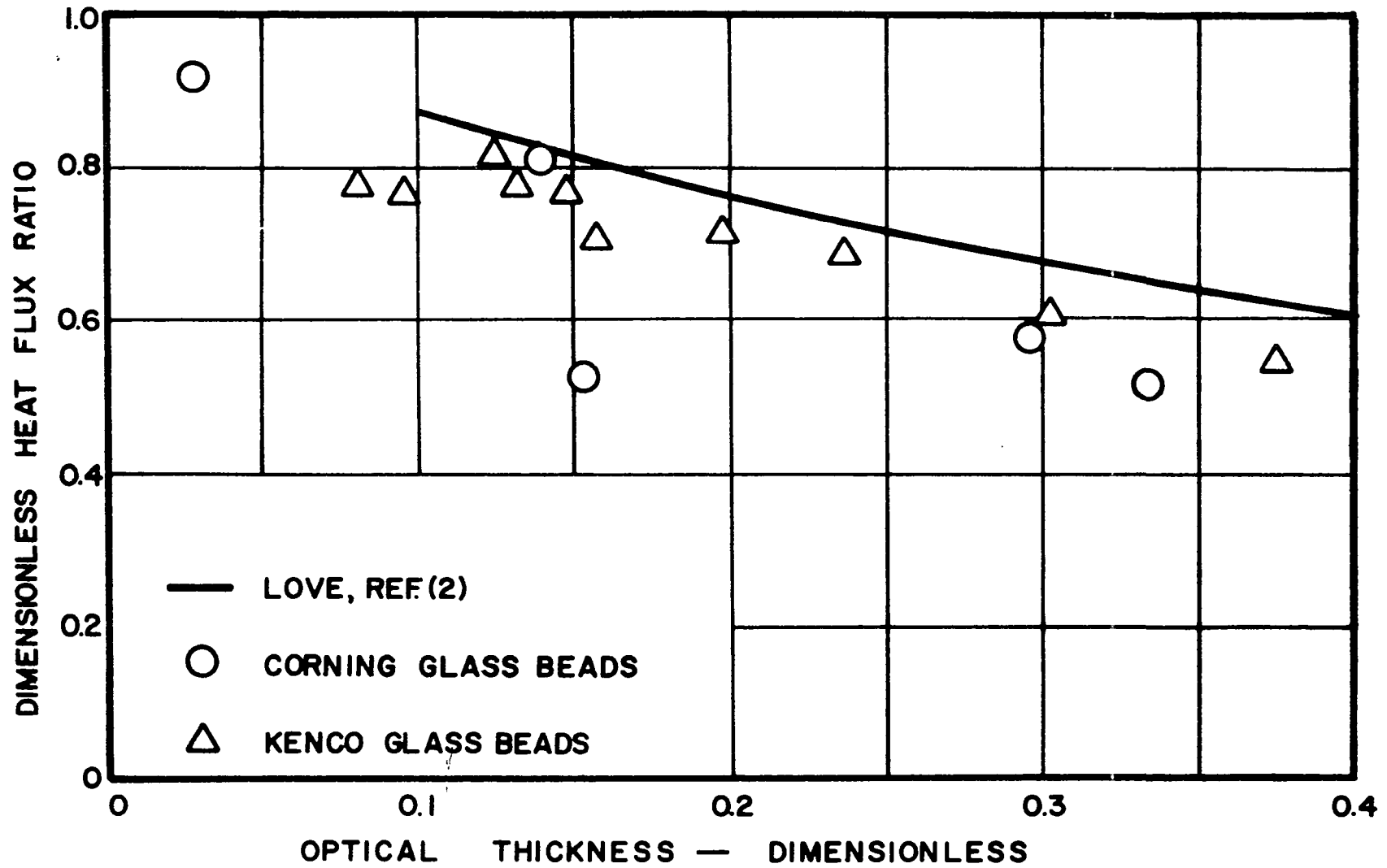


FIGURE 25. DIMENSIONLESS HEAT FLUX RATIO VERSUS OPTICAL THICKNESS

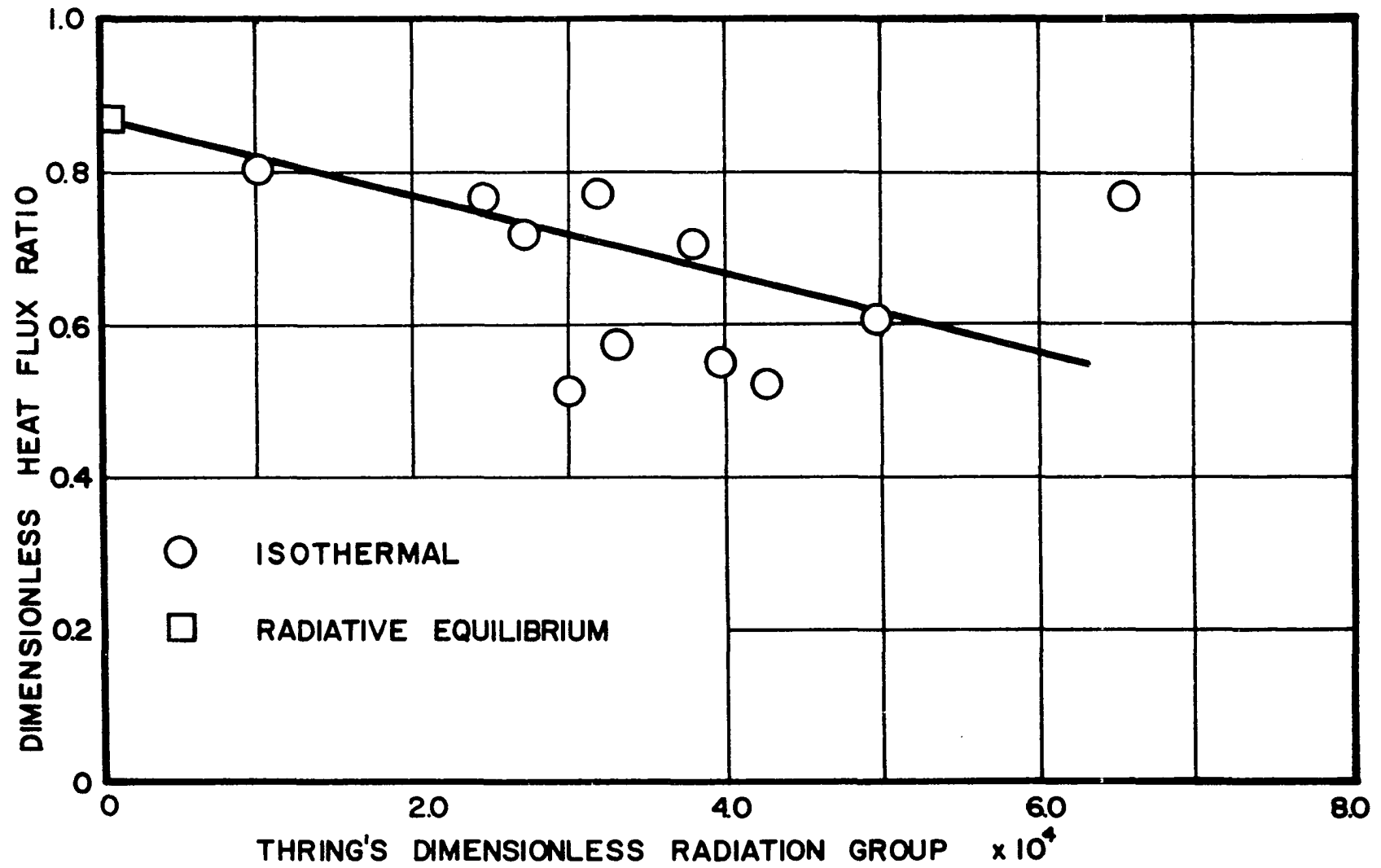


FIGURE 26. DIMENSIONLESS HEAT FLUX RATIO VERSUS THRING'S RADIATION GROUP

radiation group. Thring's radiation group was obtained from reference (30) and is given as:

$$N_{th} = \frac{\rho C_p V}{\epsilon \sigma T^3}$$

where

ρ = apparent cloud density

C_p = specific heat of cloud material

V = velocity of cloud

ϵ = total hemispherical emittance

σ = Stefan-Boltzmann constant

T = absolute temperature

This dimensionless group was viewed with interest because a majority of the variables encountered in the experiment could be grouped together for observation.

An apparent inability to accurately predict the mass flow rate of the glass beads is displayed in figure 27. This is a primary cause for the scatter in the calculation of Thring's radiation group. A major cause for the scatter is the inability of being able to account for the loss of material and the inability to measure the density simultaneously with optical thickness.

The results show a trend of decreasing radiative flux ratio with increasing Thring's radiation group, with the case of radiative equilibrium at the far left of the graph. This type of result is expected since increasing Thring's radiation group is equal to an increase in optical thickness, hence a lower radiative flux ratio.

A sample calculation is presented in Appendix VIII.

By using the definition of optical thickness

$$\tau = \rho\beta x$$

where

τ = optical thickness

ρ = apparent cloud density

β = extinction coefficient

x = normal distance

and obtaining an extinction coefficient from reference (5) for the wave length corresponding to the peak of wave length versus energy curve for the hot wall yields the curve plotted in figure 28. The experimental points scatter once again because of the density measurement. This result shows in a limited way the validity of Love and Beattie's (5) data.

An additional calculation was performed for determining the temperature rise of the dust cloud. This calculation was based upon the definition of optical thickness and the data presented by Love and Beattie (5).

By selecting an optical thickness and obtaining an extinction coefficient, for this case the lowest possible value, an apparent cloud density was calculated.

For example:

$$\tau = 0.1$$

$$\beta = 16 \text{ ft.}^2 \text{ per lb.}$$

$$x = 0.5 \text{ in.}$$

Therefore,

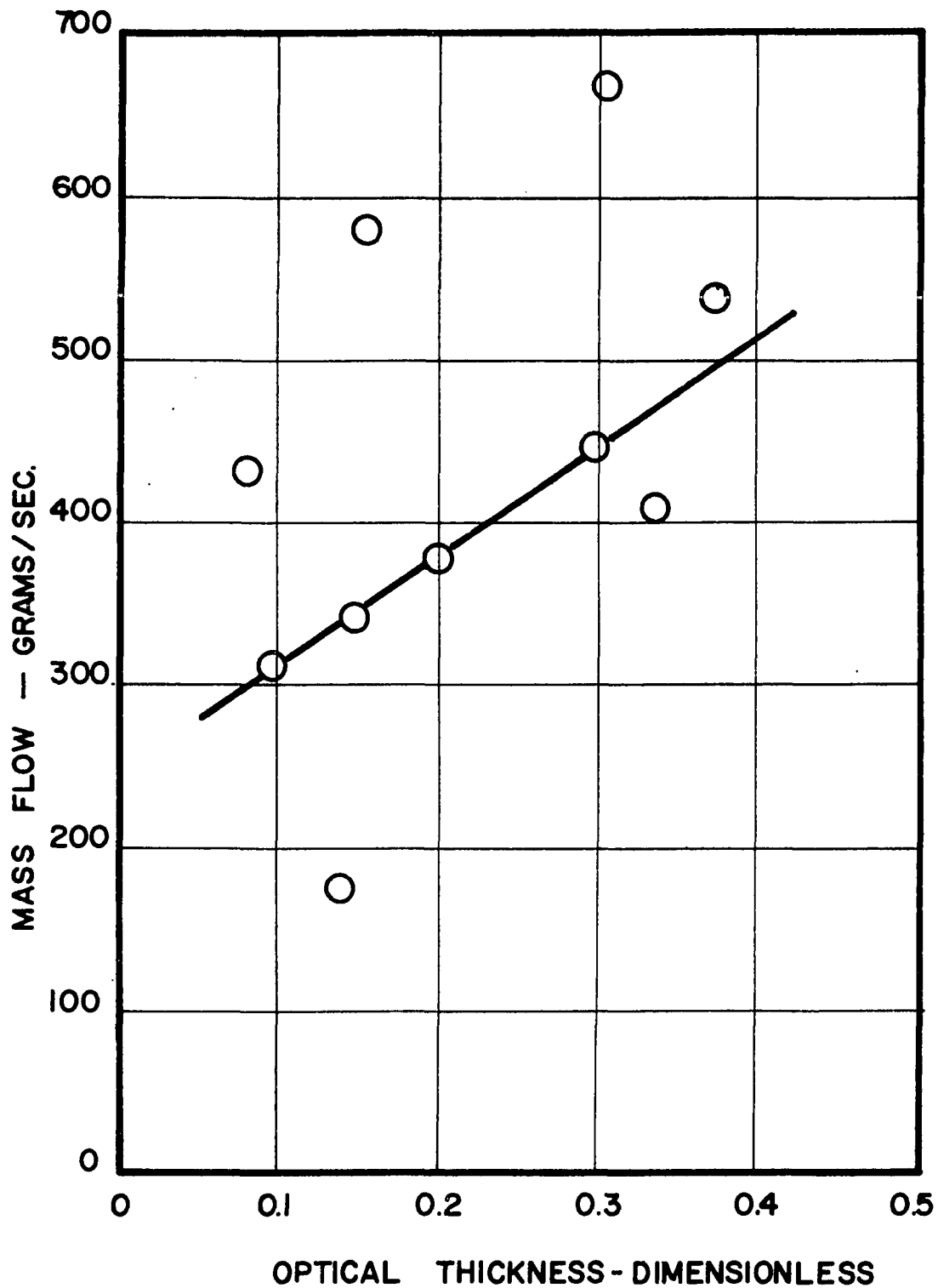


FIGURE 27. MASS FLOW VERSUS OPTICAL THICKNESS

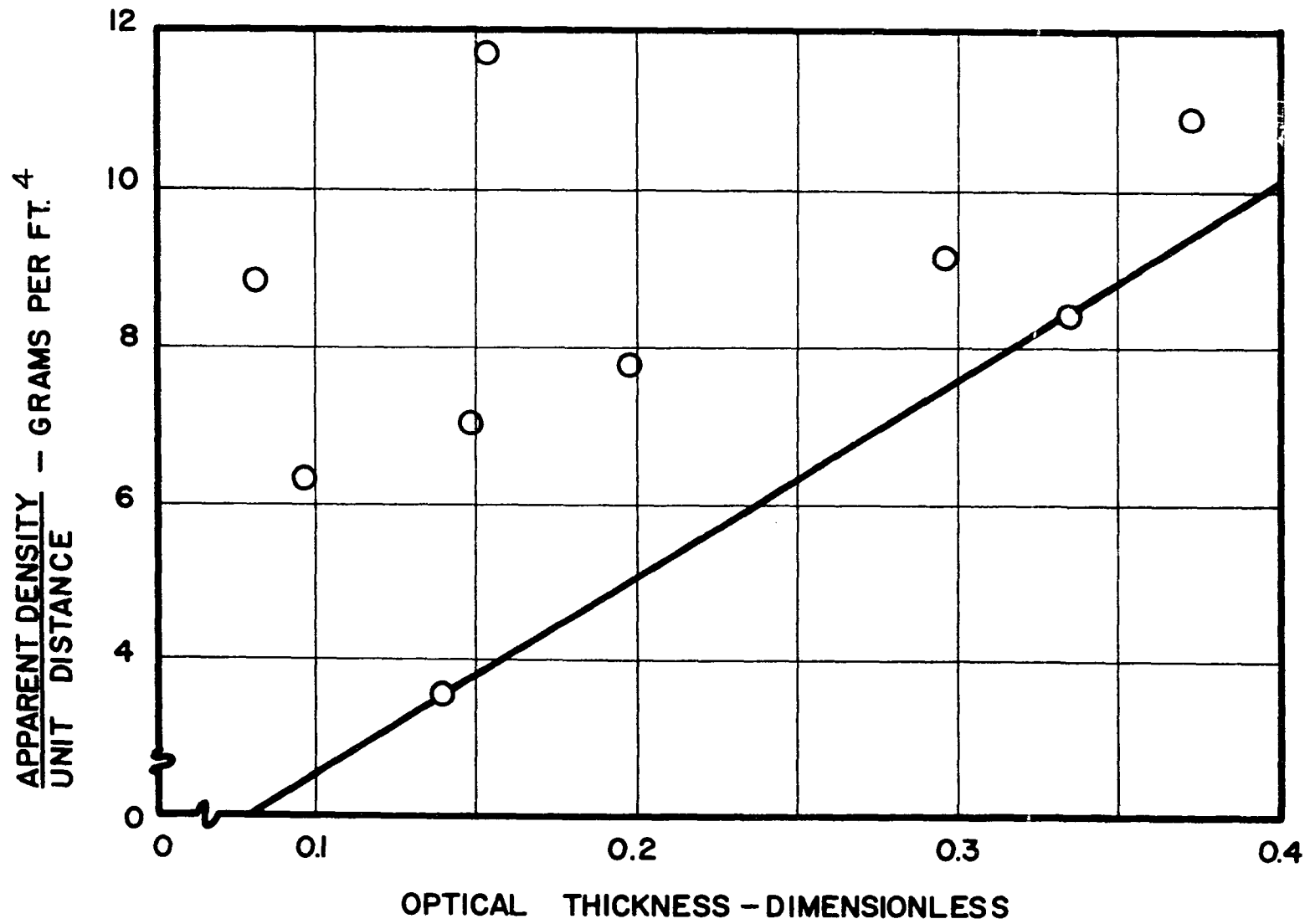


FIGURE 28. APPARENT DENSITY PER UNIT DEPTH VERSUS OPTICAL DEPTH

$$\rho = 0.15 \text{ lb. per ft.}^3$$

which yields a temperature rise of

$$\Delta T = 1.12^\circ \text{F.}$$

for the previously mentioned example case.

A final graph, figure 29, presents a typical velocity profile obtained in the test section. The shift in the curve was caused by a slight off-center location of the secondary air stream.

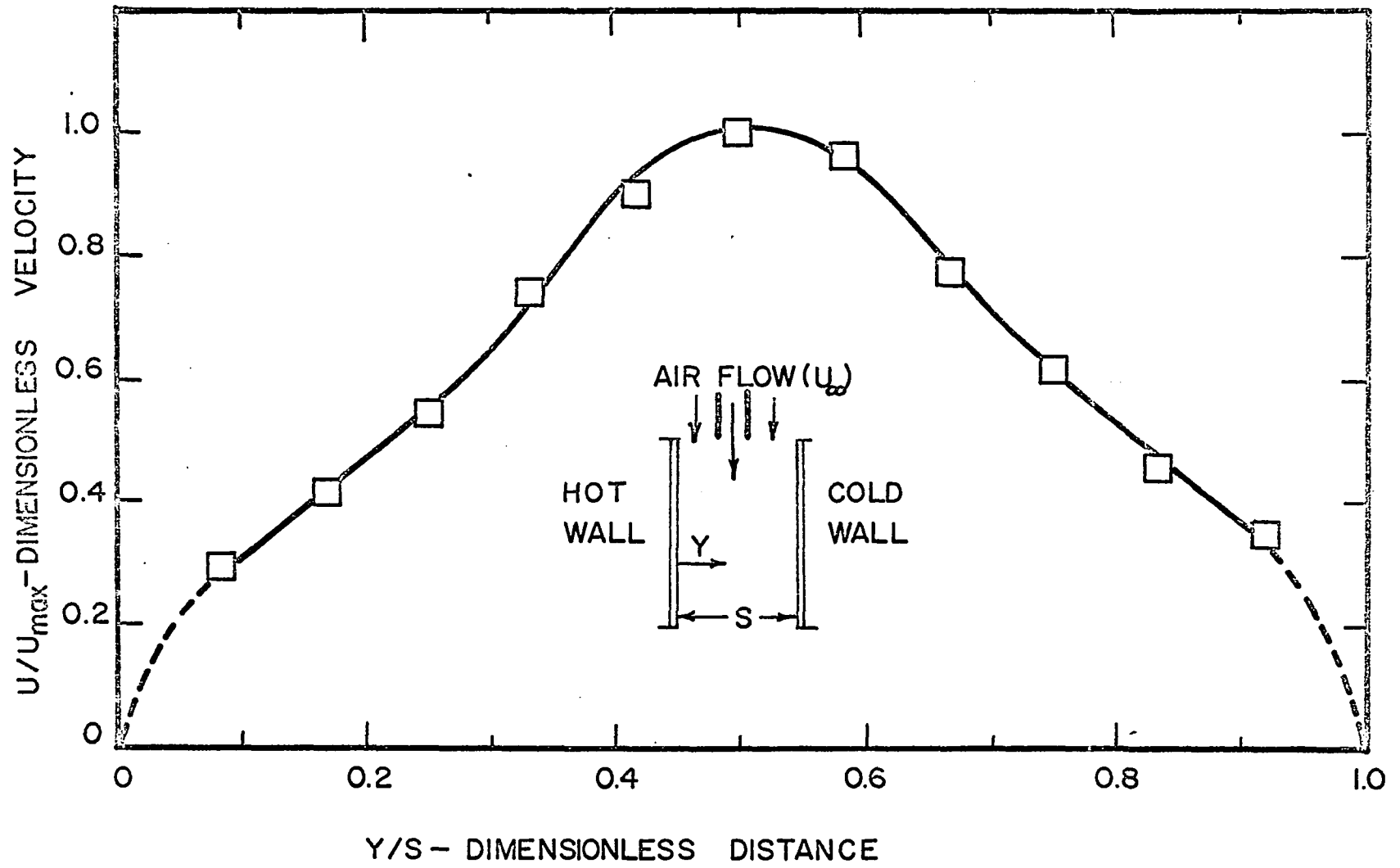


FIGURE 29. DIMENSIONLESS VELOCITY PROFILE

CHAPTER VI

CONCLUSIONS

This experimental investigation has attempted to show how particles, specifically glass beads, influence radiative heat transfer between parallel walls. The equipment with which to perform such an experiment is scarce and considerable time was spent in development of the apparatus. This is probably due in part to the fact that until recently little demand existed for this type of information.

The observed and recorded data show conclusively that particles do influence radiative heat transfer between parallel walls. There are some difficulties in attempting such an experiment, especially in a vacuum chamber. The amount of material which may be placed in a vacuum chamber is critical because of outgassing, therefore, a limit is placed on the amount of particles for maintaining a cloud. In addition the overall size of the vacuum chamber, and the size of pumps are probably the most critical pieces of equipment used in this study. A major problem encountered in operation of the particle tunnel was a limitation on the amount of material added to the secondary air stream because this reduced the fan speed and hence changed the flow characteristics.

The conclusions which may be drawn from this experimental

investigation may be stated as follows:

I. The dimensionless parameters, presented by Love (2), from theoretical considerations for isotropic scattering may be used to compute radiative heat transfer in real particle clouds.

II. The dimensionless parameter presented by Love (2) for the case of radiative equilibrium may be used for a real particle cloud in radiative equilibrium.

III. The information obtained by Beattie and Love (5) for glass beads can be used in most engineering calculations.

IV. Convective heat transfer coefficients obtained in this investigation are in good agreement with published information.

Measurements of thermal radiation involving a particular media were made, specifically glass beads; hence, a logical extension of this study would be measurements involving other media. Beattie and Love (5) investigated such materials as silica, carbon, iron, and aluminum. These would be logical extensions since their properties of scattering, absorbing, and emitting of thermal radiation have been investigated.

LIST OF REFERENCES

1. Love, T.J., Jr., Radiative Heat Transfer, Charles E. Merrill Publishing Company, Columbus, Ohio, 1968.
2. Love, T.J., Jr., "An Investigation of Radiant Heat Transfer in Absorbing, , Emitting, and Scattering Media", Norman, Oklahoma: University of Oklahoma Research Institute, 1963, Contract AF 33(657)-8859, ARL 63-3.
3. Hsia, H.M., and Love, T.J., Jr., "Radiative Heat Transfer Between Parallel Plates Separated by a Nonisothermal Medium with Anisotropic Scattering", ASME, Paper No. 66-WA/HT-28, 1966.
4. Love, T.J., Jr., and Wheasler, R., "An Experimental Study of Infra-Red Scattering by Clouds of Particles," Aerospace Research Laboratories, Wright-Patterson Air Force Base, Ohio, ARL 65-109, June 1964.
5. Love, T.J., Jr., and Beattie, J.F., "Experimental Determination of Thermal Radiation Scattering by Small Particles," Aerospace Research Laboratories, Wright-Patterson Air Force Base, Ohio, ARL 65-110, June 1965.
6. Lee, F.C., "Radiative Heat Transfer in an Emitting Absorbing and Scattering Boundary Layer", Ph.D. thesis, University of Oklahoma, 1967.
7. Love, T.J., Jr., and Gilbert, J.S., "Experimental Study of Radiative Heat Transfer Between Parallel Plates," Aerospace Research Laboratories, Wright-Patterson Air Force Base, Ohio, ARL 66-0103, June 1966.
8. Schornhorst, J.R., and Viskanta, R., "An Experimental Examination of the Validity of the Commonly Used Methods of Radiant Heat Transfer Analysis", ASME, Paper No. 68-HT-42, 1968.
9. Usiskin, C.M., and Sparrow, E.M., "Thermal Radiation Between Parallel Plates Separated by an Absorbing-Emitting Nonisothermal Gas", International Journal of Heat and Mass Transfer, Vol. 86, Series C, May 1964.

10. Howell, J.R., and Perlmutter, M., "Monte Carlo Solution of Thermal Transfer Through Radiant Media Between Gray Walls," ASME, Paper 63-AHGT-1, 1963.
11. Sparrow, E.M., and Cess, R.D., Radiation Heat Transfer, Brooks/Cole Publishing Company, Belmont, California, 1966.
12. Cess, R.D., "The Interaction of Thermal Radiation with Conduction and Convection Heat Transfer", Advances in Heat Transfer, Vol. 1, Academic Press, N.Y., 1964.
13. Pai, S.I., Radiation Gas Dynamics, New York: Springer-Verning, New York, Inc., 1966.
14. Soo, S.L., Fluid Dynamics of Multiphase Systems, Blaisdell Publishing Company, Waltham, Massachusetts, 1967.
15. Briller, R., and Peskin, R.L., "Gas Solids Suspension Convection Heat Transfer at a Reynolds Number of 130,000", ASME, Paper 68 HT-8, 1968.
16. Gilbo, C.F., American Society for Testing and Materials, 1961 Standards, Part 4, Philadelphia, Pa.
17. Gier, J.T., and Boklter, L.M.K., "The Silver-Constantan Plated Thermopile", Temperature, Its Measurement and Control in Science and Industry, New York: Reinhold Publishing Co., 1941.
18. Morse, Bonard E., "Development of an Albrecht Type Meter for the Measurement of Heat Flux in the Soil", Electrical Engineering Research Laboratory, University of Texas, Report No. 4-01.
19. Frazine, D.F., "The Design of a Total Radiation Thermopile Detector," AEDC-TDR-64-271, January 1965.
20. Harris, Louis, "Rapid Response Thermopiles", Journal of the Optical Society of America, Vol. 36, No. 10, October 1946.
21. Hornig, Donald F., and O'Keefe, R.J., "The Design of Fast Thermopiles and the Ultimate Sensitivity of Thermal Detectors", The Review of Scientific Instruments, Vol. 18, No. 7, July 1947.
22. Streeter, V.L., Handbook of Fluid Dynamics, McGraw-Hill Book Company, Inc., New York, 1961, First Edition.
23. Lawrence, D.E., "The Design and Construction of a Subsonic Low Turbulence Wind Tunnel", M. Engr. 1965.
24. Dryden, H.L., and Schubauer, G.B., "The Use of Damping Screens for the Reduction of Wind-Tunnel Turbulence", Journal of the Aeronautical Sciences, April 1947.

25. Pope, A., and Harper, J.J., Low-Speed Wind Tunnel Testing, John Wiley & Sons, Inc., New York, 1966.
26. Pankhurst, R.C., and Holder, D.W., Wind-Tunnel Technique, Sir Isaac Pitman & Sons, Ltd., London, 1952.
27. Silverman, L., and Billings, C.E., "Methods of Generating Solid Aerosols", Journal of Air Pollution Control, Vol. 6, No. 2, August, 1956.
28. Richmond, O., "Gravity Hopper Design", Mechanical Engineering, Vol. 85, No. 1, January, 1963, p. 46.
29. Dumbaugh, George D., "Vibratory Hoppers", Mechanical Engineering, Vol. 88, No. 5, May 1966, p. 197.
30. Boucher, D.F., and Alves, G.E., "Dimensionless Numbers," Chemical Engineering Progress, Vol. 55, No. 9, September 1959, pp. 55-65.
31. Love, T.J., Jr., Stockham, L.W., Lee, F.C., Munter, W.A., and Tsai, Y.W., "Radiative Heat Transfer in Absorbing, Emitting and Scattering Media", Aerospace Research Laboratories, Wright-Patterson Air Force Base, Ohio, ARL 67-0210, December 1967.
32. Letham, Darly, L., "High Vacuum Systems", Machine Design, Vol. 37, No. 3, February 1965.
33. Barrington, A.E., "High-Vacuum Engineering," Mechanical Engineering, Vol. 86, No. 11, November 1964, p. 26.
34. Steinherz, H.A., Handbook of High Vacuum Engineering, New York: Reinhold Publishing Corporation, 1963.
35. Harrison, W.H., and Richmond, J.C., "Total Hemispherical Emission of Coated and Uncoated Inconel and Types 321 and 430 Stainless Steel", Journal of Research, Vol. 66C, No. 3, September 1962.
36. Deissler, R.G., and C.S. Eian, "Analytical and Experimental Investigation of Fully Developed Turbulent Flow of Air in a Smooth Tube with Heat Transfer with Variable Fluid Properties", NACA TN 2629, February 1952.
37. Rohsenow, W.M., and Choi, H.Y., Heat, Mass and Momentum Transfer, Prentice-Hall, Inc., Englewood Cliffs, New Jersey, 1961.
38. Deissler, R.G., "Analysis of Turbulent Heat Transfer and Flow in the Entrance Regions of Smooth Passages", NACA TN 3016, October 1953.

39. Bird, R., Stewart, W., and Lightfoot, E., Transport Phenomena, John Wiley & Sons, Inc., New York, 1960.
40. Sparrow, E.M., "Analysis of Laminar Forced-Convection Heat Transfer in Entrance Region of Flat Rectangular Ducts", NACA TN 3331, January 1955.
41. Mercer, W.E., Pearce, W.M., and Hitchcock, J.E., "Laminar Forced Convection in the Entrance Region Between Parallel Flat Plates", ASME, Paper 66 WA/HT-16, 1966.
42. Eckert, E.R.G., and Jackson, T.W., "Analysis for Turbulent Free-Convection Boundary Layer of Flat Plate", NACA TN 2207, October 1950.
43. Eckert, E.R.G., and Jackson, T.W., "Analysis of Turbulent Free-Convection Boundary Layer of Flat Plate", NACA, Report 1015, 1951.
44. Schlichting, H., Boundary Layer Theory, translated by J. Kestin, McGraw-Hill Book Company, 4th Edition, 1960.
45. Ostrach, S., "An Analysis of Laminar Free-Convection Flow and Heat Transfer about a Flat Plate Parallel to the Direction of the Generating Body Force", NACA TN 2635, February 1952.

APPENDIX I

A CLOUD OF DUST IN RADIATIVE EQUILIBRIUM

In order to have an experimental verification of the radiative equilibrium analysis presented by Love (2) the previously described apparatus was placed in a vacuum chamber. Also, inside the vacuum chamber a particle hopper was mounted above the parallel walls. A detailed description of the particle hopper is presented in reference (31).

A schematic diagram of the system is shown in figure 30. The vacuum enclosure consists of a bell jar on a stainless steel base plate with the vacuum being provided by a mechanical pump and an oil diffusion pump as shown. A hopper located at the top of the bell jar with doors and vibrators, which were actuated by electrical signals feed through the base plate, formed the particle cloud generator. The hot wall and cold wall were the same as those described previously. A photocell mounted over one of the walls monitors the optical thickness of the cloud during the drop.

Due to the limited number of channels at the time of the experiment two channels were used to monitor the wall temperatures, one channel to monitor the heat flow meter output and one channel monitoring the optical thickness.

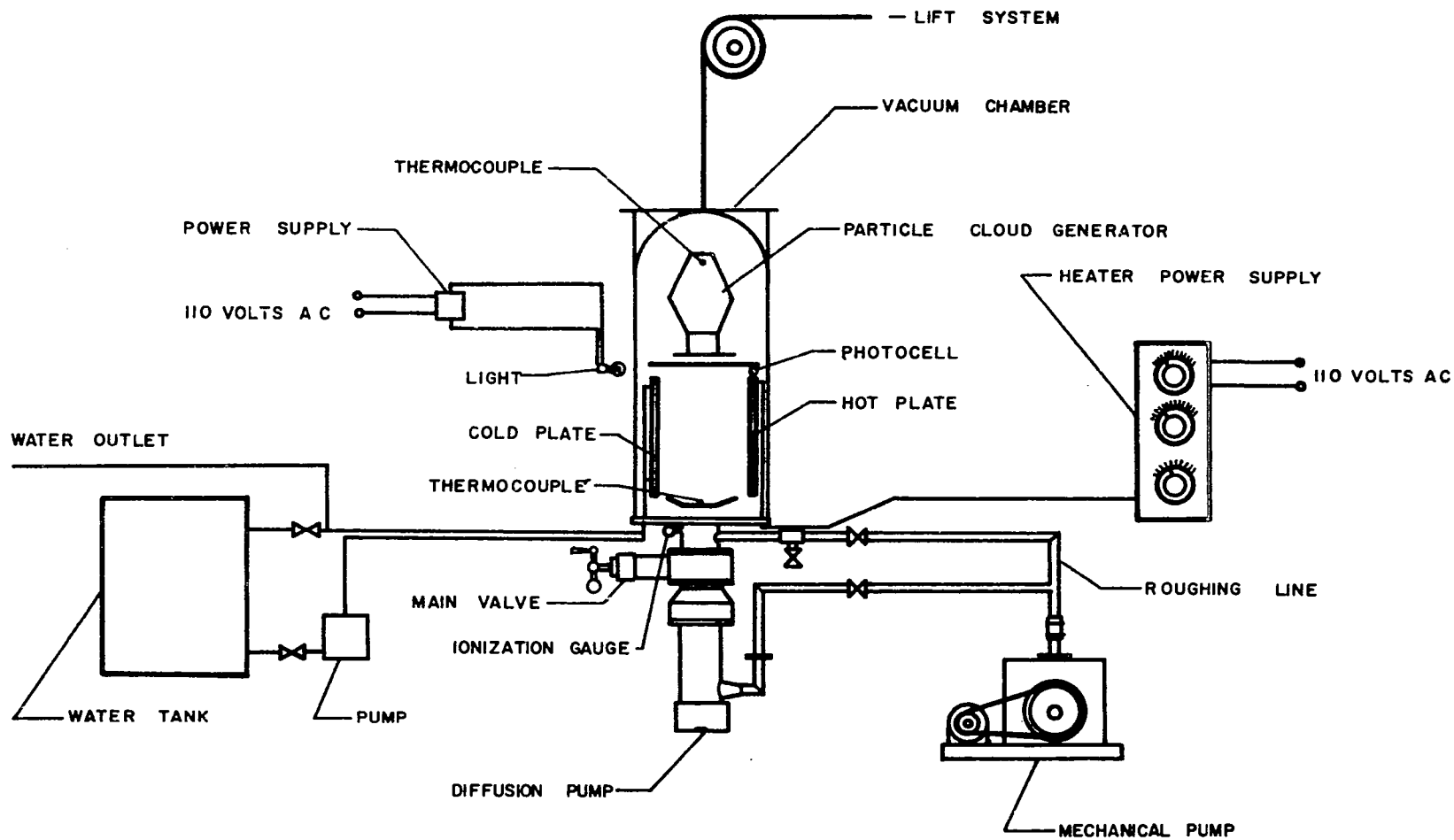


FIGURE 30. SKETCH OF OVERALL SYSTEM

The recorder and its associated apparatus is the same as that described previously in Chapter II. The temperature measurement apparatus was also identical to that described previously.

Once the particles were in the generator a check-out procedure of all electrical components was initiated. This consisted of standardizing the potentiometer, checking all thermocouples to determine if they read room temperature, running of the shaker motors, testing of the particle drop mechanism, and finally a check was made on all heater circuits for shorts or possible hazards.

The vacuum system was started and calibrated according to the operating and maintenance manual received with the vacuum system.

As soon as all systems were checked and passed, the Bell jar was lowered; the gasket between the Bell jar and base plate was greased with silicone vacuum grease. When the pressure reached 1×10^{-5} mm Hg. voltage was supplied to the heaters. Before starting the water pump for the cold wall cooling system, the cold wall was allowed to reach 200°F. This enabled the vacuum system to backout to a lesser degree, hence a lower ultimate pressure was obtained. Approximately twelve hours were allowed before particle drop was considered. During this period of time pressure and temperature readings were taken at one hour intervals; this provided a dual purpose enabling a constant check on the system's operation and provided information for the prediction of particle drop time. Meanwhile, all recording instrumentation was checked, calibrated, and observed under operating conditions.

The heat flow meter and the thermocouples were calibrated by means of a Leeds and Northrup potentiometer. This was accomplished

by applying a known input voltage to the recorder and noting the response, thus the calibration was carried out. The millivolt response was later converted to temperature by means of a Leeds and Northrup calibration chart.

After approximately twelve hours, if the hot wall temperatures had stabilized, all temperatures are read and then re-read after thirty minutes to test the stability of the hot wall. The hot wall is assumed stable by two conditions: 1) temperature difference across the pyrex should be less than 10°F , and 2) hot face temperatures change should be less than 5°F . Once these stability conditions have been satisfied the recording instruments are turned on, photocell activated, and shaker motors tested. Upon successful completion of all previous steps the particle shake mechanism is activated to remove trapped gas in the particle tray and this continues until the original vacuum is established. At such time the drop mechanism is activated and the particles are allowed to fall.

Glass beads proved to be the only type of particles which could be dropped in a uniform cloud with a minimum of "out-gasing." Uniform optical thickness of 1.1 could be maintained for periods of approximately 14 seconds. Three runs were made with the hot plate at 1285°R and the cold plate at 530°R . The optical spacing at the center of the plate was computed to be 0.75 based on the optical thickness measured by the photocell and the free fall acceleration of the particles. The wall reflectance for both surfaces was 0.5 and was approximately diffuse. The ratio of the radiative heat flux before and during the particle drop was determined. These values were compared to the

TABLE I

COMPARISON OF RADIATIVE EQUILIBRIUM RESULTS

(q) PARTICLES
(q) INFINITE PARALLEL WALLS

EXPERIMENT	PREDICTED
0.840	0.835
0.740	0.835
0.810	0.835

predicted values computed using the results of Love (2) which are tabulated in Table II, III, and IV. During the period of the particle drop, the chamber pressure rose from 2.0×10^{-6} torr to 4.2×10^{-5} torr.

Figure 31 represents a sample output record developed by the oscillograph during a particle drop. The photocell monitors the optical depth while the heat flow meter monitors the heat flux at the walls. The thermocouple readings indicate the hot wall temperature and the back of the cold wall. It will be noted that the heat flow meter has not reached an equilibrium reading by the end of the particle drop. The curve has undergone an inflection, however, and the heat fluxes listed above have been computed on the basis of the maximum reading which occurs just after the particle drop is completed.

The above experiment thus supports the theoretical predictions of radiative heat transfer through absorbing, emitting, and scattering material. It would, of course, be desirable to have a wider range of experiments. However, the difficulties encountered in the development of the cloud generator and the rapid response heat flow meter prevented extensive tests.

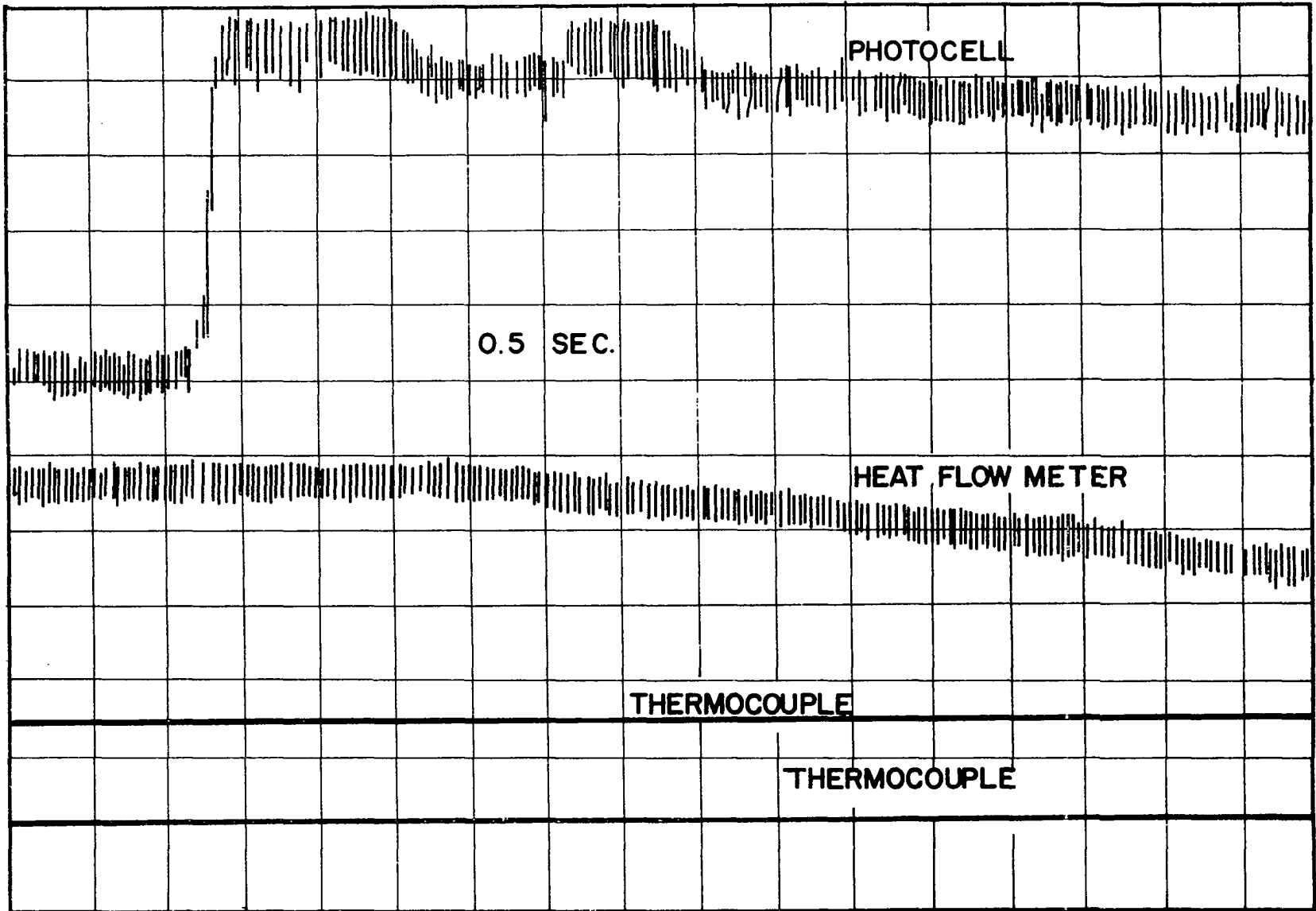


FIGURE 31. SKETCH OF ORIGINAL DATA FROM VACUUM

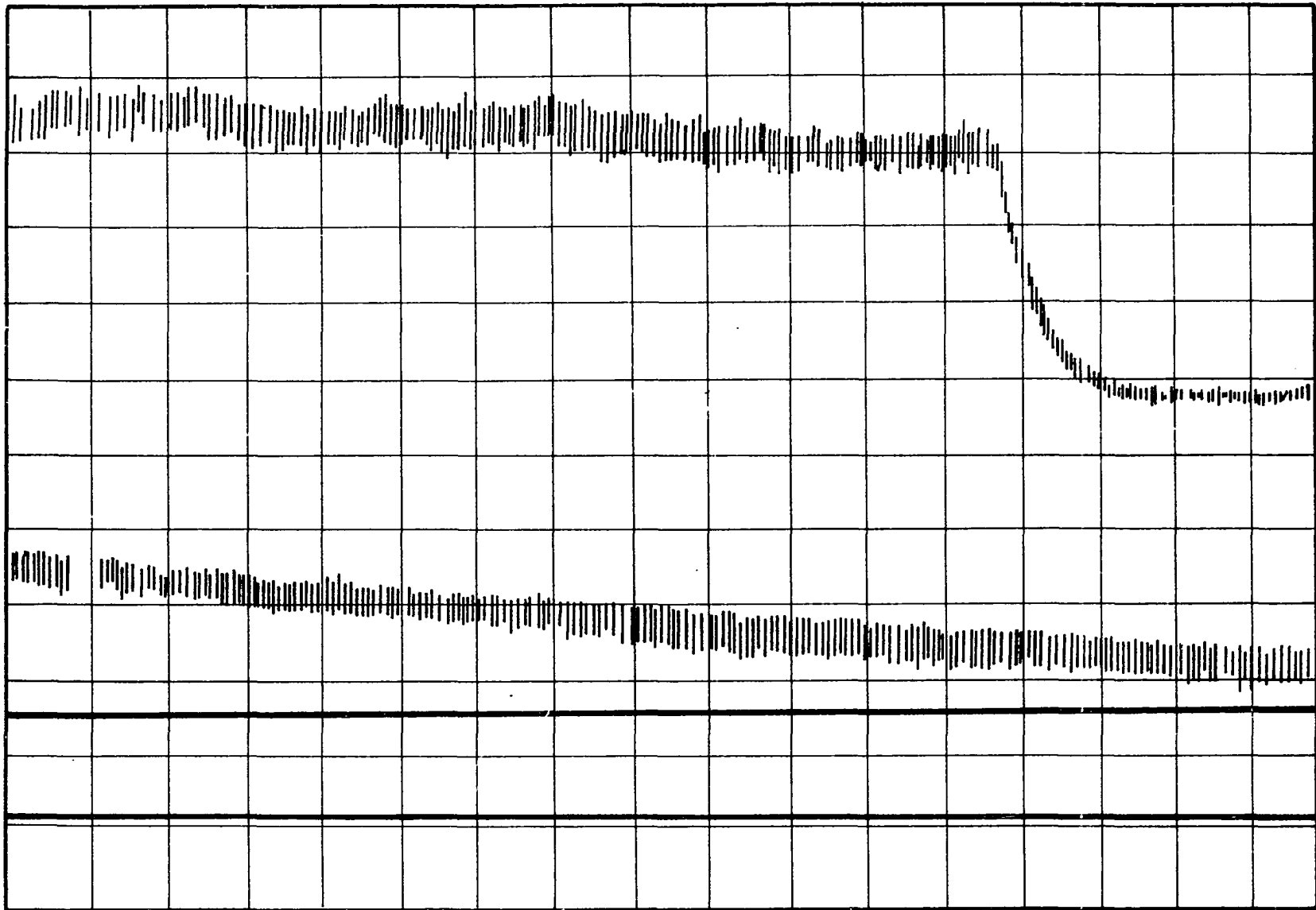


FIGURE 32. ORIGINAL DATA CONTINUED

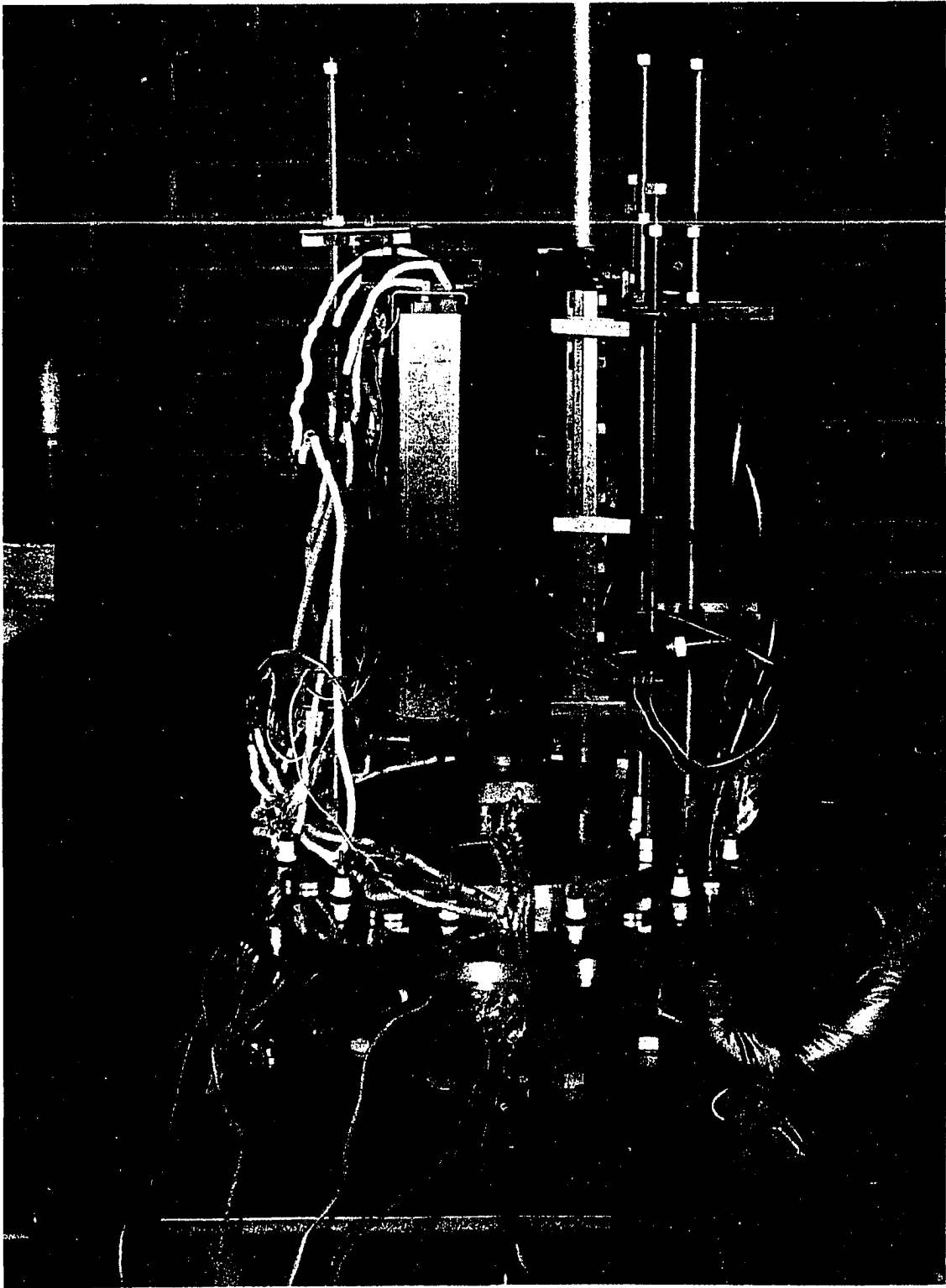


FIGURE 33. VIEW OF PARALLEL WALLS

APPENDIX II

RADIATIVE HEAT TRANSFER BETWEEN PARALLEL WALLS

Consider the system, that is the parallel walls of the heat transfer section, operating in a vacuum without the particles and analyze the governing parameters with existing theoretical considerations.

From most heat transfer texts we find the following basic equation:

$$q = \frac{\sigma(T_1^4 - T_2^4)}{1/\epsilon_1 + 1/\epsilon_2 - 1}$$

where

q = net radiant heat exchange

σ = Stefan-Boltzmann constant

T = absolute temperature

ϵ = total hemispherical emittance

subscript

1 = hot wall surface

2 = cold wall surface

The heater inputs for the cases considered, or input points, correspond to the following heat fluxes from the hot wall:

$$q(1) = 1559.66 \text{ BTU/hr. sq. ft.}$$

$$q(2) = 926.05 \text{ BTU/hr. sq. ft.}$$

$$q(3) = 349.30 \text{ BTU/hr. sq. ft.}$$

$$q(4) = 219.33 \text{ BTU/hr. sq. ft.}$$

$$q(5) = 170.59 \text{ BTU/hr. sq. ft.}$$

For all calculations the total hemispherical emittance values were assumed constant with respect to temperature. The emittance value used, $\epsilon = 0.535$, was obtained by Richmond and Harrison (35) for Type 321 stainless steel. The surface preparation was the same as the technique used by Richmond and Harrison (35) in preparing samples of stainless steel Types 321 and 430. Gilbert (7) obtained measurements for Type 302 stainless steel and found an emittance value of 0.556 to be suitable in the temperature range of 600° F.

In figure (34) the experimental flux (heat input) from the hot wall is plotted versus the fourth power difference of the wall temperatures. This data was obtained in the vacuum system described in Appendix I at a plate spacing of 3.00 inches. Also, two curves are presented using the experimental temperatures along with emittance values obtained from the literature.

From the experimental data it was possible to calculate an average emittance value, which turned out to be 0.556, assuming gray infinite parallel walls. Also, the assumption that emittance is not a function of temperature is used.

Gilbert (7) covers fully the case of parallel walls with attention to plate spacing and guarded edges for a similar apparatus. Schornhorst and Viskanta (8) present a similar analysis.

From figure (34) the assumption of finite parallel walls

for this experimental apparatus, at a spacing of three inches,
is reasonable.

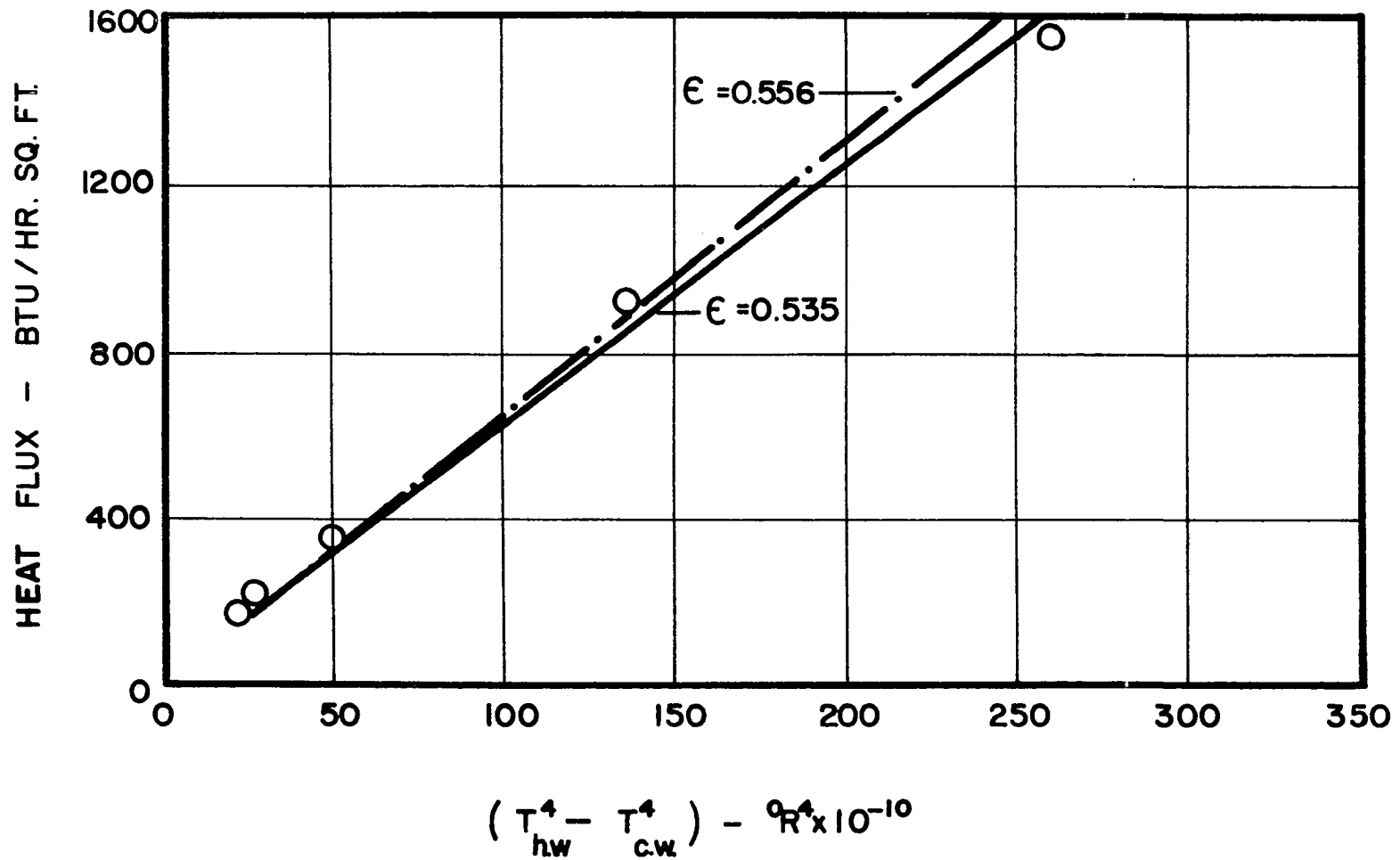


FIGURE 34. VACUUM DATA FOR FINITE PARALLEL WALLS

APPENDIX III

CALIBRATION OF HEAT FLOW METER

The measurements obtained in this study were acquired by means of the heat flow meter located in the cold wall. Since this was the primary sensor in the acquisition of data, the calibration was given considerable thought. In figure 6 a cutaway of the cold wall is shown giving details of location of the heat flow meter.

In order to calibrate the heat flow meter it was first necessary to obtain a stable hot wall temperature. This was accomplished by accurately monitoring the voltages to the heater with a Hewlett-Packard digital voltmeter and allowing a warm-up time of approximately four hours. Also, the air stream was operated at the velocity of which the data was to be taken.

After this period of time all temperatures are read and then re-read after thirty minutes to test the stability of the hot wall. The hot wall is assumed stable by two conditions:

1. Internal temperature difference should be less than 10°F ,
2. Hot wall face temperature change should be less than 5°F .

Once these stability conditions have been satisfied the cold wall temperature is adjusted to the free stream temperature of the air, the stability criteria being 1°F . This criteria is tested over

a period of one hour.

The cold wall temperature is regulated by adjusting the cooling water flow rate through the labyrinth channel located in the cold wall. This is accomplished by using two valves and a pressure gage on the water line, enabling a constant pressure to be maintained on the water channel.

The heat flow meter and the thermocouple readings were then recorded along with the power input to the heater. This information is then analyzed along with similar data taken in a vacuum chamber.

Figure 34 shows the vacuum and tunnel data in the form heat input to the hot wall verses hot wall surface temperature. Since the cold wall was in equilibrium with the air temperature the convective mode of heat transfer is erased leaving only the radiative component to be removed by the cooling water. Therefore, the heat flow meter reading is due entirely to radiative heating. In order to correlate this reading to the radiative output of the hot wall, the vacuum data must be used to obtain this radiative flux.

Since the walls had been run originally in a vacuum chamber to obtain heat input-surface temperature curves the convective effects at the hot wall could be calculated or the radiative flux could be obtained directly from the vacuum data for a given surface temperature.

The above experimental procedure supports the calibration of the heat flow meter and the results are presented in figure 35.

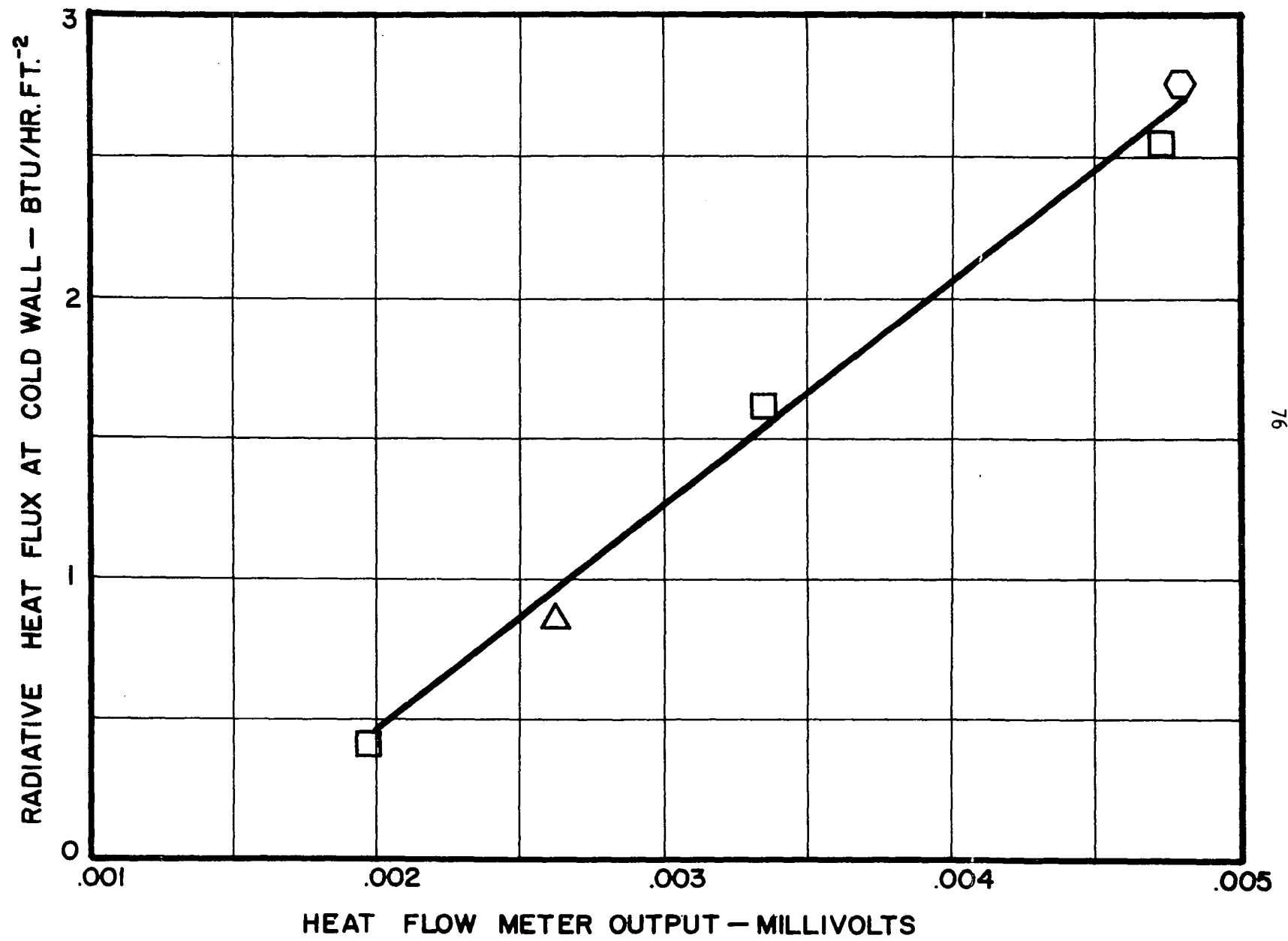


FIGURE 35. CALIBRATION OF HEAT FLOW METER

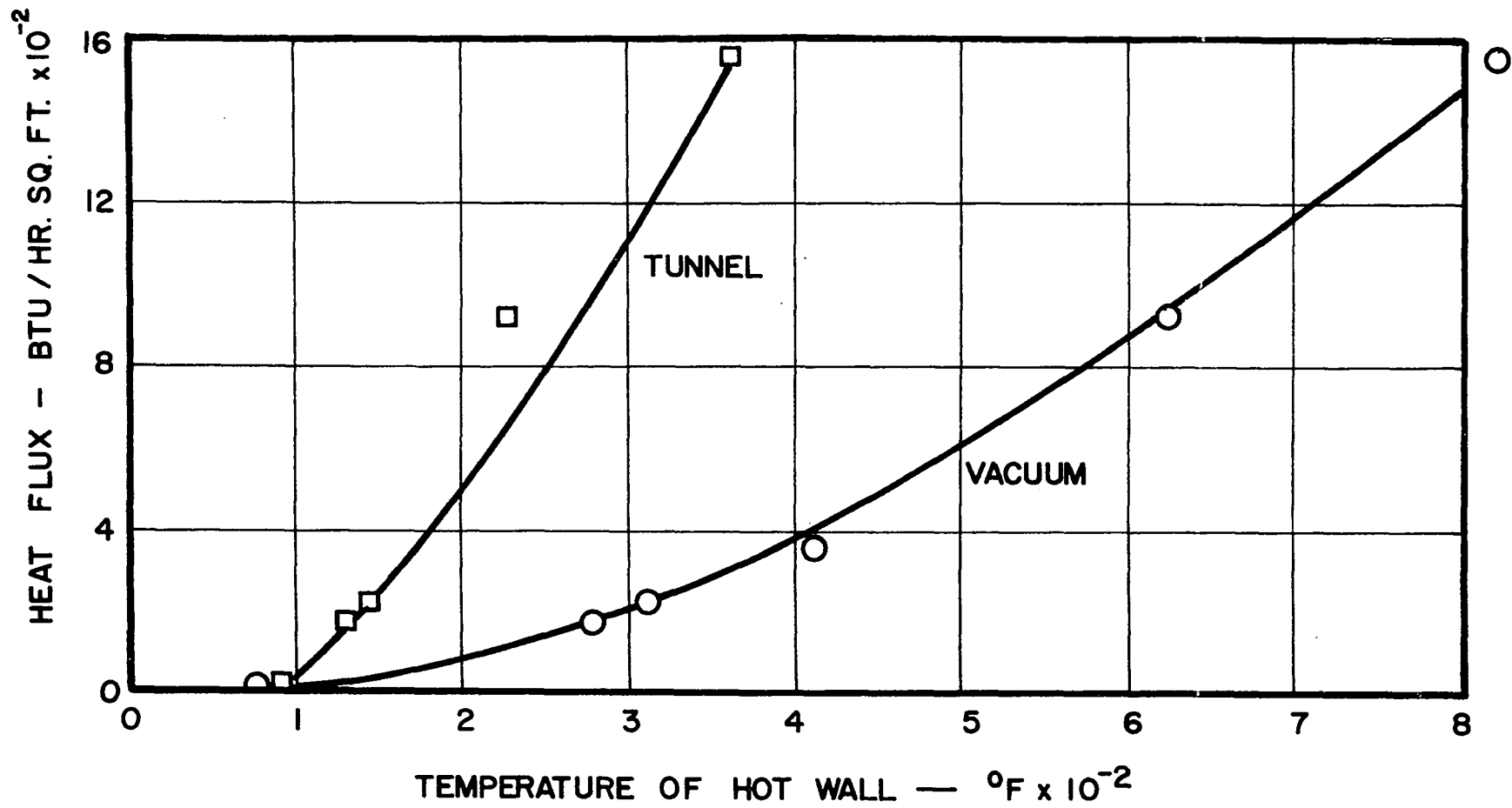


FIGURE 36. HEAT FLUX INPUT VERSUS HOT WALL SURFACE TEMPERATURE

APPENDIX IV

CONVECTIVE HEAT TRANSFER COEFFICIENTS

To accurately describe the radiative mechanism of heat transfer in this experimental apparatus a complete survey of the equipment had been performed in a vacuum chamber. The vacuum was sufficiently high to eliminate all convective heating effects, hence measurements of the radiative component of heat transfer could be made. Therefore, for a given wall temperature the radiative heat transfer component could be described to a great degree of accuracy during operation of the walls in the tunnel. This experimental operation produced curves of the form shown in figure 36, heat flux input to the heater versus hot wall temperature. The same experimental information was recorded in the particle tunnel.

Evaluation of the convective heat transfer coefficient requires a heat balance at the surface of the hot wall be made. This heat balance would be of the following form:

$$\begin{array}{l} \text{Input} \\ \text{(Electrical Power)} \end{array} = \sum \text{Heat Loss}$$

for steady state condition. The input to the hot wall was measured for each particular data run and the radiative loss was obtained from the vacuum data curves. There are two assumptions used here: (1)

conduction effects are small, (2) effect of air on the transport of radiative component is small.

Typical calculation:

Input = 1559.6 BTU per hr. sq. ft.

Hot Wall Temperature = 348°F

Free Stream Temperature = 91°F

Radiative Flux (figure 36) = 260 BTU per hr. sq. ft.

$$h = \frac{(\text{Input} - \text{Radiative Flux})}{(\text{Temp. Hot Wall} - \text{Temp. Free Stream})}$$

where h = average convective heat transfer coefficient.

$$h = 5.05 \text{ BTU per hr. sq. ft. } ^\circ\text{F}$$

This type of calculation was performed for all data runs and is presented in figure 37 along with comparative data from Diessler and Eian (36), Colburn (37), and McAdams (37).

Deïssler and Eian (36) and Deïssler (38) present an analysis for the investigation of fully developed turbulent flow of air in a smooth tube along with experimental information. Deïssler (38) indicates that results for turbulent heat transfer in tubes can be used, for flat plates when an equivalent diameter equal to twice the plate spacing is used. Bird, Stewart, and Lightfoot (39) suggest that for turbulent flow the velocity distribution and the average velocity are given by:

$$\frac{U}{U_{\max}} = \frac{4}{5}$$

The data presented in figure 37 in terms of dimensionless parameters was analyzed using these two engineering approximations mentioned.

The fluid properties were evaluated at a film temperature which was equal to the average of the wall temperature and the free stream temperature.

Sparrow (40) presents an analysis of laminar forced-convection heat transfer between parallel walls where both walls have the same uniform temperature. A second case is treated in which one wall is insulated and the opposite wall is held at a uniform temperature. A similar experimental analysis is presented by Mercer, Pearce and Hitchcock (41). Due to the turbulence in the test section caused by the secondary air stream this flow condition could not be created.

Eckert and Jackson (42), (43), and (44) developed an analysis for the heat transfer coefficient in free-convection. An analysis for laminar free-convection for a flat plate oriented with the direction of the body force is presented by Ostrach (45).

Free convection heat transfer coefficients were obtained by using an experimental technique similar to the method utilized for force convection heat transfer coefficients but without forcing air through the test section and the results are presented in figure 38 for comparison to Eckert and Jackson (42).

The results for both forced and free convection obtained by this method are in reasonable agreement with the literature.

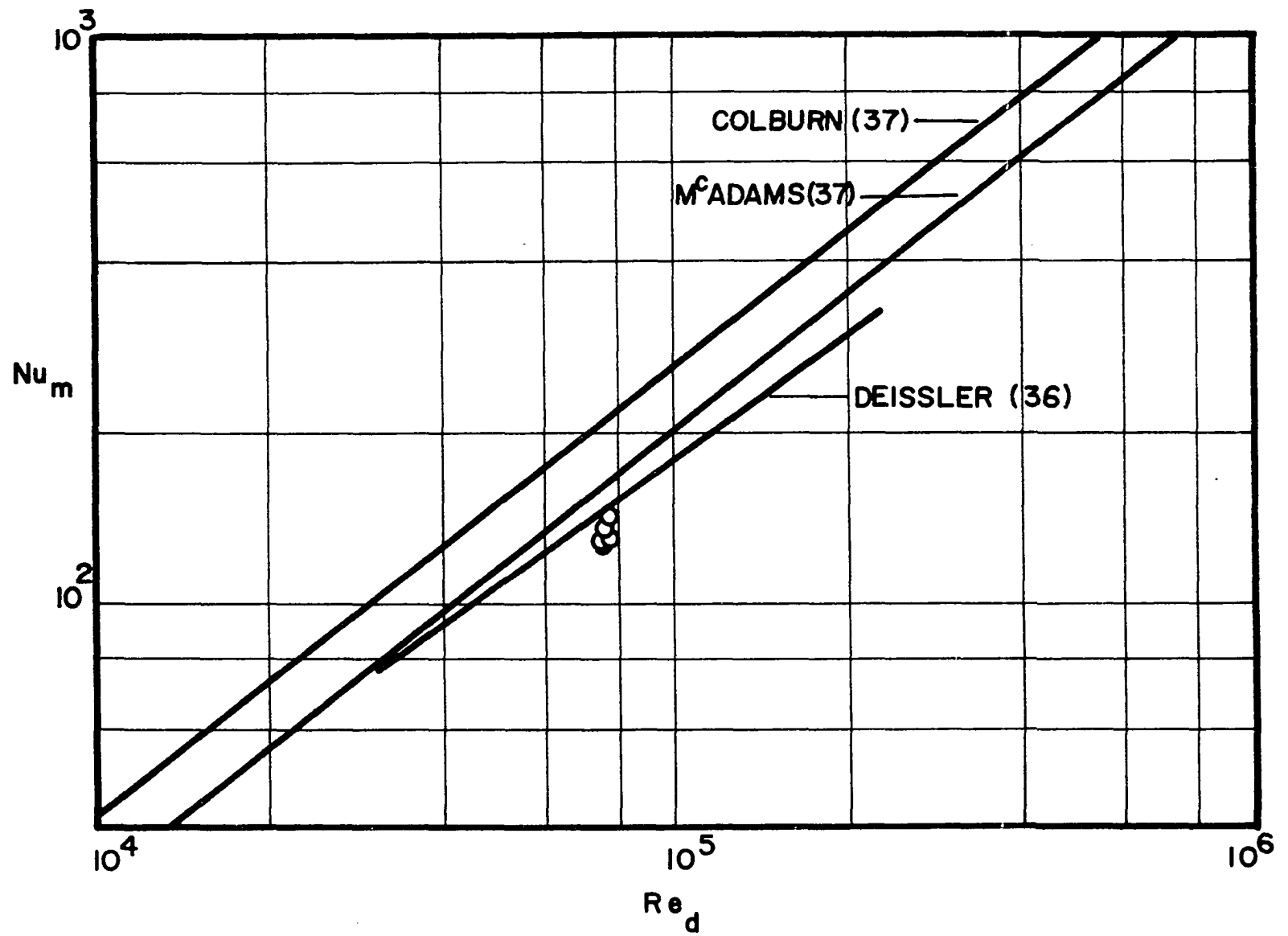


FIGURE 37. FORCE CONVECTION HEAT TRANSFER DATA

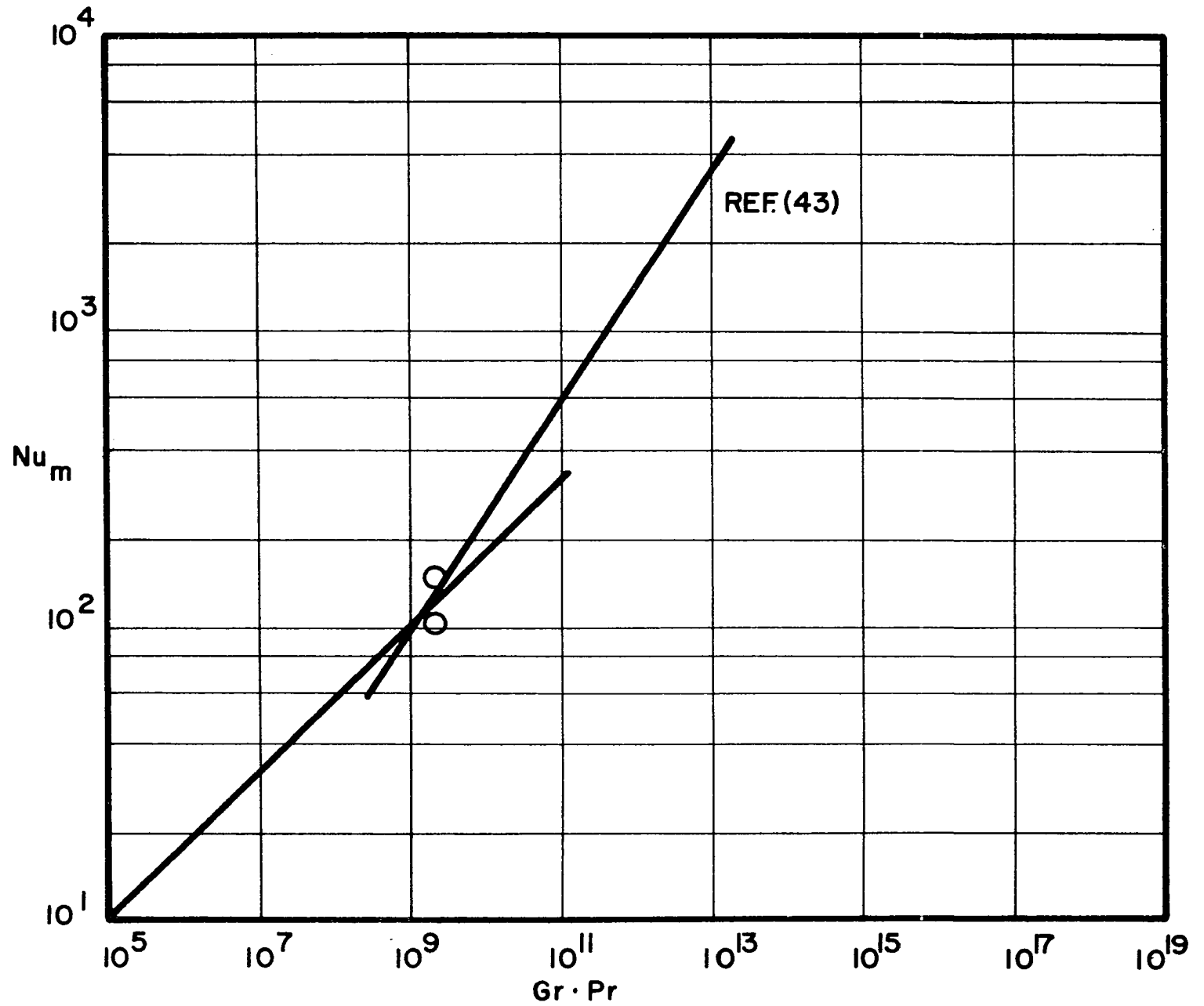


FIGURE 38. FREE CONVECTION HEAT TRANSFER DATA

APPENDIX V

GLASS BEADS

Glass beads were selected as the material to be used for generating dust clouds, because of their ability to flow without clogging or bridging as do many particles of this size.

During the testing period beads were purchased from three different suppliers. The beads ranged in size from 100 microns to about 1600 microns in diameter. But, a majority of the data was taken with glass beads of 200 micron diameter.

Photomicrographs of the glass beads are presented in figures 41 and 42. The ruled grid represents a spacing of 50 microns.

Love and Beattie (5) obtained figures 39 and 40 for glass beads, 100 microns in diameter, and they were used in the calculations for the transfer of thermal radiation involving the glass beads.

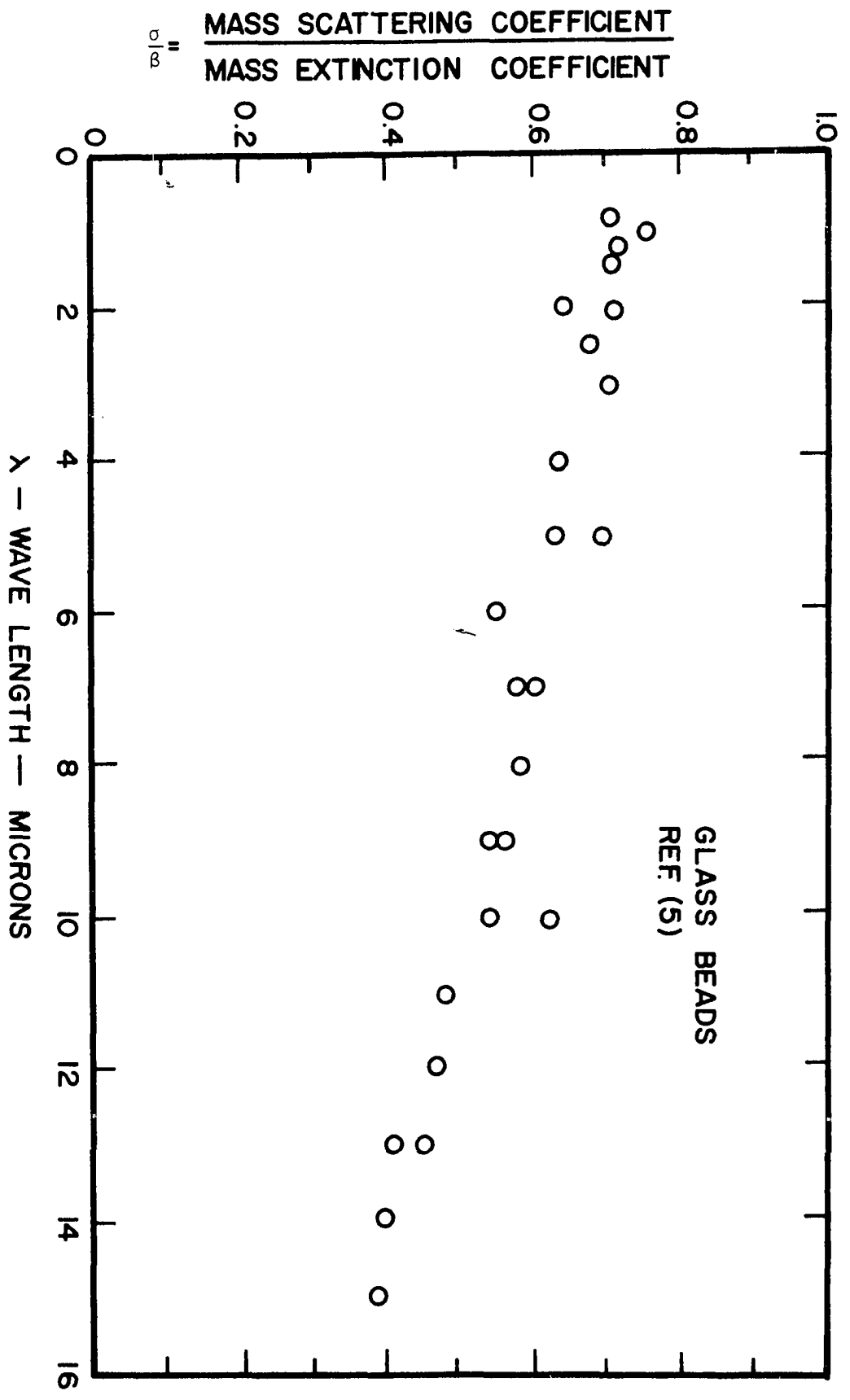


FIGURE 39. VARIATION OF σ_s/σ_t WITH WAVE LENGTH

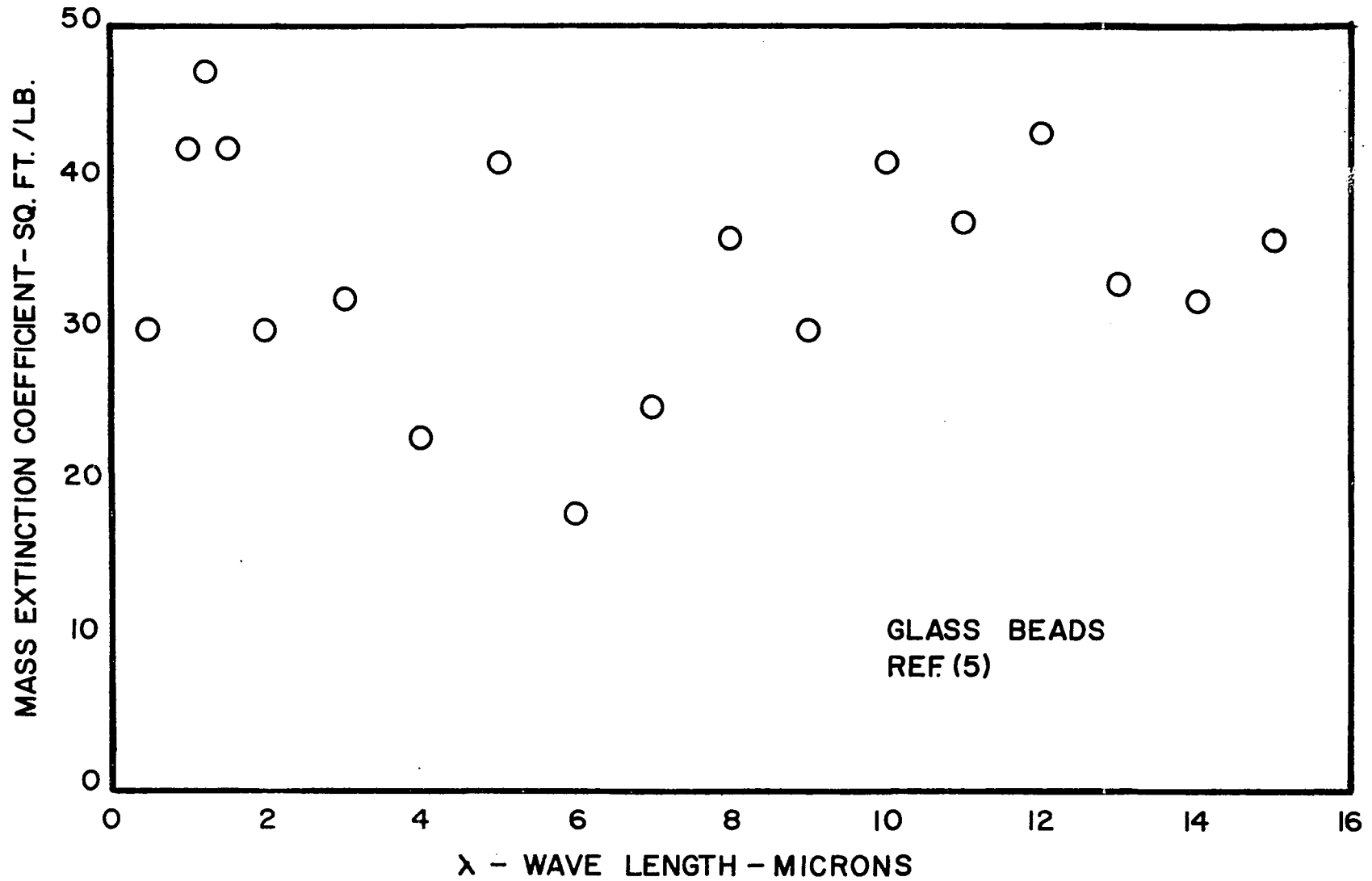


FIGURE 40. VARIATION OF MASS EXTINCTION WITH WAVE LENGTH

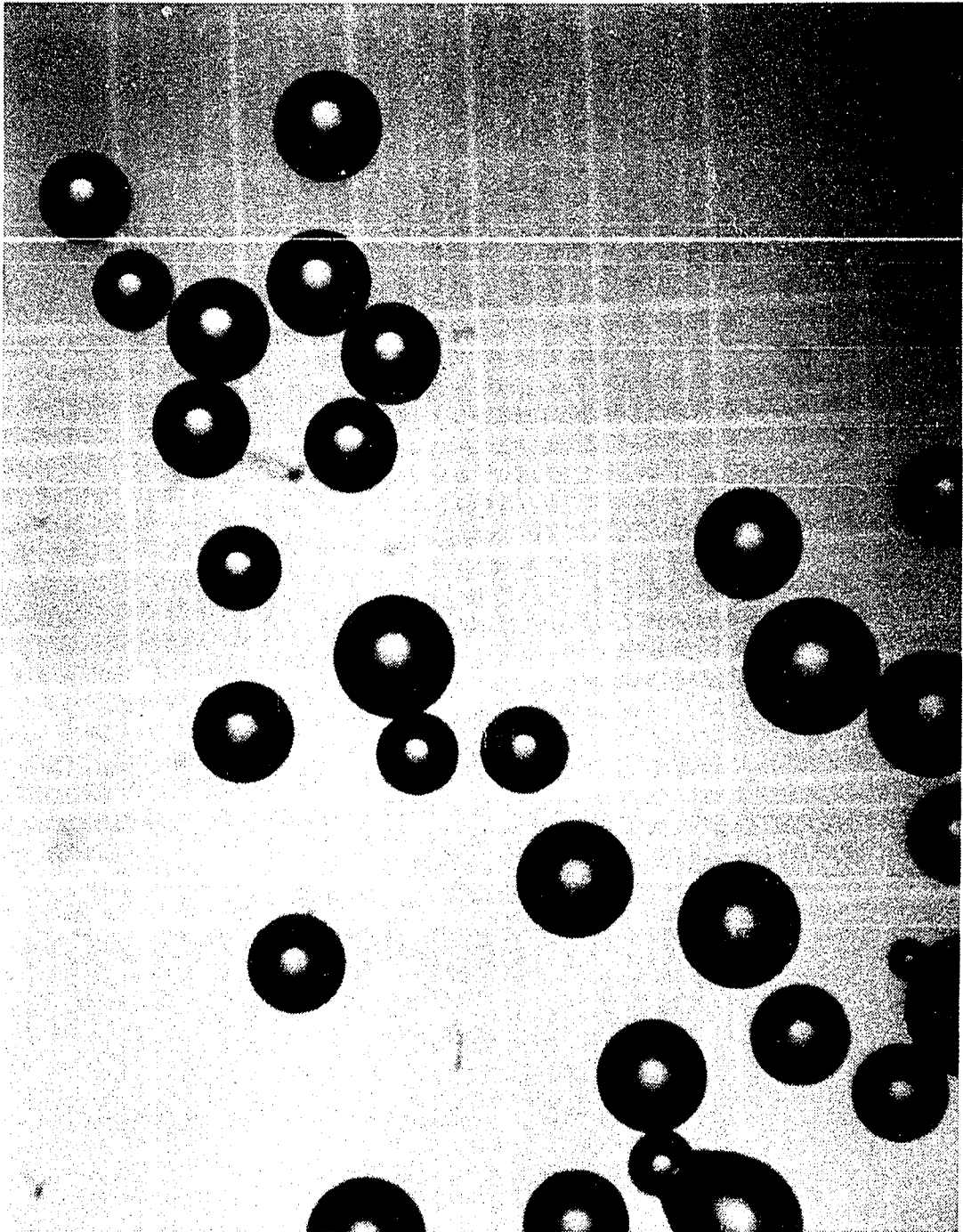


FIGURE 41. PHOTOMICROGRAPHS OF CORNING BEADS

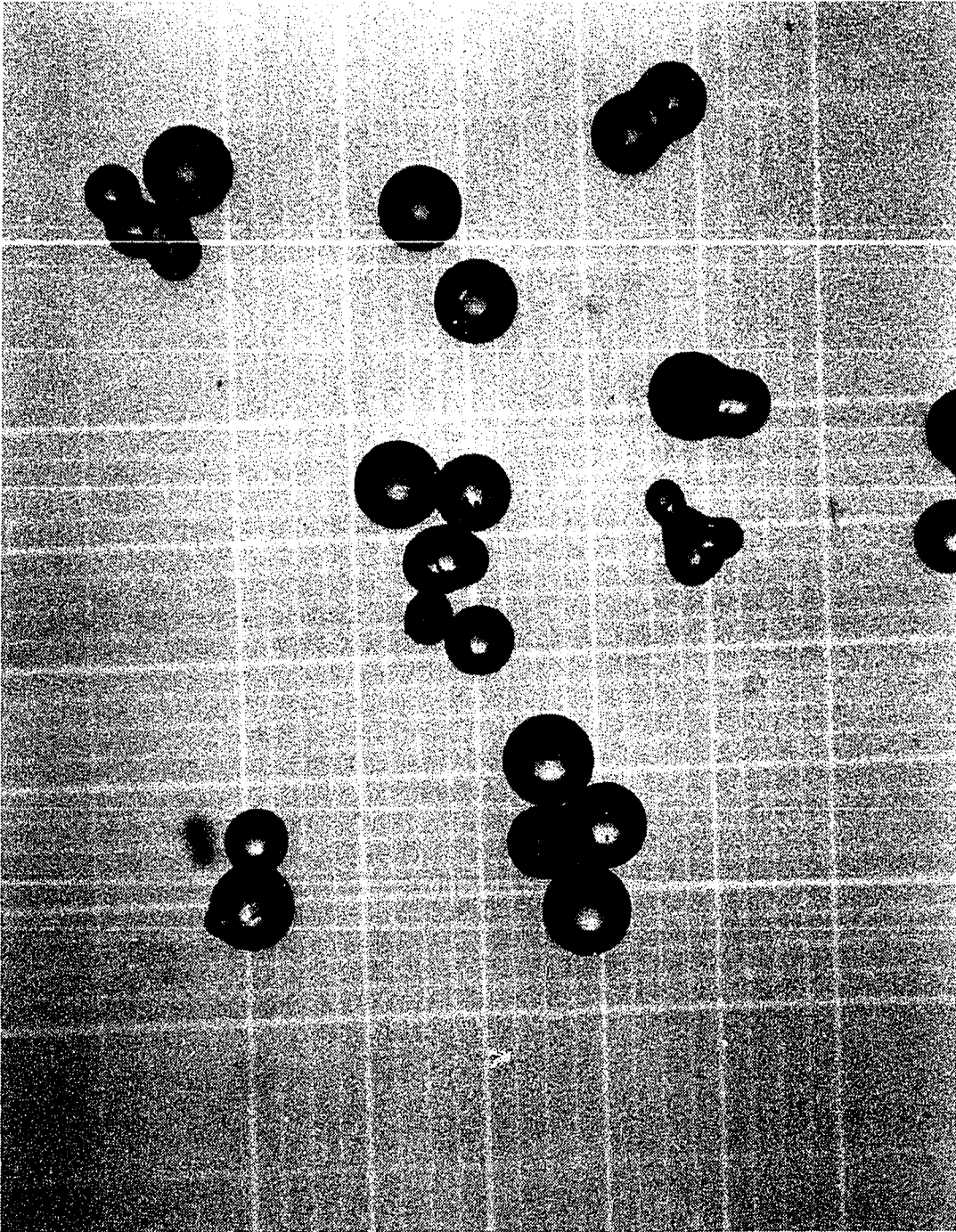


FIGURE 42. PHOTOMICROGRAPHS OF KENCO BEADS

APPENDIX VI

DIMENSIONLESS RADIATIVE HEAT TRANSFER PARAMETERS

Isotropic Case

Scattering to Extinction Ratio = 0.6

Reflectivity of Wall 1 = 0.5

Reflectivity of Wall 2 = 0.5

Optical Spacing	M	N	Q
0.1	1.1247	0.9072	0.2175
0.2	1.1823	0.7959	0.3864
0.3	1.2265	0.7035	0.5230
0.4	1.2609	0.6251	0.6358
0.6	1.3095	0.4990	0.8105
0.8	1.3405	0.4026	0.9379
1.0	1.3606	0.3272	1.0334
1.5	1.3861	0.1988	1.1873
3.0	1.4004	0.0476	1.3528
5.0	1.4013	0.0074	1.3939
∞	1.4013	0.0	1.4013

Isotropic Case

Scattering to Extinction Ratio = 0.475

Reflectivity of Wall 1 = 0.5

Reflectivity of Wall 2 = 0.5

Optical Spacing	M	N	Q
0.1	1.1529	0.8790	0.2739
0.2	1.2258	0.7528	0.4730
0.3	1.2787	0.6522	0.6265
0.4	1.3181	0.5694	0.7487
0.6	1.3709	0.4411	0.9297
0.8	1.4024	0.3469	1.0556
1.0	1.4219	0.2754	1.1464
1.5	1.4446	0.1587	1.2858
3.0	1.4556	0.0332	1.4225
5.0	1.4561	0.0044	1.4517
∞	1.4562	0.0	1.4562

VALUE OF PARAMETER M^e

Case of Radiative Equilibrium

Reflectivity of Wall 1 = 0.5

Reflectivity of Wall 2 = 0.5

Optical Spacing	M^e
0.1	1.10159
0.2	0.9889
0.3	0.9638
0.4	0.9406
0.6	0.8982
0.8	0.8602
1.0	0.8256
1.5	0.7508
3.0	0.5918
5.0	0.4619

APPENDIX VII

SAMPLE DATA RECORDING

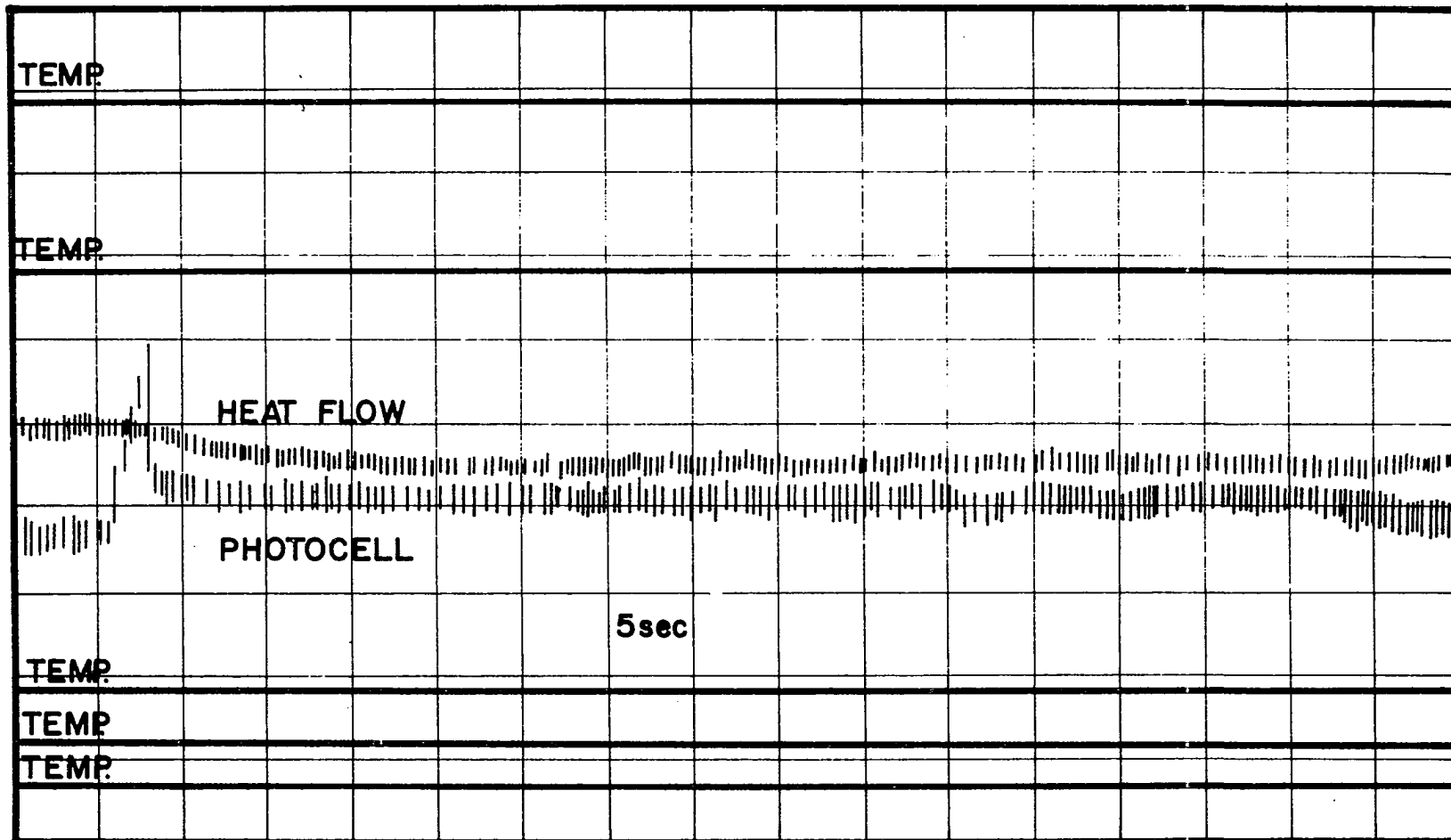


FIGURE 43. SAMPLE DATA RECORDING FROM TUNNEL

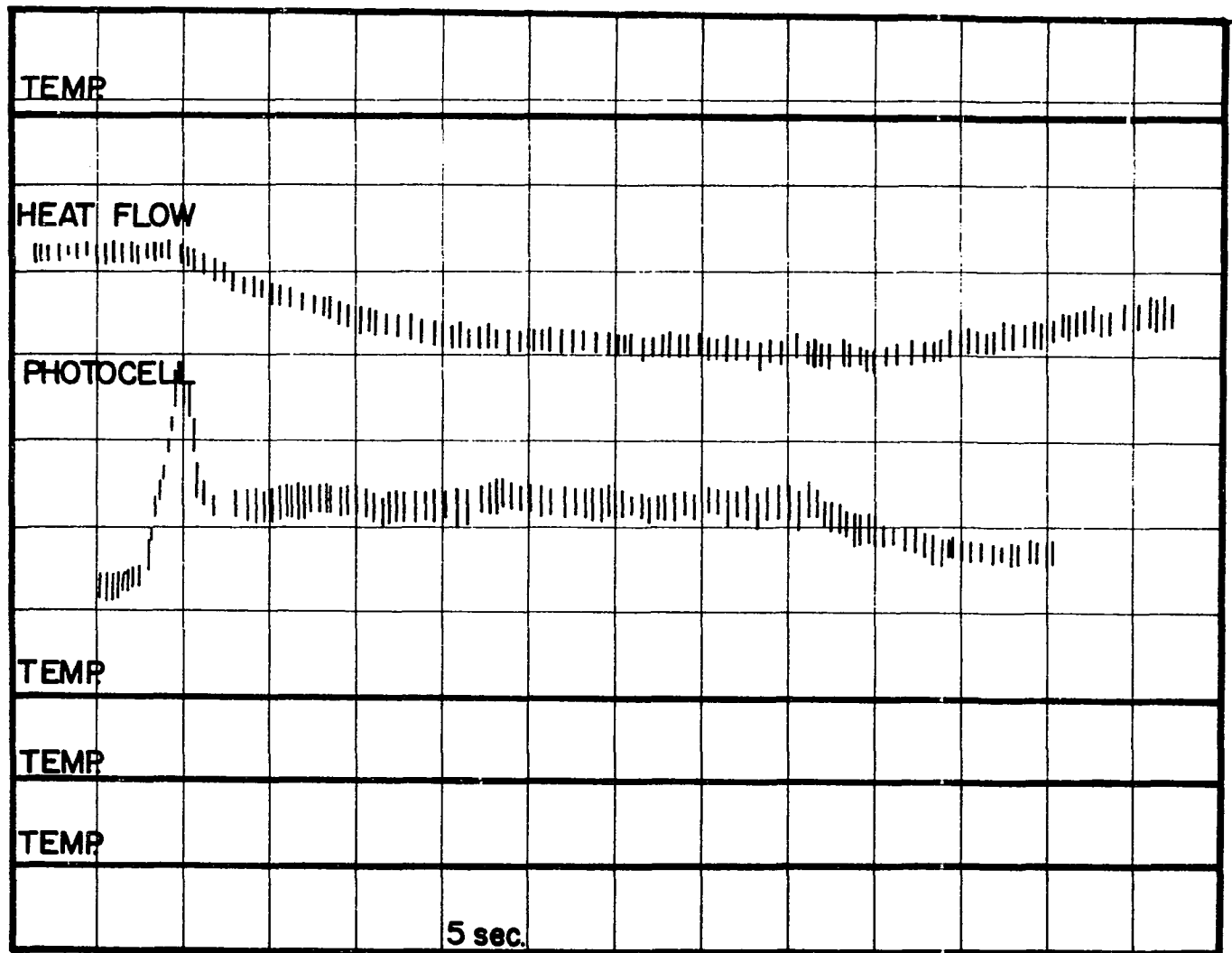


FIGURE 44. SAMPLE DATA RECORDING FROM TUNNEL

APPENDIX VIII

EXAMPLE CALCULATIONS

EXAMPLE CALCULATION FOR ISOTROPIC SCATTERING

$$q = \frac{\sigma}{\pi} [MT_1^4 - NT_2^4 - QT_a^4]$$

where:

q = net radiant flux at wall 1

T = absolute temperature

M, N, Q = dimensionless parameters from Table

σ = Stefan-Boltzmann constant

Subscript

1 = surface 1

2 = surface 2

a = particles

Wall 1 - - Temperature = 820.5°R

Emittance = 0.50

Wall 2 - - Temperature = 554.0°R

Emittance = 0.50

Particles - - Temperature = 554.0°R

Let τ (optical spacing) = 0.1

(Assume a scattering to extinction ratio of 0.6)

$$q_1 = \frac{\sigma}{\pi} [1.1247 (46.3)(10)^{10} - 0.9072 (9.61)(10)^{10} - 0.2175 (9.61)(10)^{10}]$$

$$q_1 = 225.2 \text{ BTU per hr. sq. ft.}$$

Net radiant flux at wall 2

$$q_2 = - 182.0 \text{ BTU per hr. sq. ft.}$$

The assumption of a scattering to extinction ratio of 0.6 is based on figure 39 from reference (5).

EXAMPLE CALCULATION FOR PARTICLES IN RADIATIVE EQUILIBRIUM

$$q = \frac{\sigma M^e (T_1^4 - T_2^4)}{\pi}$$

where

q = net radiant flux

T = absolute temperature

σ = Stefan-Boltzmann constant

M^e = dimensionless parameters from Table

π = 3.1416

Subscript

1 = hot wall surface

2 = cold wall surface

Wall 1 - - temperature = 1291.69°R

emittance = 0.50

Wall 2 - - temperature = 711.69°R

emittance = 0.50

$$q = \frac{0.1713(10)^{-8}(0.7801)[(1291.69)^4 - (711.69)^4]}{3.14}$$

q = 1116.54 BTU per hr. sq. ft.

INFINITE PARALLEL WALL SAMPLE CALCULATION

$$q = \frac{\sigma(T_1 - T_2)}{\frac{1}{\epsilon_1} + \frac{1}{\epsilon_2} - 1}$$

where

q = net radiant flux

T = absolute temperature

σ = Stefan-Boltzmann constant

ϵ = total hemispherical emittance

subscript

1 = hot wall surface

2 = cold wall surface

Wall 1 - - temperature = 1291.69°R

emittance = 0.50

Wall 2 - - temperature = 711.69°R

emittance = 0.50

$$q = 1.713(10)^{-8} \frac{[(1291.69)^4 - (711.69)^4]}{\frac{1}{.5} + \frac{1}{.5} - 1}$$

q = 1585.73 BTU per hr. sq. ft.

RADIATIVE EQUILIBRIUM CALCULATION

Particles: Glass Beads

Density of Particles: 2.80 grams per cc.

Total Particle Weight: 1400 grams

Duration of Cloud: 6 seconds

Velocity at Center of Walls: 8 ft per sec.

Density of Cloud: (ρ_c)

$$\text{Weight (lb)} = 2.2046(1.4) = 3.082$$

$$\text{Volume (cubic feet)} = 8 \text{ ft per sec} (6 \text{ sec}) (1 \text{ ft}) (0.25 \text{ ft})$$

$$= 12 \text{ cubic feet}$$

$$\rho_c \text{ (lb per cubic ft)} = (3.082)/(12)$$

$$= 0.2561 \text{ (lb per cubic ft)}$$

Mass Flow Rate: (m)

$$m = \rho_c av$$

$$= (0.2561)(0.25)(8)$$

$$= 0.5122 \text{ (lb per sec)}$$

Specific Heat Glass = $c_p = 0.199$

Heat Transfer:

$$q'' = 1559.66 \text{ BTU per hr}$$

$$q'' = mc_p \Delta T$$

$$\text{or } \Delta T = (q'')/(mc_p)$$

$$= (1559.66)/(0.5122 \times 3600 \times 0.199)$$

$$= 4.24(10)^0$$

$$= 4.24^{\circ}\text{F}$$

SAMPLE CALCULATION OF OPTICAL THICKNESS

$$\frac{I}{I_0} = e^{-\tau}$$

I_0 = Intensity of source

I = Intensity for given optical thickness

Experimentally:

$$I/I_0 = \frac{\text{Maximum Deflection} - \text{Deflection at Time (t)}}{\text{Maximum Deflection}}$$

Sample Calculation:

Maximum Deflection = 2.5

Deflection at Time (t) = 1.7

$I/I_0 = 0.32$

$\tau = 1.14$

SAMPLE CALCULATION OF THRING'S RADIATION GROUP

$$N_{th} = \rho c_p v / \epsilon \sigma T^3$$

Volume of Cloud: 6.78 sec. x 7.3 ft/sec. = 49.6 ft.

0.25 ft. x 49.6 ft. = 12.398 cubic ft.

Density of Cloud: 3.082 lb./12.398 cubic ft. = 0.249 lb/cubic ft.

$\epsilon = 0.5$ (dimensionless)

$\sigma = 0.1713 \times 10^{-8}$ BTU/hr ft² °R⁴

$C_p = 0.199$ BTU/hr lb °F

$T = 1292$ °R

$N_{th} = 0.249(0.199)(7.3) / (0.5)(0.1713 \times 10^{-8})(1292)^3$

$N_{th} = 0.07039$

APPENDIX IX

EQUIPMENT

- (1) Digital Voltmeter
Hewlett-Packard Company
Model 3440 A
- (1) DC Micro Volt Ammeter
Hewlett-Packard Company
Model 425 A
- (1) Oscilloscope
Tektronic
Type 561 A
- (1) Differential Amplifier
Tektronic
Type 2A63
- (1) Time Base
Tektronic
Type 2B67
- (1) Vacuum Tube Voltmeter
Hewlett-Packard Company
Model 410 B
- (4) Differential Amplifier
Sanborn Division of Hewlett-Packard Company
Model 8875 A
- (1) Ammeter
Weston Company
110 volts, 1-50 amps.
- (1) Voltmeter
Heath Company
1.5 - 1500 volts

- (1) Potentiometer
Leeds and Northrup Company
Model 8686
- (1) Rotary Selector Switch
Leeds and Northrup Company
Model 8248-16
- (1) Visicorder Oscillograph
Honeywell Corporation
Model 906 C
- (1) Wattmeter
General Electric Company
Volts 100/200, Amps. 5/10
- (1) Variable Auto Transformer
Standard Electrical Products Company
230 Volts, 9.0 Amps.
- (1) Variable Auto Transformer
Superior Electric Company
240 Volts, 9.0 Amps.
- (1) Variable Auto Transformer
General Radio Company
115 Volts, 6.0 Amps.
- (1) AC/DC Range Unit
(For Digital Voltmeter)
Hewlett-Packard Company
Model 3440 A
- (1) Vacuum Pumping System
NRC Equipment Corporation
Number 3307
- (1) Micromanometer
Flow Corporation
Model MM-3
- (1) Pitot Tube
F.W. Dwyer Mfg. Co.
0.125 Inches Diameter